Band structure of ²³⁵U

D. Ward,[1] A. O. Macchiavelli,[1] R. M. Clark,[1] D. Cline,[2] M. Cromaz,[1] M. A. Deleplanque,[1] R. M. Diamond,[1,*]
P. Fallon,[1] A. Görgen,[1,3] A. B. Hayes,[2] G. J. Lane,[1,4] I.-Y. Lee,[1] T. Nakatsukasa,[5] G. Schmidt,[6] F. S. Stephens,[1]
C. E. Svensson,[1,7] R. Teng,[2] K. Vetter,[1,8] and C. Y. Wu[2,6]

[1]*Nuclear Science Division, Lawrence Berkeley National Laboratory, Berkeley, California 94720, USA*
[2]*Department of Physics, University of Rochester, Rochester, New York, USA*
[3]*Department of Physics, University of Oslo, Oslo, Norway*
[4]*Nuclear Physics Department, Australian National University, Canberra, Australia*
[5]*RIKEN Nishina Center, Wako 351-0198, Japan*
[6]*Lawrence Livermore National Laboratory, Livermore, California 94550, USA*
[7]*Department of Physics, University of Guelph, Guelph, Ontario N1G 2W1, Canada*
[8]*Department of Nuclear Engineering, University of California Berkeley, Berkeley, California 94720, USA*

Over a period of several years we have performed three separate experiments at Lawrence Berkeley National Laboratory's 88-Inch Cyclotron in which ²³⁵U (thick target) was Coulomb-excited. The program involved stand-alone experiments with Gammmasphere and with the 8pi Spectrometer using ¹³⁶Xe beams at 720 MeV, and a CHICO-Gammasphere experiment with a ⁴⁰Ca beam at 184 MeV. In addition to extending the known negative-parity bands to high spin, we have assigned levels in some seven positive-parity bands which are in some cases (e.g., [631]1/2, [624]7/2, and [622]5/2) strongly populated by $E3$ excitation. The CHICO data have been analyzed to extract $E2$ and $E3$ matrix elements from the observed yields. Additionally, many $M1$ matrix elements could be extracted from the γ-ray branching ratios. A number of new features have emerged, including the unexpected attenuation of magnetic transitions between states of the same Nilsson multiplet, the breakdown of Coriolis staggering at high spin, and the effect of $E3$ collectivity on Coriolis interactions.

I. INTRODUCTION

The spectroscopy of ²³⁵U has hardly been extended since the work of Stephens *et al.* in 1968 [1]. In the intervening years, techniques in γ-ray spectroscopy have been advanced enormously, and on this basis we decided to revisit this most important nuclide. The initial motivation was to investigate Coriolis interactions between the rotational bands of ²³⁵U, and we would argue that the origin of the attenuation of these interactions observed by many authors, in many nuclei, has yet to be fully understood. But in pursuing the Coriolis effects, other interesting features have emerged and are included in this work.

In their paper of 1968, Stephens *et al.* [1] recognized the unique role of ²³⁵U as a laboratory for the study of Coriolis effects in nuclei. First, Coriolis matrix elements increase with increasing j of the orbitals, and the $j_{15/2}$ multiplet is the highest j value accessible in nuclei. Second, because the Fermi surface lies close to the middle of the system, near the $K = 7/2$ member (with [743]7/2 being in fact the ground state), rotational bands on all eight members of the multiplet, $K = 1/2$ through $K = 15/2$ should lie reasonably low in the spectrum, and in principle they might be observable. Third, although several nuclei near ²³⁵U might satisfy these conditions, ²³⁵U and ²³⁷Pu are the only cases where a member of the $j_{15/2}$ multiplet is the ground state; this property is essential if we are to measure $E2$ matrix elements between members of the multiplet by Coulomb excitation, and hence determine some of the mixing amplitudes directly. Finally,

the intruder $j_{15/2}$ orbitals having the opposite parity to that of the shell are not mixed with other Nilsson levels; hence their properties are more robust and less dependent on the Nilsson parameters than is the case for the resident orbitals. With these advantages, it should be possible in ²³⁵U to obtain a very detailed view of the Coriolis interaction.

In the 1968 paper, only the $5/2, 7/2$, and $9/2$ members of the $j_{15/2}$ multiplet were unambiguously identified and measured. A complication is the existence of γ-vibrational bands with $K = 3/2$ and $K = 11/2$ ($K \pm 2$ on the $K = 7/2$ ground state), which can in principle mix with the multiplet bands.

In the present work we have populated rotational bands of ²³⁵U by Coulomb excitation with ¹³⁶Xe and with ⁴⁰Ca beams at energies below the Coulomb barrier, where cross sections may be related to $E\lambda$ matrix elements. Gamma decays were detected in experiments with both the 8pi Spectrometer and with Gammasphere, and for the ⁴⁰Ca beam, a coincidence with scattered beam particles in the CHICO detector system was also required. Although some 80 new levels were assigned in this work, we could not identify any new K members of the $j_{15/2}$ multiplet.

Several points of interest have arisen out of these studies— for example, the inferred $B(M1)$ values, both within a band and between bands built on the $j_{15/2}$ multiplet. There have been hardly any reported measurements of absolute $B(M1; K \to K \pm 1)$ values between rotational bands belonging to different members of a high-j intruder multiplet in any nucleus. These $B(M1)$ values are generally predicted to be very large, typically in the range of 0.5–1.0 nuclear magnetons. By calibrating against the competing in-band γ-ray branch, for which the transition strength can be reliably predicted, we

have obtained a large data set for such $B(M1)$ strengths in ^{235}U. We find that, in all cases, they are retarded by at least an order of magnitude compared with a Nilsson-particle-rotor calculation. These results are presented in Sec. III.

By extending the known bands to much higher spins, we find a further problem with the Coriolis prediction. Stephens *et al.* [1] were able to obtain a good fit to the spacing and staggering of the energy levels known at that time by decreasing some of the Coriolis matrix elements $\langle K + 1|j_+|K\rangle$ calculated in the Nilsson model by arbitrary factors $\alpha(K + 1, K)$. The best-fit values were $\alpha \approx 0.5$ for $K = 5/2$ and $7/2$. We now find that the energy staggering predicted with these attenuation factors becomes too large for spins above those originally included in the fit and diverges from experiment with increasing spin. These results are discussed in Sec. V.

Because the γ-vibrational bands with $K = 3/2$ and $K = 11/2$ are mixed with the ground-state band via $\Delta K = 2$ Coriolis interactions, all the K components of the $j_{15/2}$ multiplet found in the ground band via $\Delta K = 1$ Coriolis interactions will find their way into the γ-vibrational bands. The rotational band on the $K = 9/2$ member of the multiplet is crossed by the $K = 11/2$ vibrational band near spin $17/2$ and we can estimate the size of the interaction as discussed in Sec. VI.

Factors that impact the attenuation of Coriolis matrix elements such as pairing and the so-called recoil effect are very briefly discussed in Secs. VII and VIII.

We were surprised to find no clear spectroscopic signal of rotational bands built on octupole vibrational states; instead we observed relatively strong populations of many positive-parity bands that have been given Nilsson assignments in the literature. In sub-barrier Coulomb excitation, the excitation of positive-parity bands from a negative-parity ground state is a sure indication of octupole character. It is apparent that in ^{235}U the octupole correlations are strong, but we believe that the expected octupole bands built on the ground state are mixed into many positive-parity Nilsson states and simply lose their identity.

The occurrence of strong octupole correlations in ^{235}U, expected theoretically, and now confirmed experimentally, suggests a mechanism to explain the attenuated Coriolis matrix elements, namely, the dilution of high-j components in the $j_{15/2}$ wave functions through mixing with the opposite-parity $g_{9/2}$ orbitals ($\Delta L = 3$). To test whether a significant attenuation of the Coriolis matrix elements would be expected at the observed level of octupole collectivity, we have performed extensive calculations in a model based on the quasiparticle random phase approximation (QRPA), as described in Sec. IX. The paper includes three appendices. Appendix A describes details of the QRPA theory; Appendix B contains detailed level schemes; Appendix C contains the main data tables.

II. EXPERIMENTS AND DATA ANALYSIS

A. The experiments

The data reported in this paper are the outcome of three separate experiments performed at the 88-Inch Cyclotron of the Lawrence Berkeley National Laboratory over a period of seven years. The same rolled foil of enriched ^{235}U

($\approx$50 mg cm^{-2}) was used throughout. The small percentage of ^{238}U in the foil posed no significant difficulty in the experiment.

In the first experiment, the foil was bombarded with a ^{136}Xe beam at 720 MeV, and in-beam γ-rays were detected in the Gammasphere array, comprising 100 Compton-suppressed HPGe detectors at that time. The trigger condition was for three or more Compton-suppressed HPGe detectors to fire in coincidence. Because of light-element contaminants in the target foil, principally carbon and oxygen, the quality of the data was restricted. The nuclide ^{235}U, as well as perhaps any odd-mass actinide, presents unusual facets in Coulomb excitation. The γ-ray transition energies of the rotational bands at low spins are very low, and thus they are strongly converted. Furthermore, excited bands directly populated by Coulomb excitation tend to decay by a single-step transition to a lower-lying band rather than by cascading in-band. Only at high spin does the partial lifetime for decay within the band become competitive with the decay out. The only exceptions to this rule in ^{235}U are the low-lying [622]5/2 and [631]1/2 bands that are so close to yrast that the γ-ray flux tends to stay in-band. The γ-ray multiplicity of radiation following Coulomb excitation in ^{235}U is then much less than the rule-of-thumb estimate $M_\gamma \approx I/2$, where I is the spin.

The resolving power of an array such as Gammasphere increases strongly with the order of the coincidence fold; however, in the Coulomb excitation of ^{235}U there are few high-fold events, and the full power of the array could not be realized. It was not practical to analyze the coincidence data as an $E_\gamma \cdot E_\gamma \cdot E_\gamma$ coincidence cube, and we had to be content with an $E_\gamma \cdot E_\gamma$ matrix. The contaminating light elements bombarded with ^{136}Xe at 720 MeV have a large cross section for fusion-evaporation reactions with a high γ-ray multiplicity, say typically $M_\gamma \approx 20$, and produce a copious background on a trigger condition of three or more Compton-suppressed HPGe coincidences used in the first experiment. For these reasons, the experiment was considered at the time to have been a failure. However, as seen below, a reanalysis of the data has produced a sensitive view of the spectroscopy of the highest spins populated in Coulomb excitation.

A reprise of the ^{136}Xe experiment was performed with the 8pi Spectrometer array when it was operated at Lawrence Berkeley National Laboratory (LBNL). Although this spectrometer is generally less efficient than Gammasphere, it had two features making this particular experiment attractive. First, the smaller HPGe detectors of the 8pi Spectrometer (25% versus 75% standard efficiency) had a better response to low-energy γ rays, say below $E_\gamma \approx 100$ keV, and it was hoped to study coincidences in the range $E_\gamma = 50$–100 keV where Gammasphere has little efficiency. Second, the BGO ball of the 8pi Spectrometer allows a good dispersion of events by K, the total number of hits on the BGO detectors. The trigger condition for this experiment was for two or more Compton-suppressed HPGe coincidences. By specifying an upper limit to the K in the data analysis (with $K \leqslant 5$ being eventually selected), it was hoped to discriminate against the background of high-spin (high-K) events from the contaminants.

In fact these expectations were borne out, and the 8pi data provided the bulk of the information concerning the principal rotational bands, particularly the γ-ray branching ratios, which

involved low-energy γ rays that could not be determined reliably in the Gammasphere experiment.

Encouraged by these results, the data from the earlier Gammasphere experiment were reanalyzed with the most restrictive multiplicity cut in the parameter K that could be applied, namely $K = 3$, and only three Compton-suppressed hits on the HPGe array, and no additional hits on the BGO array. Only a small subset of the data was retained with this condition, but in the $E_\gamma \cdot E_\gamma$ coincidence matrix we found a clean result. Typically, these data allowed us to add one or two transitions to the tops of the principal rotational bands and gave a view of decays from the highest spins of excited bands not seen in the 8pi data.

Although these experiments with Gammasphere and with the 8pi Spectrometer had given us much new data on the level scheme and spectroscopy of ^{235}U, there remained a problem in attempting to extract accurate experimental yields for comparison with the yields calculated in Coulomb excitation with the Winther–de Boer code [2]. This was the bias introduced by the trigger and analysis conditions on the K parameter, which distorted the instrumental response. One might suppose that this could be accounted for in a Monte Carlo simulation, and indeed it probably could, but it would be an elaborate calculation with potentially large uncertainties. For example, some of the interesting levels in our study were not detected at all in these experiments because their effective γ-ray multiplicity was essentially unity.

A third experiment was performed with the Gammasphere array and the University of Rochester's CHICO detector [3]. This latter system comprises 20 parallel-plate avalanche counters (PPACs) covering 67% of the 4π solid angle around the target. Only the backward hemisphere was used in this experiment. The target foil was that used in the earlier experiments and was thick enough to stop the beam, chosen to be ^{40}Ca at 184 MeV for this experiment. Backscattered ^{40}Ca ions were detected in the CHICO detectors in the laboratory angular range from ≈ 110 degrees to ≈ 170 degrees in coincidence with γ rays registered in Gammasphere. The trigger condition was one or more Compton-suppressed HPGe detectors and a CHICO detector to fire in coincidence. The trigger bias on the γ-ray multiplicity was therefore eliminated, and background from fusion-evaporation reactions was entirely suppressed since neither evaporated neutrons, nor protons, nor α particles registered in the CHICO detectors.

B. Data analysis: ^{136}Xe experiments

The data collected in the ^{136}Xe experiments were replayed into $E_\gamma \cdot E_\gamma$ coincidence matrices with conditions on multiplicity given in the previous section. The Gammasphere matrix contained 160×10^6 coincident pairs, and the 8pi matrix contained 13×10^6 pairs. The matrices were processed with the RADWARE analysis package to build level schemes and to determine γ-ray energies and intensities. Where possible, the levels were organized into rotational bands and intrinsic states assigned to them as summarized in Table XIX.

The bands built on the ground-state, Nilsson [743]7/2$^-$, and on the first and second excited states, [631]1/2$^+$ and [622]5/2$^+$, readily lend themselves to such a treatment. The
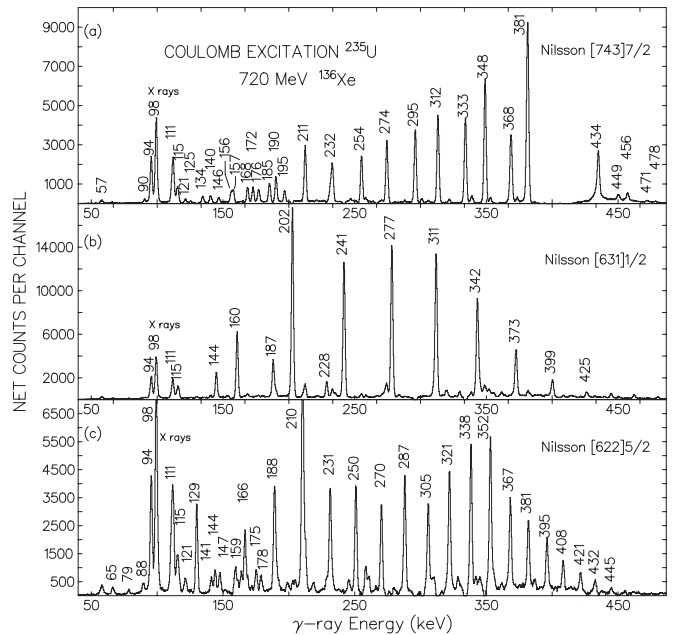

FIG. 1. Coincidence γ-ray spectra showing the features of the principal bands to high spin in the Gammasphere stand-alone experiment. (a) Coincidence spectrum with a single gate set at $E_\gamma = 409$ keV, the $43/2^- \rightarrow 39/2^-$ transition in the ground-state rotational band. The $45/2^- \rightarrow 41/2^-$ and $41/2^- \rightarrow 37/2^-$ transitions are not in coincidence with the gate and are absent in the spectrum. The decrease in peak height with decreasing spin represents the increasing conversion coefficient. The decay down this band is seen to spread the population to both signatures very quickly. (b) Coincidence spectrum summed over the gates $E_\gamma = 241$, $E_\gamma = 277$, and $E_\gamma = 311$ keV, respectively, the $23/2^+ \rightarrow 19/2^+$, $27/2^+ \rightarrow 23/2^+$, and $31/2^+ \rightarrow 27/2^+$ transitions in the Nilsson [631]1/2 band. Compared to panel (a), the population is seen to stay more closely to the signature in which the gates were set. (c) Coincidence spectrum summed over the gates $E_\gamma = 250$, $E_\gamma = 270$, and $E_\gamma = 288$, $E_\gamma = 305$, and $E_\gamma = 322$ keV, respectively, the $23/2^+ \rightarrow 19/2^+$, $25/2^+ \rightarrow 21/2^+$, $27/2^+ \rightarrow 23/2^+$, $29/2^+ \rightarrow 25/2^+$, and $31/2^+ \rightarrow 27/2^+$ transitions in the Nilsson [622]5/2 band.

lowest states could not be seen in either the Gammasphere or the 8pi experiments but these states are well studied in the literature (e.g., Ref. [4]), and there is no doubt as to how the γ rays and rotational levels seen in these experiments should fit together. Examples of spectra related to these bands are shown in Fig. 1, and the level schemes for the bands seen to high spin in these experiments are shown in Fig. 2. Detailed level schemes for all bands observed are presented in Appendix B.

In Fig. 2, we also show a fourth band seen to high spin and identified as Nilsson [631]3/2. This band decays primarily to the [631]1/2 band rather than to the ground-state band. Although it is firmly tied to the [631]1/2 band, as shown by the coincidence data in Fig. 3, we could not make the Nilsson assignment on these data alone, but the lowest state seen with the ^{136}Xe beam ($E_x = 791$ keV) is identical to a state seen in the ^{40}Ca experiments, which has been firmly identified with spin 15/2$^+$ in the Nilsson [631]3/2 band. In that experiment it was the highest level identified in the band (cf. Figs. 20 and 23).
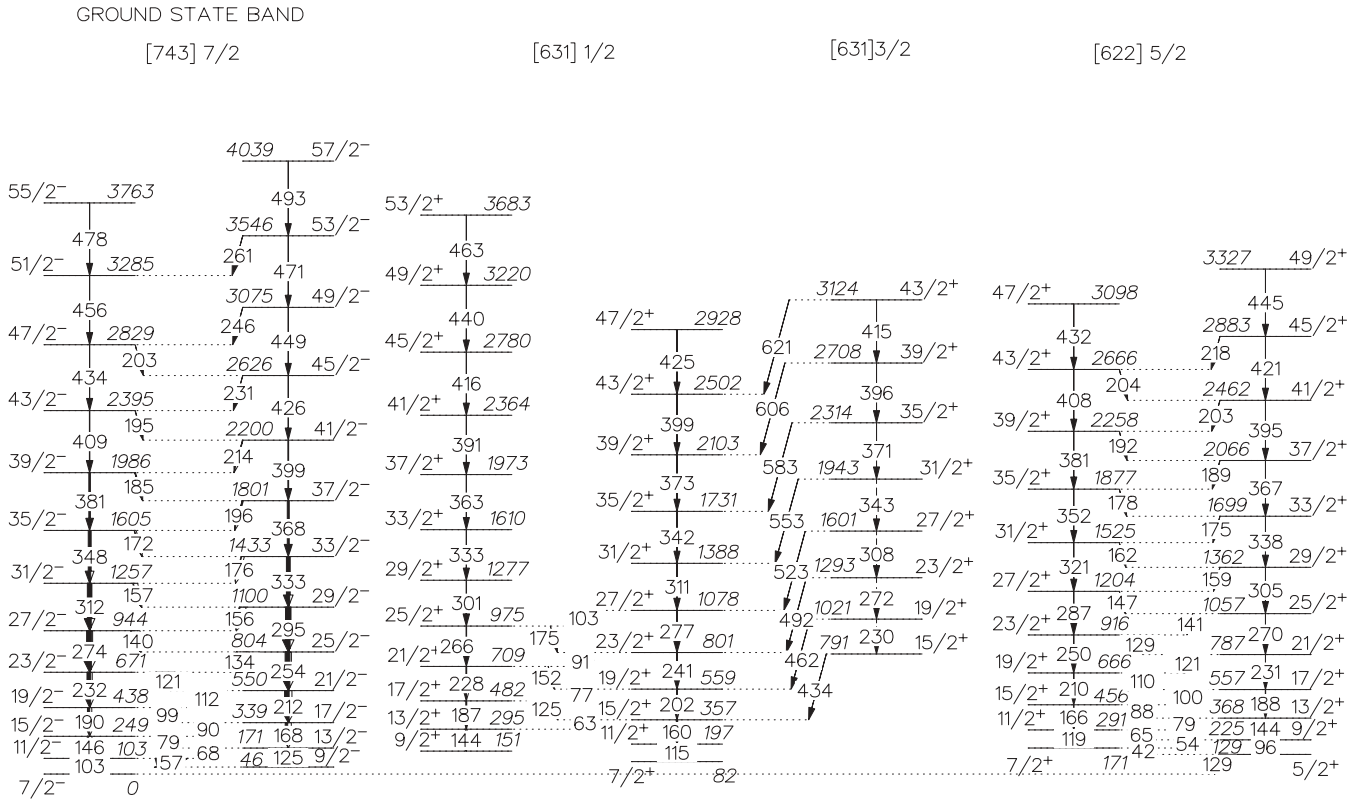
FIG. 2. The principal high-spin rotational bands seen in the ^{136}Xe experiments
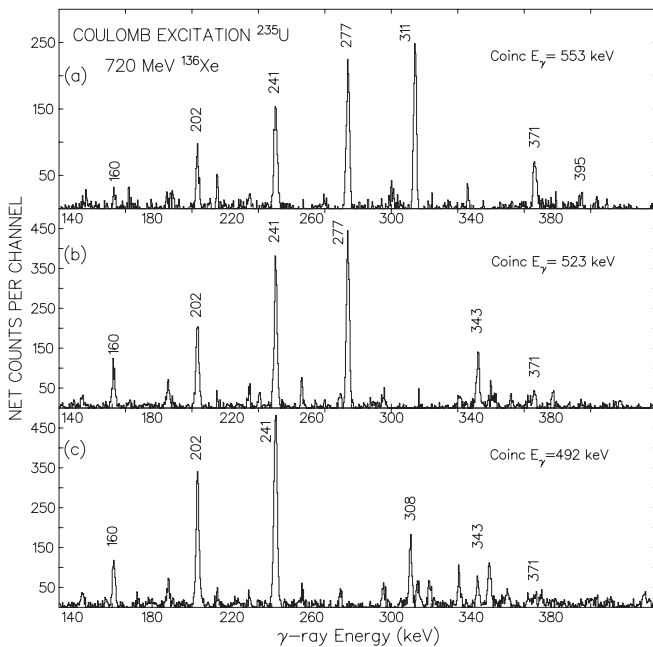

FIG. 3. Examples of the decay from the Nilsson [631]3/2 band to the Nilsson [631]1/2 band with Gammasphere in the ^{136}Xe experiments. The gates shown correspond to the $23/2^+ \rightarrow 23/2^+$, $27/2^+ \rightarrow 27/2^+$, and $31/2^+ \rightarrow 31/2^+$ transitions. The spectra illustrate where each of these gates feed into the [631]1/2 band, and also weak cascade transitions lying above the gates at $E_\gamma = 308, 343, 371,$ and 395 keV in the [631]3/2 band (cf. the detailed level scheme in Fig. 20).

Coulomb excitation of the positive-parity [631]1/2, [631]3/2, and [622]5/2 bands from the negative-parity [743]7/2 ground state are predominantly $E3$ excitations.

A complete documentation of the experimental results is given in the tables shown in Appendix C. Spins, excitation energies, and Nilsson assignments are given in Tables XIX–XXXII. Results from the CHICO experiment that were input to the Coulomb excitation calculations for the principal bands are shown in Tables XXXIII–XXXVI. Results for γ-ray energies and intensities from the ^{136}Xe experiments are shown in Tables XXXVII–XLVIII. The Gammasphere results, and to a lesser extent, the 8pi results for relative γ-ray intensities were strongly influenced by bias introduced through the trigger conditions. The intensities quoted in Tables XXXVII–XXXIX for the principal high-spin bands are taken mainly from the 8pi experiment, and there the γ-ray branching ratios $I_\gamma(J \rightarrow J - 2):I_\gamma(J \rightarrow J - 1)$ are reliable and an important input to the quantitative analysis of the ^{40}Ca experiments presented below. Tables XLIX–LX present γ-ray intensities from the ^{40}Ca experiment in coincidence with the CHICO detectors and also used in the Coulomb excitation calculations.

Rotational bands built on higher-lying intrinsic states were not observed in the 8pi experiments because of the statistical accuracy. Such bands were observed in the Gammasphere experiments with the ^{136}Xe beam. The spectrum shown in Fig. 4 gives an example of the data quality. Excitation energies were based on the particular state at which their γ decay populated the ground-state band as determined in γ-ray coincidence spectra. Levels were then associated into bands as signalled by cascade transitions between
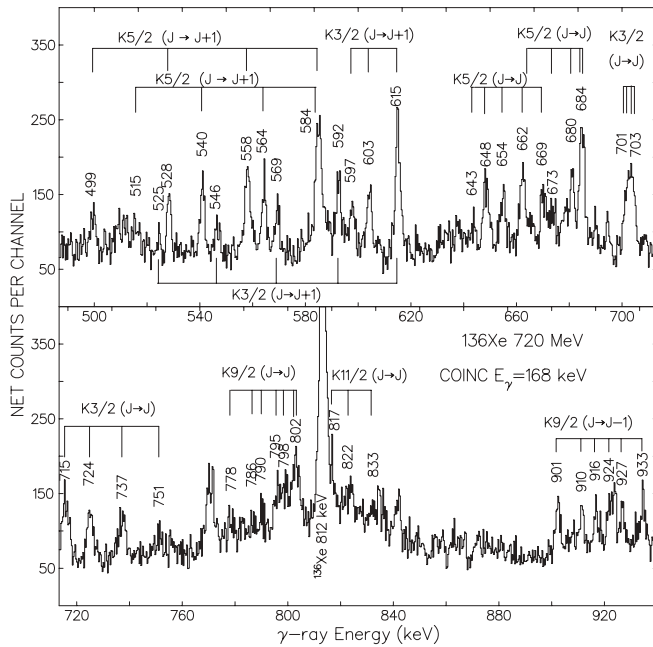
FIG. 4. Portion of the spectrum of γ rays in coincidence with $E_\gamma = 168$ keV, the $17/2^- \to 13/2^-$ transition in the ground-state rotational band. Data are taken in the Gammasphere experiment with ^{136}Xe at 720 MeV. With a few exceptions, the peaks may be identified with transitions from the [752]5/2 and [734]9/2 members of the $j_{15/2}$ multiplet together with the $K = 3/2$ and 11/2 γ-vibrational bands. For the $K = 3/2$ and 5/2 bands, the signatures are labeled separately in this figure (cf. the detailed level schemes in Figs. 20–22).

members. A good illustration of this technique is shown in Fig. 3.

C. Data analysis: CHICO detectors and the ^{40}Ca experiment

The E_γ CHICO data were reduced to a single histogram after correcting for random coincidences. Portions of the histogram are shown in Fig. 5 and in Fig. 6. The spectrum contains 19.5×10^6 counts. In addition, we built a CHICO-gated $E_\gamma \cdot E_\gamma$ coincidence matrix, with 1.2×10^6 coincidence pairs. Since we anticipated processing the singles γ-ray data with search procedures by energy-sum techniques (Ritz principle), the histogram was analyzed to extract the energies and intensity of as many peaks as possible. We found that there were more than 300 peaks in the energy interval 50–1400 keV. As an example, consider the intense line near 675 keV (cf. Fig. 6): we analyzed the region 664–687 keV, finding no fewer than eleven peaks. In fact the density of lines makes the analysis by energy sums on anything but the strongest lines unattractive; there are too many chance sums.

We have examined the signal content of energy sums in some detail. For example, we scanned the database of the approximately 300 transitions, histogramming the frequency of occurrence of γ-ray energy differences binned in 1-keV steps. If there were any signal content relevant to the ^{235}U level scheme, one would expect to see peaks in this histogram at energy differences of 46 keV, corresponding to the lowest $9/2^- - 7/2^-$ energy difference, and probably at 56.8 keV,
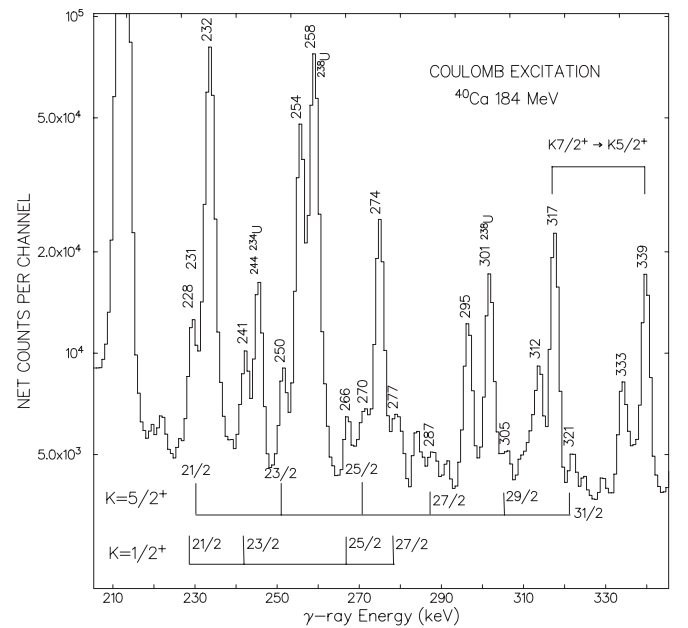

FIG. 5. Portion of the spectrum of γ rays in coincidence with the CHICO detectors with a ^{40}Ca beam at 184 MeV. The cascade transitions indicated in the rotational bands built on the Nilsson [631]1/2 (cf. Fig. 23) and [622]5/2 (cf. Fig. 24) levels are those used to measure the cross section and derive $E3$ matrix elements as discussed in the text. The peaks labeled at $E_\gamma = 317$ and 339 keV are decays of the Nilsson [624]7/2 band to the [622]5/2 band originating from spin $7/2^+$ and $9/2^+$ states (cf. Fig. 24). These γ rays are relatively intense in this figure because the other transitions depicted originate from much higher spins. Gamma rays labeled only by their energy are cascades of the ^{235}U ground-state band ranging from $E_\gamma = 232$ keV, $23/2^- \to 19/2^-$ to $E_\gamma = 333$ keV, $33/2^- \to 29/2^-$.

corresponding to the $11/2^- - 9/2^-$ energy difference. There were no such peaks in the histogram, and we conclude that, at least with the present energy resolution, say ± 0.5 keV, energy-sum techniques will be very unreliable. The idea that correlations should exist in the γ-ray energies may be applicable to direct Coulomb excitation with light ions, where the selection rules constrain the states excited to lie within 2 spin units of the ground state. No doubt the present experiment populates too many states that are outside that spin range, and it is interesting to speculate that, with a much lighter ion, say a ^{4}He beam, such energy-sum correlations might be observable.

In the singles-γ CHICO data at the point where the low intensities become problematic, there is enough statistics in the CHICO-gated $E_\gamma \cdot E_\gamma$ coincidence matrices to firmly identify the continuation of rotational bands to higher spin. An example is shown in Fig. 7.

III. RESULTS

A. Comparison with previously assigned band structures

1. Ground-state band [743]7/2

The level scheme is shown in Fig. 20. The energies of states to spin $13/2^-$ were taken from the compilation [4], which for
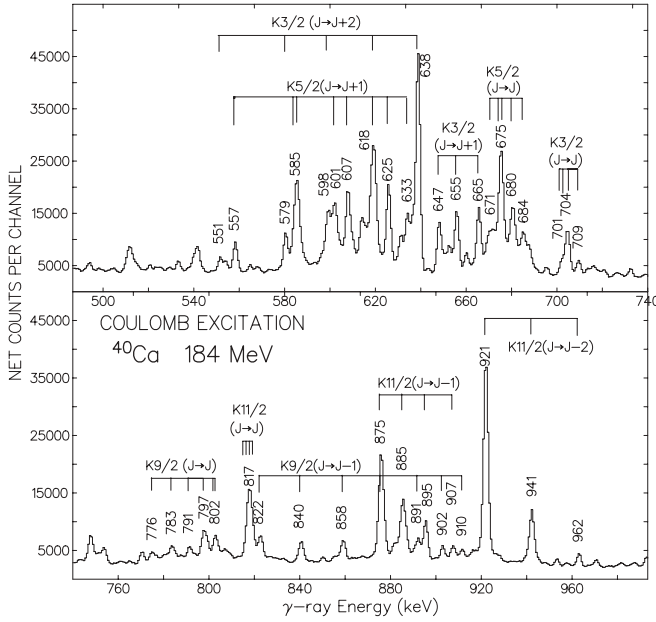
FIG. 6. Portion of the spectrum of γ rays in coincidence with the CHICO detectors with a ^{40}Ca beam at 184 MeV. The peaks are labeled by their energy (keV) and are grouped together in bands which belong to the negative-parity [752]5/2 and [734]9/2 (cf. Fig. 27) members of the $j_{15/2}$ multiplet together with the $K = 3/2$ and 11/2 γ-vibrational bands (cf. Fig. 26). The labeled peaks are decays to the ground-state band in all cases. Note that the [734]9/2 Nilsson band is crossed by the $K = 11/2$ γ-vibrational band at spin 17/2.

such low-energy transitions is more accurate than the present experiment. The transition energies given by Simon *et al.* [5] agree from spin $13/2^-$ to $57/2^-$ to within 1 keV in all cases, but there is a systematic difference in our respective calibrations which results in an accumulated difference of ≈ 4 keV in state energies at the top of the band. We prefer our values because the experiment of Simon involved a large Doppler correction, which could have led to a systematic error of this magnitude.

2. The [631]1/2 band

To spin $13/2^+$ the state energies were taken from the compilation [4]. For spin $15/2^+$ we agree with the previous assignment to better than 1 keV, but the states of spin $17/2^+$ through $23/2^+$ assigned by de Bettencourt *et al.* [6] are very different from ours and we believe their values to be in error. The discrepancies are so large that the previous authors must have assigned the wrong γ-ray peaks to this band. For spins above $23/2^+$ the present assignments are new. The level scheme is shown in Fig. 20.

3. The [622]5/2 band

The state energies to spin $11/2^+$ are taken from the compilation [4]. Our assignments differ from those of de Bettencourt *et al.* [6] by ≈ 2 keV at spin 15/2 and by ≈ 5 keV at spin 19/2 and we assume that the wrong transitions were assigned in their work. Above spin $23/2^+$, the present assignments are new. The level scheme is shown in Fig. 21.
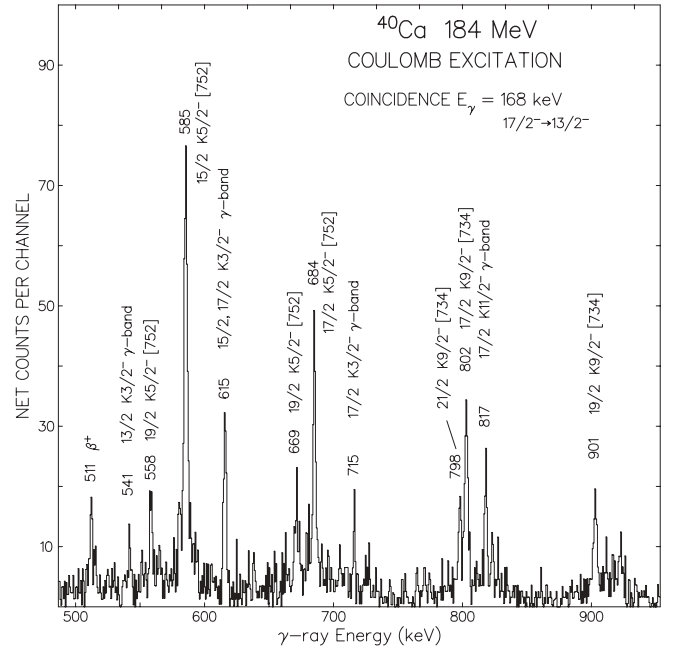
FIG. 7. Portion of the spectrum of γ rays in coincidence with $E_\gamma = 168$ keV, the $17/2^- \rightarrow 13/2^-$ transition in the ground-state rotational band, taken from the $E_\gamma \cdot E_\gamma$ coincidence matrix gated by the CHICO detector. The beam was ^{40}Ca at 184 MeV incident energy. In comparison with the corresponding spectrum taken in the ^{136}Xe experiment it can be seen that the highest spins seen in the ^{40}Ca experiment overlap the lowest spins identified in the ^{136}Xe experiment.

4. The [631]3/2 band

To spin $13/2^+$, we assume the assignments given in the compilation [4] and there is a good correspondence between previous transition energies and peaks seen in the CHICO-γ coincidence spectrum (cf. Fig. 23). Beginning at spin $15/2^+$, we see the coincidence between the odd-signature ($J \rightarrow J$) transitions to the [631]1/2 band and the corresponding ($J \rightarrow J - 2$) transition within the [631]1/2 band. The level scheme is shown in Fig. 20. The even-signature states $17/2^+$, $21/2^+$, and $25/2^+$ assigned by de Bettencourt *et al.* [6] were not seen in this experiment. The odd-signature transitions, spin $19/2^+$ and $23/2^+$, assigned in de Bettencourt *et al.* [6] differ by more than 10 keV from our own assignments, and we believe that these authors assigned the wrong transitions to these decays. States of spin $27/2^+$ and above are new assignments in the present work.

5. The [633]5/2 band

No new assignments were made in the present work. The states $5/2^+$, $7/2^+$, and $9/2^+$ were assumed to be populated based on the correspondence of previously assigned transitions [4] and those seen in the CHICO-γ spectrum (cf. Figs. 24 and 25).

6. The [624]7/2 band

The spin $7/2^+$ and $9/2^+$ levels in this band have characteristic decays to the [622]5/2 band known from previous work [4].

These transitions were seen very strongly in the CHICO-γ-γ spectrum and the sequence beginning at 316.5, 338.7, and 359.7 keV shown in Table LVIII can be extended to spin $15/2^+$ (cf. Fig. 24). The present energies for the $11/2^+$, $13/2^+$, and $15/2^+$ transitions differ from those of de Bettencourt *et al.* [6] to an extent that suggests that these authors assigned the wrong peaks to this band.

7. *Bands that decay into the [624]7/2 band: tentative new assignments for the [613]7/2 and [615]9/2 bands*

The characteristic decay pattern of the [624]7/2 band allowed us to identify several transitions in the CHICO-γ-γ matrix which feed into the [624]7/2 band at specific levels, thereby defining the excitation energies of the new states (cf. Fig. 25). Transitions with the appropriate energies to correspond with decays from these new states to the ground-state band can also be seen in the CHICO-γ spectrum as shown in Tables LVI, LVII, and LX. However, the decay to the ground-state band is not observed in γ-γ coincidence data because the corresponding in-band transitions have low energy and are highly converted. The new levels can be organized into bands as shown in Tables XXV, XXVI, and XXVIII. Based on the particle-rotor calculation described later, we suggest the Nilsson assignments [613]7/2 for the band beginning at $E_x = 986.7$ keV (Table XXV) and [615]9/2 for the band beginning at $E_x = 1192.9$ keV (Table XXVI). The band beginning at $E_x = 1052.9$ keV (Table XXVIII) is less well developed, and we have not suggested any assignment. Its level energies, 1052.9 and 1100.3 keV, correspond very closely with the 1053- and 1099-keV levels observed by Stephens *et al.* [1]. In this latter work it was thought to be a β-vibrational band because of the very strong $E0$ components in its $J \rightarrow J$ transitions to the ground-state band. If these bands are the same band, as seems rather certain, its parity must be the same as the ground-state band, i.e., negative.

The levels at 986.7 keV (7/2) and 1042.9 keV (9/2) in the suggested 7/2 band (cf. Table XXV) probably correspond to levels observed in (d, d') reactions by Thompson *et al.* [7] at 986 and 1041 keV. Braid *et al.* [8] have tentatively suggested from (p, t) and (t, p) reactions that the Nilsson states [613]7/2 and [615]9/2 lie higher with bandheads at 1236 and 1438 keV, respectively. We cannot confirm the existence of these bands in the present data without invoking energy-sum arguments. We reiterate that the levels we are proposing in this section are placed by clear γ-γ coincidence data that pins their decay to specific levels in the [624]7/2 band.

8. *The $K = 3/2^-$ γ-vibration band*

The states 3/2 through 9/2 are assigned on the basis of the compilation [4] and the correspondence of transitions seen in the CHICO-γ spectrum with these previous assignments (cf. Fig. 26). For spin 11/2 and above, the present assignments are based on γ-γ coincidence data as shown in Fig. 20. Beginning at spin 17/2, and above, we note serious discrepancies with the results of de Bettencourt *et al.* [6] (e.g., 10 keV at spin 17/2), which suggests that these authors have assigned the wrong transitions to this band. Above spin 23/2, the assignments in the present work are new.

9. *The [752]5/2 band*

The assignments to spin 15/2 (excluding spin 13/2) are based on the correspondence of the compilation [4] (mainly Ref. [1]) with transitions observed in the CHICO-γ spectrum (cf. Fig. 27). Above spin 15/2, and including spin 13/2, the present assignments are based on γ-γ coincidences (cf. Fig. 22). To spin 21/2 these are in agreement with the results of de Bettencourt *et al.* [6]. The 23/2 and 25/2 assignments differ from those of Ref. [6] by 3 and 6 keV, respectively. Above spin 25/2 the present assignments are new.

10. *The [734]9/2 band*

The assignments to spin 15/2 are based on the correspondence of the compilation [4], (mainly Ref. [1]) with transitions observed in the CHICO-γ spectrum (cf. Fig. 27). At spin 17/2 and above the present assignments are based on γ-γ coincidences (cf. Fig. 21). Our assignments differ from those of Ref. [6] by ≈ 10 keV at spin 17/2, increasing to ≈ 30 keV at spin 23/2, indicating that the wrong transitions were assigned in that work. Above spin 23/2, the present assignments are new.

11. *The $K = 11/2^-$ γ-vibration band*

The 11/2 and 13/2 assignments are based on the correspondence of the compilation [4], (mainly Ref. [1]) with transitions observed in the CHICO-γ spectrum (cf. Fig. 26). At spin 15/2 and above the present assignments are based on γ-γ coincidences (cf. Fig. 22). The energies to spin 17/2 agree well with previous assignments. The state at spin 19/2 is a new assignment in this work. The state at spin 23/2 differs by ≈ 30 keV from that of Ref. [6], indicating that the wrong transition was assigned in that work.

The [734]9/2 band and the $K = 11/2$ γ-vibrational band undergo an avoided crossing at spin 17/2. This is analyzed in Sec. VI B below. The quoted energies and intensities tabulated for spins above the crossing are given under the original band assignments made at spins below the crossing.

12. *The "missing" Nilsson state [761]3/2*

A state of great interest to the present study is the $K = 3/2$ member, [761]3/2, of the $j_{15/2}$ multiplet. The energy spacings of its rotational band would define the first step of the Coriolis mixing that carries the oscillations of the $K = 1/2$ band spacings through all members of the multiplet.

It has been claimed that its bandhead lies at (1) 806 keV [4], at (2) 1039 keV [6], and at (3) 1243 keV [9]. These assignments were tentative and have not been accepted in refereed compilations. In their calculations, Gareev *et al.* [10] considered the $K = 3/2$ state at 638 keV to be the bandhead of the [761]3/2 state. As discussed later, simple Nilsson models place the level at approximately 1300 keV.

The low-spin states (say J less than 11/2) of the [761]3/2 band will be populated very weakly in direct Coulomb excitation. This is because the $K = 3/2$ band is expected to have small admixtures into the $K = 7/2$ ground state: for example, in Stephens *et al.* [1] the $K = 3/2$ and $K = 5/2$ states of spin 7/2 have ground-state $K = 7/2$ admixtures $\epsilon = 0.008$ and 0.092, respectively. Therefore, in direct Coulomb excitation,

we expect that the cross section to the $K = 3/2$ band will be approximately 100 times smaller (i.e., ϵ^2) than that to the $K = 5/2$ band, making it difficult to observe experimentally.[1]

Multiple Coulomb excitation involving excitation across two bands, e.g., $K = 7/2 \to K = 5/2 \to K = 3/2$, will also have low probability at low spin because it involves two small connecting moments. In very strongly coupled multiple Coulomb excitation with heavy projectiles (as with the present ^{136}Xe beam), involvement of high-spin states, where the wave function admixtures should be much stronger, may make it possible to induce measurable population into the $K = 3/2$ band at high spin.

Our failure to observe a high-lying $K = 3/2$ band in the present experiments might be because it decays by many γ-ray pathways. We supposed that very fast $M1$ transitions expected between the $K = 3/2$ and $K = 5/2$ members of the same high-j multiplet in the Nilsson model would provide a characteristic signature of the $K = 3/2$ band, i.e., decaying to specific members of the $K = 5/2$ band in γ-γ coincidence. Unfortunately, where $M1$ transitions between members of the $j_{15/2}$ multiplet have been observed (cf. Sec. III E below), they are inhibited by one or two orders of magnitude compared with the calculations.

These factors taken together indicate that it is not surprising that we could not identify the [761]3/2 level in these experiments. In Sec. VI C below, we discuss the possibility that the $K = 3/2$ γ-vibrational band may have some structural overlap with the [761]3/2 band.

B. Magnetic properties of the principal bands

In examining the magnetic properties of a rotational band it is convenient to define ratios for the γ-ray intensity branching between signature partners by

$$\lambda = I_\gamma(J \to J - 2)/I_\gamma(J \to J - 1), \quad (1)$$

where it is understood that $I_\gamma(J \to J - 1)$ has both $M1$ and $E2$ components. The photon transition strengths are given in inverse seconds by

$$T(M1) = 1.7584 \times 10^{13} E_\gamma^3 B(M1), \quad (2)$$

$$T(E2) = 1.2253 \times 10^{13} E_\gamma^5 B(E2). \quad (3)$$

The reduced transition probability $B(M1)$ is in nuclear magnetons, $B(E2)$ is in $e^2\,{\rm b}^2$, and the γ-ray energy E_γ is in MeV. From these equations it follows that the ratio $B(M1; J \to J - 1)/[B(E2; J \to J - 2)$ is given by

$$\frac{B(M1)}{B(E2)} = \frac{0.6968}{\lambda(1 + \delta^2)} \frac{E_\gamma(J \to J - 2)^5}{E_\gamma(J \to J - 1)^3}, \quad (4)$$

where the units are $[\mu_N/(e\,{\rm b})]^2$, and δ is the mixing ratio in the $(J \to J - 1)$ transition expressed as the amplitudes $(E2/M1)$.

In the rotational model, the reduced $E2$ transition probabilities between members of the same rotational band are given

---

[1]In this argument, we assume that all transition moments between members of the multiplet result from admixtures in the wave functions and that the direct moments are essentially zero (cf. discussion in Secs. IV A and V A).
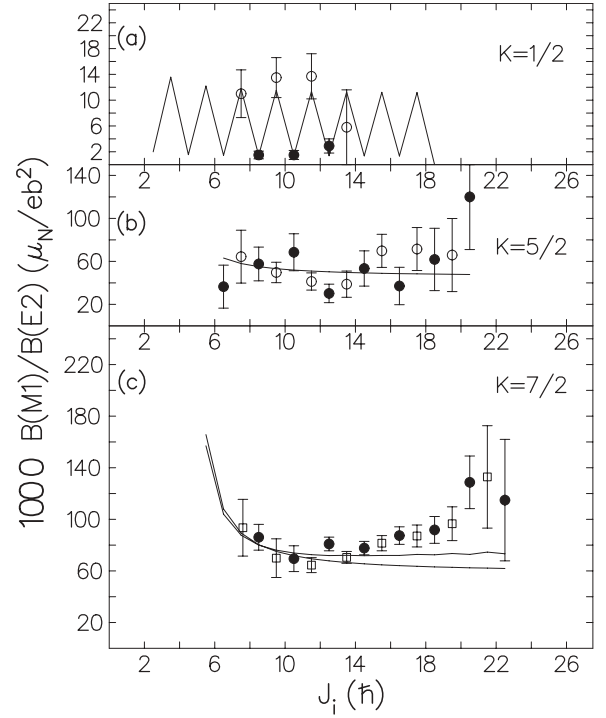
FIG. 8. Ratios of $B(M1)/B(E2)$ values derived from measured γ-ray branching ratios in these experiments. The experimental values have been corrected for the small effect of $E2/M1$ mixing in the $(J \to J - 1)$ transitions based on a simple model. In panels (a) and (b), solid lines correspond to the rigid-rotor model with parameters chosen to best reproduce the results. For $K = 5/2$ there is only one free parameter, namely, $(g_K - g_R)^2$, and values are discussed in the text. For the special case $K = 1/2$, there is an additional parameter usually called the magnetic-decoupling parameter, b, which governs the magnitude and phase of the oscillation in $B(M1)$ values. Two calculations are shown in panel (c). The lower fitted curve is a rigid-rotor calculation with the one free parameter $(g_K - g_R)^2$ fitted at low spin. The higher fitted curve is a particle-rotor calculation with attenuated Coriolis matrix elements (cf. text).

in terms of Clebsch-Gordan coefficients by

$$B(E2; J_i \to J_f) = (5/16\pi)e^2 Q_0^2 \langle J_i K 20 | J_f K \rangle^2, \quad (5)$$

where Q_0 is the intrinsic quadrupole moment, and K is the quantum number giving the angular momentum projection on the symmetry axis, which in the simplest model is a constant for any given band. In ^{235}U the quadrupole moment Q_0 has been measured for the lowest states of the ground-state rotational band with the result $Q_0 = 9.75e$ b [4]. With Eq. (5) we can therefore predict values for $B(E2; J \to J - 1)$ for

TABLE I. Measured magnetic properties. Comments: (a) data averaged over spin; (b) average magnetic moment of literature values from the Table of Nuclear Moments [23].

Band	Experiment $(g_K - g_R)$	Experiment $\mu(\mu_N)$	Comments
[743]7/2	$\pm 0.38(5)$	$-0.39(6)$	a,b
[622]5/2	$\pm 0.47(5)$		a

TABLE II. Derived magnetic properties from the results in Table I. The terms "old" and "new" refer to different parametrizations of the Nilsson model (cf. text).

Band	Derived g_K (experiment)	Assumed g_R or derived	Nilsson g_K new style [13]	Nilsson g_K old style [17,18]	Chasman g_K Woods-Saxon [12]
[743]7/2	−0.20(5)	0.18(5)	−0.21	−0.20	−0.19
[622]5/2	−0.22(5)	0.25(5)	−0.24	+0.10	−0.20

the ground-state band, and if we further assume that all the rotational bands in ^{235}U have the same intrinsic quadrupole moment then we can predict $B(E2; J \rightarrow J - 1)$ for all the bands. This allows us to derive the $E2/M1$ mixing ratio in the $J \rightarrow J - 1$ transitions, thereby extracting the $M1$ contribution needed in Eq. (4).

A summary of $B(M1)/B(E2)$ ratios derived from the branching ratios measured in these experiments is given in Fig. 8, where the ratios have been corrected for the mixing amplitude. This is model dependent, but in all the cases shown it is a small correction usually not exceeding 5%.

In the rotational model, the magnetic transitions between signature partners ($K \neq 1/2$) are given by

$$B(M1; J_i \rightarrow J_f) = (3K^2/4\pi)(g_K - g_R)^2 \langle J_i K 10 | J_f K \rangle^2. \quad (6)$$

For $K = 1/2$, there is an additional factor multiplying Eq. (6):

$$[1 + b(-1)^{I_i+1/2}]^2 \quad (7)$$

where b is the magnetic-decoupling parameter. The parameters g_K and g_R are gyromagnetic ratios for the intrinsic state and the collective rotation of the core, respectively.

Results from fitting the γ-ray branching data for the [743]7/2$^-$ and [622]5/2$^+$ bands to the rotor model given above are summarized in Table I. The [631]1/2$^+$ band needs a different treatment because of the magnetic-decoupling-term, b, as will be described in the following discussion.

For the ground-state band we can invoke the static magnetic moment measured for the ground state, $\mu = -0.39(6)$ [4], and since in the rotor model we have for $K \neq 1/2$

$$\mu = g_R J \mu_N + (g_K - g_R)K^2 \mu_N / (J + 1), \quad (8)$$

we can derive separate values for g_K and g_R as shown in Table II. The static magnetic moment for the [622]5/2$^+$ band is not known, but if we estimate $g_R = 0.25(5)$, then $g_K = -0.22(5)$ as shown in Table II.[2]

For $K = 1/2$, there is an additional multiplying factor operating on the second term in Eq. (8), namely,

$$[1 + (2J + 1)b(-1)^{I_i+1/2}], \quad (9)$$

which for the $I = 1/2$ ground state reduces to $(1 - 2b)$.

---

[2]Many authors in the literature assume that $g_R = Z/A$ (=0.39 for ^{235}U), but there is ample evidence that pair blocking reduces g_R in odd-neutron nuclei and increases it in odd-proton nuclei (cf. page 303 of Ref. [11]).

C. Discussion of the magnetic properties of the principal bands

The results for the $B(M1)/B(E2)$ ratios can be compared with a variety of theoretical predictions. In the review paper of Chasman *et al.* [12], matrix elements are presented for calculating the magnetic properties of heavy nuclei, $A \geqslant 228$, based on a momentum-dependent Woods-Saxon potential.

In general, the factor is given by

$$g_K = [g_s \langle s_3 \rangle + g_l \langle l_3 \rangle]/K, \quad (10)$$

where g_s is the intrinsic gyromagnetic ratio for the odd particle, a neutron in this case: we take as a typical renormalization given in the literature (e.g., [12]) $g_s = 0.6g_s^{\text{free}} = -2.296$ and $g_l = 0$ for neutrons. The average projection of the intrinsic spin on the symmetry axis is denoted $\langle s_3 \rangle$, and this term contains the dependence on nuclear structure.

Interpolating Chasman's results between $A = 232$ and $A = 238$ to the deformation appropriate to ^{235}U, we find the values shown in Table II.

We can compare with a simple Nilsson model, for which it is convenient to use the tables of Browne and Femenia [13]. A table of Nilsson $\langle s_3 \rangle$ and g_K values by Stuchbery [14] also provides a convenient and user-friendly reference. The parameters of the Nilsson model used in Refs. [13,14] are $\kappa = 0.05$ with $\mu = 0.434$ ($N = 7$) and $\mu = 0.448$ ($N = 6$), taken from the paper of Chi [15]. For convenience we refer to these parameters as the "new style." The predictions of both Woods-Saxon and the new-style calculations are in agreement with the measurements for the [743]7/2$^-$ and [622]5/2$^+$ bands, as seen in Table II.

The Nilsson model we have employed for our particle-rotor calculations with the code GAMPN [16] has parameters $\kappa = 0.062$ with $\mu = 0.26$ ($N = 7$) and $\mu = 0.34$ ($N = 6$); they are based on the work of Nilsson *et al.* [17] and are prescribed in Ragnarsson *et al.* [18]: this parameter set we call "old style." In our work, a hexadecapole deformation was also included with $\epsilon_4 = -0.035$. The calculation predicts $g_K = -0.20$ for the [743]7/2$^-$ band, also in agreement with the data and with the other calculations. For the [622]5/2$^+$ band g_K is predicted to be $+0.1$, in disagreement with the experiment, and with the other calculations (cf. Table II). The source of this discrepancy is that the [633]5/2 and [622]5/2 orbitals are crossing as a function of deformation. In the Woods-Saxon calculation of Chasman *et al.* [12], and with the new-style Nilsson parameters used by Browne and Femenia [13] and by Stuchbery [14], this happens near deformation $\beta = 0.1$, after which the [633]5/2 orbital lies lower. In our particle-rotor calculations, with the old-style parameters, this crossing does not occur until $\beta = 0.3$, and the calculated g_K for the lowest $K = 5/2^+$ band is dominated by the wave function for [622]5/2.

Understanding the properties of the $N = 6$ levels above the 126-neutron shell gap has been a long-standing problem [19]. The underlying problem is associated with the single-particle levels originating from the $g_{9/2}$ and $i_{11/2}$ spherical states. In Woods-Saxon and with the new-style parameter set of the Nilsson model, $g_{9/2}$ and $i_{11/2}$ are close in energy at zero deformation and interact strongly with increasing deformation and level crossings occur at small deformations. In contrast, with the old-style parameters used in our particle-rotor calculations, the $i_{11/2}$ system lies higher in energy and is much displaced from the $g_{9/2}$ system, resulting in smaller interactions, and level crossings occur only for large deformations. To rationalize the situation, attempts have been made to fit the κ and μ parameters such that the Nilsson calculation best reproduces the level energies produced in a Woods-Saxon calculation at zero deformation as mentioned in Ref. [19]; for example, a fit obtained in this way by Rozmej *et al.* [20] has been employed by Herrmann *et al.* [21]. However, we note that the Rozmej parameters, $\kappa = 0.0526$ with $\mu = 0.457$ ($N = 7$), are very similar to the new-style parameters mentioned above.

Results for the [631]1/2 band are interesting because they allow us to test some properties of the rotational model for which experimental data are rare. We compare the measured properties with three calculations, namely, (a) Stuchbery [14], (b) the Woods-Saxon calculation of Chasman *et al.* [12], and (c) the particle-rotor code of Ragnarsson and Semmes [16].

The energy-decoupling parameter $a = -0.295$ in ^{235}U is found from fitting the experimental energies of the [631]1/2 band to the formula

$$E(J) = \left(\frac{\hbar^2}{2\mathcal{J}}\right)[J(J+1) + a(-1)^{J+1/2}(J+1/2)], \quad (11)$$

where $\mathcal{J}$ is the nuclear moment of inertia.

The magnetic-decoupling factor is given by

$$b(g_K - g_R) = g_R a + g_s \langle s_+ \rangle. \quad (12)$$

Now since

$$\langle s_+ \rangle = -(-)^l(1/2 + \langle s_3 \rangle) \quad (13)$$

then in the case of the [631]1/2 orbital $\langle s_+ \rangle + \langle s_3 \rangle = -0.5$. For $K = 1/2$, it follows from Eq. (10) that $g_K = 2\,g_s \langle s_3 \rangle$.

We can proceed in one of two ways. If we take a common renormalization of g_s in Eqs. (10) and (12), then it follows that the energy-decoupling parameter, a, and the magnetic-decoupling parameter, b, are quite generally related by (page 303 of Ref. [11])

$$b(g_K - g_R) = -a(g_l - g_R) - \tfrac{1}{2}(-1)^l(g_s + g_K - 2g_l). \quad (14)$$

For the [631]1/2 band, l is even, and we are assuming that $g_l = 0$; therefore Eq. (14) simplifies to

$$b(g_K - g_R) = ag_R - \tfrac{1}{2}(g_s + g_K), \quad (15)$$

but it has been pointed out by Bochnacki and Ogaza [22] that the renormalization of g_s could be different between $\langle s_+ \rangle$, arising from the so-called transverse polarization, Eq. (12), and $\langle s_3 \rangle$, the longitudinal polarization, Eq. (10). In that case, Eq. (14) would not hold, and one must extract separate
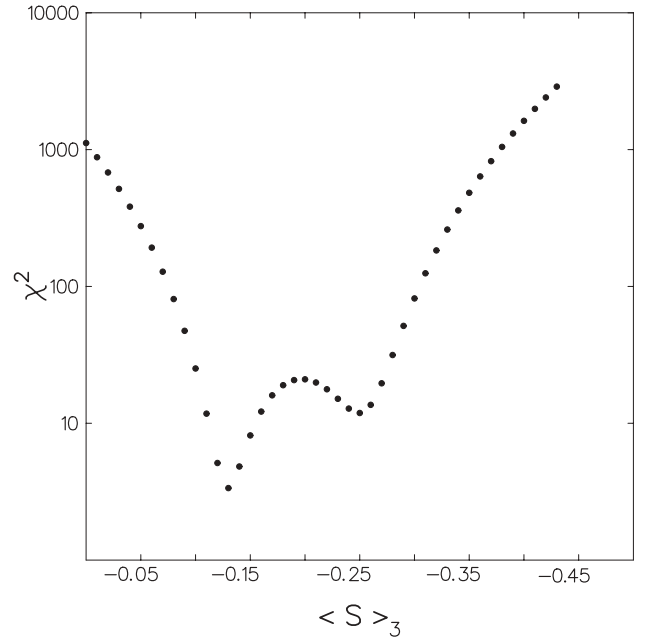
FIG. 9. Goodness of fit to the data shown for the $K = 1/2$ band in Fig. 8. For the seven data points and one free parameter, the un-normalized chi-squared, shown should minimize at the value 6. The lower minimum is therefore statistically favored.

renormalizations of g_s for the transverse and longitudinal components.

The magnetic-decoupling factor, b, can be estimated from the magnitude of the observed oscillation of the $B(M1)$ values, and we find from Eqs. (6) and (7) that $b \sim 2.5$ or $b \sim 0.40$. However, to test the relationship between a and b [Eq. (15)] we note that the magnetic parameters defining the $B(M1)$ values, namely, g_K and b, depend only on the value of $\langle s_3 \rangle$ if we take the values for g_s, g_R, and a as given, i.e., $g_s = -2.296$, $g_R = 0.25$, and $a = -0.294$ based on the experimental data. We have scanned the parameter $\langle s_3 \rangle$ over its full range (-0.5 to $+0.5$), computing the goodness of fit to the experimental $B(M1)$ values at each step as shown in Fig. 9. This procedure uses the theoretical relationship between a and b, and the results may be viewed as a test of this relationship. As would be expected from the quadratic nature of the b dependence of the $B(M1)$ values, there are two minima corresponding to $\langle s_3 \rangle = -0.135$, or $\langle s_3 \rangle = -0.25$, with associated b values of $b = 2.1$ or $b = 0.56$, respectively. The minimum at $\langle s_3 \rangle = -0.135$ is more significant statistically, and we have adopted this value.

These parameter values reproduce the observed $B(M1)$ values as seen in Fig. 8. It seems that there is a wave function that can consistently describe the observed oscillation in the level spacing (a) and that in the $B(M1)$ values (b). The result is compatible with a common renormalization of g_s in Eqs. (10) and (12), and therefore there is no reason to invoke the theory of Bochnacki and Ogaza [22].

The magnetic moment of the [631]1/2 bandhead has not been determined, but our experimental and our assumed values (Table III) in Eqs. (8) and (9) predict $\mu = -0.07\mu_N$. The [631]1/2 Nilsson level is also known in the nuclide ^{239}Pu,

TABLE III. Comparison of measured and predicted magnetic properties of the [631]1/2 Nilsson band.

	Decoupling parameter a	$\langle s_3 \rangle$	g_K	Magnetic decoupling b	Comments
Experiment	−0.294	−0.135(10)	+0.62(5)	+2.1(4)	$g_R = 0.25$, $g_S = -2.30$
Chasman *et al.*	−0.48	−0.10	+0.46	+3.8	$g_R = 0.25$, $g_S = -2.30$
Stuchbery	−0.92	−0.11	0.58	+2.8	$g_R = 0.30$, $g_S = -2.68$
GAMPN	−0.23	−0.02	+0.09	−3.4	$g_R = 0.39$, $g_S = -2.30$

where it is the ground state. The measured magnetic moment is $+0.203\mu_N$ [23], and the experimental energy-decoupling factor is $a = -0.58$. Since the deformations of ^{235}U and ^{239}Pu are very similar (the quadrupole deformations of ^{235}U and ^{239}Pu being quoted by Lobner *et al.* [25] as $\epsilon_2 = 0.24$ and 0.23, respectively), we would expect the properties of the [631]1/2 band to be similar in the two nuclides. The fact that they are not is another indication of the difficulties in predicting properties of $K = 1/2$ bands in this region.

D. Magnetic properties of the ground-state band in a particle-rotor model

With the particle-rotor code GAMPN by Ragnarsson and Semmes [16] we can calculate the effects of Coriolis mixing on the ground-band $B(M1)$ values. The details of this code are described later. For this particular calculation we considered only the interactions between the members of the $j_{15/2}$ multiplet, and we attenuated the Coriolis matrix elements by a factor of 0.5 throughout. This choice seems to be the closest we can get to reproducing all the data without opening up many free parameters as discussed later. The moment of inertia and aligned spin of the ground-state band were reproduced up to spin 35/2. Although the mixing amplitudes at spin 35/2 are large (e.g., 33% $K = 5/2$ and 29% $K = 9/2$ into the $K = 7/2$ level), the effect only increases the $B(M1)$ values by approximately 15%. In Fig. 8 it can be seen that this is in the right direction, but it is at least a factor of 2 too small to explain the data.

The parameters originally derived in Ref. [1] also fit the moment of inertia and signature staggering of the ground-state band at low spin, but they begin to deviate by spin 29/2, after which the predicted staggering diverges from experiment as discussed later. At spin 35/2, the mixing amplitudes in this calculation are 46% $K = 5/2$ and 28% $K = 9/2$, and the result for the $B(M1)$ values in the $K = 7/2$ band should be similar to the particle-rotor calculation.

E. $M1$ transitions between states of rotational bands built on members of the $j_{15/2}$ multiplet

The data set gives us a rare chance to study the $M1$ strengths between rotational bands built on Nilsson orbitals belonging to the same multiplet: indeed, scarcely any measurements of such $B(M1)$ values appear in the literature for any nucleus. As shown below, these are predicted to be very strong for intruder multiplets, but the experimental values are much smaller than predicted.

The reduced transition probability for $M1$ transitions between rotational states built on different Nilsson states differing by $K = \pm 1$, and for K_i, $K_f \neq 1/2$, are given by

$$B(M1; J_i \rightarrow J_f) = (3/4\pi)\mu_o{}^2 \langle J_i 1 K_i (K_f - K_i)|J_i 1 J_f K_f \rangle^2$$
$$\times G_{M1}(K_i \rightarrow K_f)^2 \quad (16)$$

and the $M1$ matrix element can be calculated from

$$G_{M1}(K_i \rightarrow K_f) = (g_s - g_R)\langle s_+ \rangle + (g_l - g_R)\langle l_+ \rangle. \quad (17)$$

For neutrons, we may estimate the matrix element assuming $g_R = 0.3$ and $g_l = 0.0$ and with $g_s = 0.6g_s^{\text{free}} = -2.296$; Eq. (17) then reduces to

$$G_{M1}(K_i \rightarrow K_f) \approx -2.6\langle s_+ \rangle - 0.3\langle l_+ \rangle. \quad (18)$$

The operators are related by

$$\langle l_+ \rangle = \langle j_+ \rangle - \langle s_+ \rangle. \quad (19)$$

When we examine $M1$ transitions (that satisfy the selection rules), between Nilsson bands belonging to the same multiplet, we find that, in general, these matrix elements will vary over a wide range. However, for high-j intruder multiplets, such as the $j_{15/2}$ considered here, the matrix elements are nearly constant and very large. This comes about because the intruders do not mix appreciably with resident orbitals of the shell ($N = 6$ in our case) and consequently "remember" their spherical shell-model heritage, namely, $j = 15/2$. Hence if we examine calculations of the matrix elements, for example, Browne and Femenia [13] or Chasman *et al.* [12], we find for the $j_{15/2}$ intruders over the whole range of the multiplet ($K = 1/2$ to $K = 15/2$) that typically $\langle l_+ \rangle$ is in the range 5.5 to 6.5, and $\langle s_+ \rangle$ is in the range 0.35 to 0.50. In Eq. (18) above, this implies G_{M1} values in the range -2.5 to -3.0 in Ref. [12] and -1.7 to -2.3 in Ref. [13]. These estimates immediately reveal the magnitude of the discrepancy—for example, the $J \rightarrow J + 1$ and $J \rightarrow J$ transitions from the [752]5/2 $\rightarrow$ [743]7/2 band at spins in the range 25/2 to 39/2 have measured $B(M1)$ values of approximately $0.02\mu_N{}^2$ and never exceed $0.05\mu_N{}^2$, as shown in Table IV, whereas the Chasman estimate above gives typically $0.8\mu_N{}^2$ to $1.0\mu_N{}^2$, and the Browne and Femenia estimate gives about a factor of 2 smaller. The discrepancy is then a factor of 20 to 50 between experiment and theory. The same is true for the [734]9/2 $\rightarrow$ [743]7/2 $B(M1)$ values shown in Table V and in Fig. 10.

Because this result is unexpected, and difficult to understand, we have conducted a literature search for nuclei where at least one γ-ray transition is known to connect rotational states based on intruders differing by $\Delta K = 1$ in the same multiplet. We considered all odd-neutron and odd-proton deformed nuclei from Sm to Es isotopes, examining neutron intruders

TABLE IV. Analysis of γ-ray branching ratios to extract $B(M1)$ values from the [752]5/2 Nilsson band to the [743]7/2 ground-state band (gsb) in the Xe experiments. Values were obtained from ratios involving the stretched-$E2$ in-band transitions.

Band (negative parity)	Initial spin	Final spin	$B(M1; J_i \rightarrow J_f)$ (μ_N^2)
[752]5/2	25/2	27/2	0.020(7)
$\rightarrow$	25/2	25/2	0.009(3)
gsb [743]7/2	25/2	23/2	0.000(1)
	27/2	29/2	0.028(7)
	27/2	27/2	0.012(4)
	29/2	31/2	0.024(8)
	29/2	29/2	0.017(6)
	29/2	27/2	0.0020(7)
	31/2	33/2	0.023(8)
	31/2	31/2	0.017(6)
	33/2	35/2	0.041(13)
	33/2	33/2	0.022(7)
	33/2	31/2	0.0047(16)
	35/2	37/2	0.041(12)
	35/2	35/2	0.024(8)
	37/2	39/2	0.066(22)
	37/2	37/2	0.017(6)
	37/2	35/2	0.0074(25)
	39/2	39/2	0.044(15)

TABLE V. Analysis of γ-ray branching ratios to extract $B(M1)$ values from the [734]9/2 Nilsson band to the [743]7/2 ground-state band in the Xe experiments (high spins) and in the Ca experiments (low spin). High-spin values were obtained from ratios involving the stretched-$E2$ in-band transitions. Low-spin values were obtained from ratios involving stretched-$E2$ transitions ($J \rightarrow J - 2$) between bands. Note that the [734]9/2 Nilsson band is crossed by the $K = 11/2$ γ-vibrational band at spin 17/2.

Band (negative parity)	Initial spin	Final spin	$B(M1; J_i \rightarrow J_f)$ (μ_N^2)
[734]9/2	13/2	15/2	0.005(3)
$\rightarrow$	13/2	13/2	0.003(2)
gsb [743]7/2	13/2	11/2	0.013(6)
	15/2	17/2	0.0025(30)
	15/2	15/2	0.018(8)
	17/2	17/2	0.005(3)
	17/2	15/2	0.009(3)
	19/2	17/2	0.004(2)
	21/2	21/2	0.0055(15)
	21/2	19/2	0.007(2)
	23/2	23/2	0.0086(18)
	23/2	21/2	0.0059(12)
	25/2	25/2	0.011(2)
	25/2	23/2	0.011(2)
	27/2	27/2	0.010(2)
	27/2	25/2	0.0060(12)
	29/2	29/2	0.009(2)
	29/2	27/2	0.011(2)
	31/2	31/2	0.010(2)
	31/2	29/2	0.011(2)
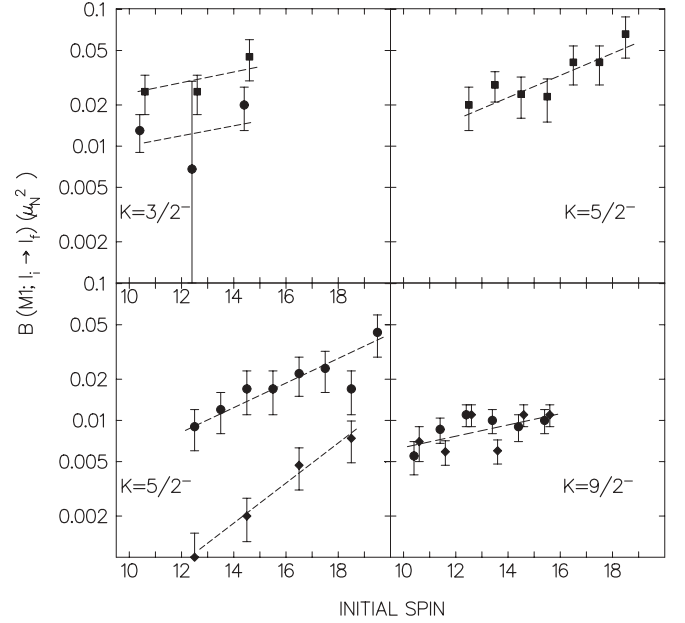
FIG. 10. Derived $B(M1)$ values from analysis of γ-ray branching data in the Xe experiments. In all cases, the final state refers to the ground band. Transitions going ($J \rightarrow J$) are shown as circles: transitions going ($J \rightarrow J + 1$) are shown as squares; and transitions going ($J \rightarrow J - 1$) are shown as diamonds. The lines are to guide the eye. Note that the [734]9/2 Nilsson band is crossed by the $K = 11/2$ γ-vibrational band at spin 17/2.

$j_{15/2}$ and $i_{13/2}$ and proton intruders $i_{13/2}$ and $h_{11/2}$. Including ^{235}U, there are nine nuclides in the odd-neutron list. For ^{183}Pt and ^{187}Os the γ-ray branch relative to the predictable in-band transition has been measured: in the other nuclides, the strength of the calibrating $E2$ transition had to be estimated from the particle-rotor code with the Coriolis mixing derived from a crude fit to the moments of inertia and rotational energy staggering (similar to the procedure described later). Relative to the particle-rotor code prediction, the attenuation of the $B(M1)$ values varied from factors of 3 to several hundred. For the seven nuclides in the odd-proton list, similar attenuations were found. Results for the $B(M1)$ values from the γ-vibrational bands to the ground-state band are shown in Table VI and in Fig. 10. These values are very small, even consistent with zero, but this is expected for γ-vibrational transitions.

IV. COMPARISON OF MEASURED YIELDS WITH COULOMB EXCITATION CALCULATIONS

A. Input parameters

In these experiments absolute cross sections were not measured; nevertheless, matrix elements can be extracted by normalizing to the relative yields of the ground-state bands for which reliable Q_0 values are known in the literature, namely, $Q_0 = 11.1 \pm 0.5e$ b for ^{238}U and $Q_0 = 9.75 \pm 0.50e$ b for ^{235}U. In strongly deformed nuclei, the yield at the bottom of the ground band is insensitive to the Q_0 value because of feeding from higher ground band members. The $E2$ and $E3$ matrix elements needed to calculate the cross sections are as

TABLE VI. Analysis of γ-ray branching ratios to extract $B(M1)$ values from the $K = 3/2$ and $K = 11/2$ γ-vibrational (vib) bands to the [743]7/2 ground-state band in the Xe (higher spins) and Ca (lower spins) experiments. High-spin values were obtained from ratios involving the stretched-$E2$ in-band transitions. Low-spin values were obtained from ratios involving stretched-$E2$ transitions ($J \rightarrow J+2$) for the $K = 3/2$ band and ($J \rightarrow J-2$) for the $K = 11/2$ band. The negative sign in parentheses is retained to indicate where the calculated $E2$ component of the tabulated transition exceeds the total observed value derived from the branching ratio. In such cases, the $B(M1)$ value is consistent with zero.

Band (negative parity)	Initial spin	Final spin	$B(M1; J_i \rightarrow J_f)$ ($\mu_N{}^2$)
$K = 3/2$ γ vib	5/2	7/2	$(-)0.0003(12)$
$\rightarrow$	7/2	9/2	0.0005(17)
gsb [743]7/2	9/2	11/2	$(-)0.0009(12)$
	11/2	13/2	$(-)0.0016(7)$
	13/2	15/2	0.0038(52)
	21/2	23/2	0.025(8)
	21/2	21/2	0.013(4)
	25/2	27/2	0.025(8)
	25/2	25/2	0.0068(23)
	29/2	31/2	0.045(15)
	29/2	29/2	0.020(7)
$K = 11/2$ γ vib	11/2	13/2	0.000(2)
$\rightarrow$	11/2	11/2	0.000(4)
gsb [743]7/2	11/2	9/2	0.000(4)
	13/2	15/2	$(-)0.0015(7)$
	13/2	13/2	0.000(5)
	13/2	11/2	0.003(8)
	15/2	17/2	$(-)0.002(2)$
	15/2	15/2	0.009(10)
	15/2	13/2	0.010(10)

follows. Within a band the reduced $E2$ transition probabilities are given by Eq. (5); that is, we assume that all rotational bands have the same intrinsic quadrupole moments, Q_0.

The Winther–de Boer code uses the symmetric form of the matrix elements given as

$$M(E\lambda; J_i \rightarrow J_f)^2 = M(E\lambda; J_f \rightarrow J_i)^2$$
$$= (2J_i + 1)B(E\lambda; J_i \rightarrow J_f). \quad (20)$$

The sign of $M(E\lambda)$ is the same sign as the Clebsch-Gordan coefficient in Eq. (5).

Reduced transition probabilities between the ground-state band and the excited bands in lowest order are given by

$$B(E\lambda; J_i \rightarrow J_f) = \frac{2\lambda + 1}{16\pi} e^2 Q_t{}^2(\lambda) \langle J_i K_i \lambda 0 | J_f K_f \rangle^2,$$
$$(21)$$

where $Q_t(\lambda = 2)$ and $Q_t(\lambda = 3)$ transition moments play an analogous role to the intrinsic moments $Q_0(\lambda = 2)$ and $Q_0(\lambda = 3)$.

The $E1$ excitation between the ground-state band and the positive-parity bands has been neglected because most $E1$

transitions will be strongly K-forbidden, in addition to the usual inhibition of $E1$ strength at low excitation energy,[3] and neglect all matrix elements between states of two different bands except where one band is the ground-state band.

Some model dependence of the matrix elements is inevitable since the number of unknown matrix elements entering into the Coulomb excitation process is very large and vastly exceeds the number of data. The number of levels and electromagnetic matrix elements required to perform semiclassical Coulomb excitation calculations simultaneously for several collective bands in ^{235}U far exceeds the capability of the Winther–de Boer code [2]. Thus only the ground band plus one side band were included simultaneously in individual calculations of the excitation process using this code.[4] Typically, the side bands are populated at the 10% level and thus a perturbation approach to the analysis of the side-band excitation is not expected to lead to large errors. However, the electromagnetic de-excitation process requires inclusion of feeding to multiple sidebands.

Coriolis mixing of the type $\Delta K = 1$ between the ground-state band, [743]7/2, and the [752]5/2 and [734]9/2 bands will occur; however, as shown by Bohr and Mottelson [11] (page 156), the intrinsic $E2$ matrix elements between rotational states belonging to different K states of a Nilsson multiplet are approximately renormalized by the mixing, and the form of Eq. (21) remains valid. In fact, if we assume that the intrinsic $E2$ transition moment is negligible, as is likely the case, then the transition takes place only by virtue of the admixed amplitudes. For this reason, $B(E2)$ values connecting states of the $K = 5/2$ and $9/2$ bands to the $K = 7/2$ ground state are a direct measure of the admixed amplitudes, as we discuss below.

For the γ-vibrational bands, $\Delta K = 2$ Coriolis mixing can be treated in lowest order by

$$M(E2; J_i K_i \rightarrow J_f K_f)$$
$$= (2J_i + 1)^{1/2} \langle J_i K_i 22 | J_f K_f \rangle$$
$$\times \{M_1 + M_2[J_f(J_f + 1) - J_i(J_i + 1)]\}, \quad (22)$$

where $K_f = K_i + 2$. (cf. Bohr and Mottelson [11], pages 149–151). The analysis of the γ-ray branching ratios between the vibrational bands and the ground-state band yields experimental values for the parameter ratio M_2/M_1, which we can then apply in Eq. (22) to derive realistic $E2$ matrix elements for the Coulomb excitation calculations. We will discuss the Coriolis mixing of the ground state and γ-vibrational bands more fully in Sec. VI.

To compare with experiment we need to run the Coulomb excitation code over the active scattering angles and

---

[3]Very few $E1$ transitions were observed in this work; however, with the present value for $g_K - g_R$ in the [622]5/2 band we can interpret γ-ray branching to the ground state quoted in the Nuclear Data Sheets [4] as giving $B(E1; K5/2, J7/2 \rightarrow K7/2, J7/2) \sim 3.3 \times 10^{-6}$ W.u. and $B(E1; K5/2, J7/2 \rightarrow K7/2, J9/2) \sim 5 \times 10^{-6}$ W.u.

[4]A difficulty with ^{235}U is the 7/2 spin of its ground state, which greatly increases the number of substates per level that must be included in the calculations compared to, say, a spin-zero ground state.

bombarding energies of events seen by the CHICO detectors. The biggest uncertainty in this is knowing the threshold and the response of the CHICO detectors to ^{40}Ca ions near threshold. This could be improved in future experiments but for this experiment we are content to include an uncertainty to cover the possible effects. After simple kinetic scattering and energy-loss calculations and assuming a sharp threshold of 5 MeV for the detectors, we find that integrating over center-of-mass angles 120–180 degrees and incident energies down to 100 MeV (from 184 MeV) in the thick target will give a good representation. These integrations were performed with a simple Simpson algorithm. With the spherical symmetry of both Gammasphere and the 8pi Spectrometer, it was not necessary to take into account γ-ray directional correlation effects.

Given that the ground-state of ^{235}U is $7/2^-$, the observation of many positive-parity bands in these experiments is strong evidence of octupole collectivity. We have included $E3$ excitations in the Coulomb excitation code. For some bands in ^{235}U the $E3$ matrix elements to the ground-state band that are needed to reproduce the observed yields are comparable to the well-known collective octupole excitations in ^{238}U, namely, 10–20 W.u. However, in ^{235}U there is no evidence for a dominant collective $K = 0^-$ octupole band as is the case in ^{238}U.

B. Extracting the experimental yields

From the Coulomb excitation code we obtain the total cross section for the independent, or direct, Coulomb excitation of each state in the problem. To compare with experiment one may proceed either by extracting experimental yields using
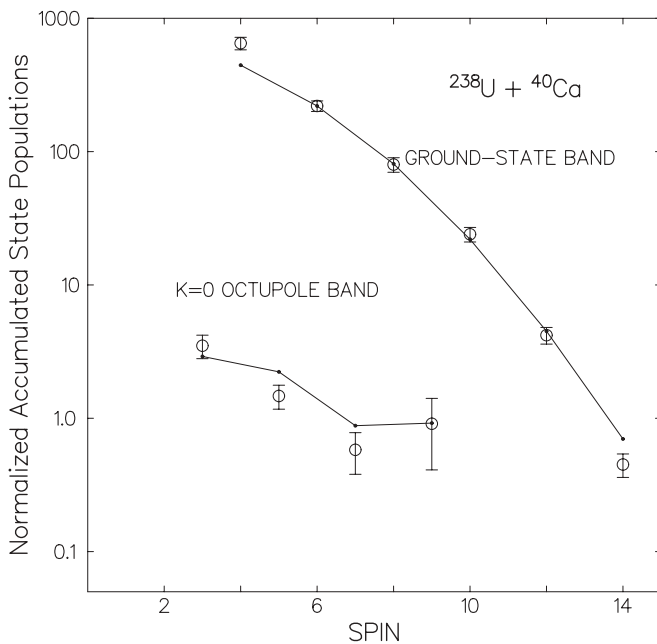

FIG. 12. Measured and calculated Coulomb excitation yields for the negative-parity bands observed in ^{235}U in the CHICO experiments. The $E2$ matrix elements in the ground-state band (GSB) and in the excited bands were taken from Eq. (5) with $Q_o = 9.75e$ b. The $E2$ matrix elements linking the ground-state band with the excited bands were taken from Eq. (21) for the $K = 5/2$ and $K = 9/2$ bands and from Eq. (22) for the $K = 3/2$ and $11/2$ γ-vibrational bands. The parameter M_2/M_1 in Eq. (22) was fixed from analysis of the present and previously measured $E2$ γ-ray branching ratios between the vibrational bands and the ground-state band. The parameter M_1 or Q_t was varied for each band to give a best fit to the relative yield. The measured yields in the ground-state band are the directly observed $E2$ γ-ray intensities normalized to the $19/2^- \rightarrow 15/2^-$ transition, $E_\gamma = 189.6$ keV, with $I_\gamma = 100$; the calculated yields were derived from the Winther–de Boer code folding in the decay properties of the band as explained in the text and are also normalized to the $19/2^- \rightarrow 15/2^-$ transition. The excited bands were treated differently: in these cases the total yield of the state obtained by summing the intensities of all γ-ray transitions depopulating the state is shown and compared with the same calculated quantity. Note that the [734]9/2 Nilsson band is crossed by the $K = 11/2$ γ-vibrational band at spin 17/2.

FIG. 11. Accumulated yields normalized to the 8^+ state in ^{238}U present as a contaminant in the ^{235}U target. The $E2$ matrix elements were taken from Eq. (5) with $Q_o = 11.1e$ b. The $E3$ matrix elements connecting the ground-state rotational band to the $K = 0$ octupole band were taken from Eq. (21) with $Q_t(\lambda = 3) = 2.3e$ 10^{-36} cm^3 chosen to fit the intensity of the octupole band.

knowledge of the decay scheme to subtract out the feeding from higher states or by building knowledge of the decay scheme into the calculation of independent yields to extract observed yields. Given the complexity of the ^{235}U level scheme we chose to take the second route for the principal bands seen to high spin. In these cases that procedure is inherently more stable. For the less strongly populated bands where the cascade feeding was very weak, it is simpler to make the small corrections needed to the observed yields in order to make the comparison at the level of the independent yields.

In calculating yields for the principal bands we are confronted with how to deal with the transitions between signature partners. We have chosen to use the fitted values for the γ-ray branching ratios discussed in Sec. III. There are a variety of reasons to do this. First, it produced a smooth result
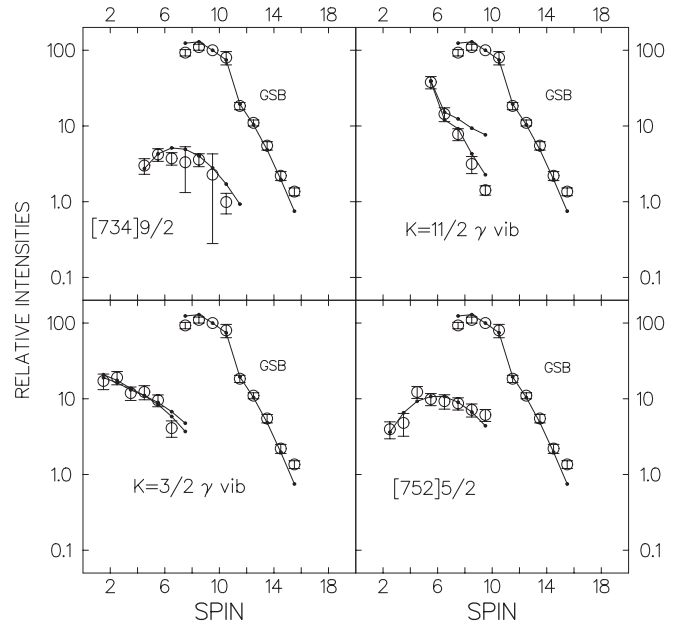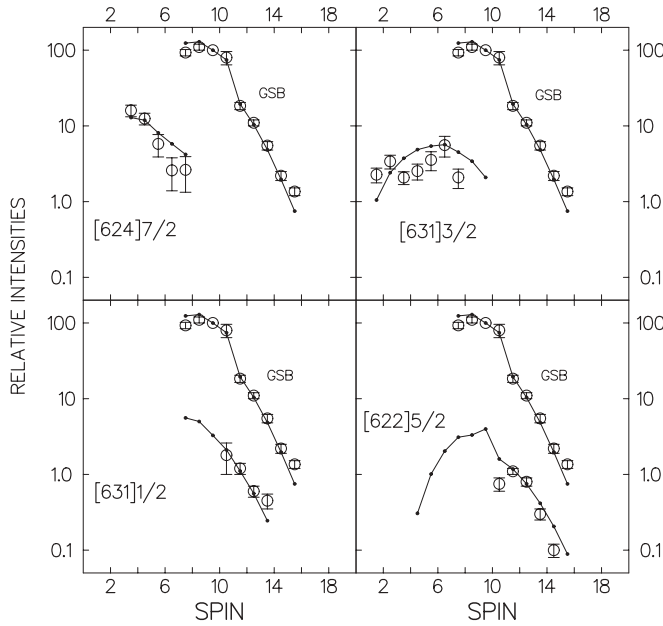
FIG. 13. Measured and calculated Coulomb excitation yields for some positive-parity bands observed in ^{235}U in the CHICO experiments. The $E2$ matrix elements in the ground-state band (GSB) and in the positive-parity bands were taken from Eq. (5) with $Q_0 = 9.75e$ b. The $E3$ matrix elements linking the ground-state band with the excited bands were taken from Eq. (21). The parameter Q_t was varied for each band to give a best fit to the relative yield. The measured yields in the ground-state band and in the [631]1/2 and [622]5/2 bands are the directly observed $E2$ γ-ray intensities normalized to the $19/2^- \to 15/2^-$ transition, $E_\gamma = 189.6$ keV, with $I_\gamma = 100$; the calculated yields were derived from the Winther–de Boer code folding in the decay properties of the bands as explained in the text and are also normalized to the $19/2^- \to 15/2^-$ transition. The [624]7/2 and [631]3/2 bands were treated differently: in these cases the total yield of the state obtained by summing the intensities of all γ-ray transitions depopulating the state is shown and compared with the same calculated quantity.

and allowed extrapolation to high spins where the experimental errors would become large. Second, the conversion coefficients of the mixed $E2/M1$ transitions between the signature partners can only be obtained from the calculated mixing ratios and this is an important delineation of the yields at low spin. The contributions to the yields from decays out of a band were corrected for conversion, either from the literature [4] or by assuming pure $M1$ for the potentially mixed cases.

In the procedure described above, there is only one free parameter, namely, Q_t (or M_1 in the case of the vibrational bands) to fit the yields of all the states in a given band. The main isotopic impurity in the target was ^{238}U. Since its ground state and low-lying octupole bands have been well studied [24], we could use it as a test of the techniques. As shown in Fig. 11, this works reasonably well and lends confidence to the analysis of ^{235}U.

Results for ^{235}U are shown in Figs. 12–14. Numerical values for the quadrupole moment are given in Sec. V below and octupole moments are given in Sec. IX.
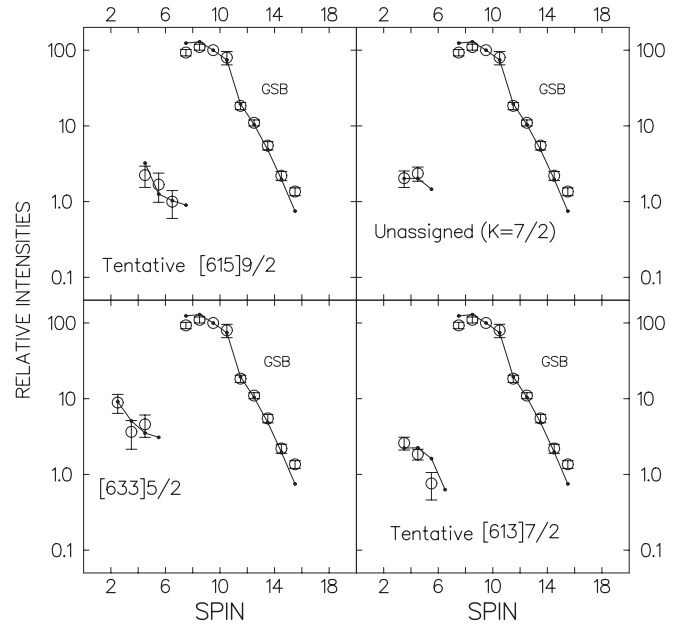
FIG. 14. Measured and calculated Coulomb excitation yields for some positive-parity bands observed in ^{235}U. The $E2$ matrix elements in the ground-state band (GSB) and in the positive-parity bands were taken from Eq. (5) with $Q_o = 9.75e$ b. The $E3$ -matrix elements linking the ground-state band with the excited bands were taken from Eq. (21). The parameter Q_t was varied for each band to give a best fit to the relative yield. The measured yields in the ground-state band are the directly observed $E2$ γ-ray intensities normalized to the $19/2^- \to 15/2^-$ transition, $E_\gamma = 189.6$ keV, with $I_\gamma = 100$; the calculated yields were derived from the Winther–de Boer code folding in the decay properties of the band, as explained in the text. For the positive-parity bands the total yield of the state obtained by summing the intensities of all γ-ray transitions depopulating the state is shown and compared with the same calculated quantity.

V. CORIOLIS EFFECTS IN THE $j_{15/2}$ MULTIPLET

A. Setting up the interaction matrix

There are two independent methods to extract the Coriolis mixing amplitudes. Following Stephens *et al.* [1], we can examine the energy spacings of the bands belonging to the $j_{15/2}$ multiplet and interpret the result, particularly the magnitude of the oscillations, in terms of the strength of the Coriolis interactions. This multiband mixing problem can be solved exactly by diagonalizing a matrix of which the elements include the interaction energies between the $\Delta K = 1$ bands. We can also examine the Q_t values from the [743]7/2 ground-state band to the [752]5/2 and [734]9/2 bands and extract the 5/2-7/2 and 9/2-7/2 mixing amplitudes directly. An important difference with the work of Stephens *et al.* [1] is that we have a much more coupled situation in the Coulomb excitation process due to the heavier projectile, and it is only meaningful to discuss Q_t values for the entire band, rather than individual $B(E2)$ values to specific levels measured in Ref. [1].

Within a Nilsson multiplet, and in the present case we are interested in the neutron $j_{15/2}$ multiplet, the rotational levels interact via a Coriolis force. The interaction energy, H_{cor},

TABLE VII. Values of the matrix elements $\langle K \pm 1 \mid j_\pm \mid K \rangle$, in keV, for the $j_{15/2}$ multiplet in ^{235}U calculated in three different models.

K	Stephens *et al.*	Chasman *et al.*	Particle-rotor
1/2			
	7.25	6.93	7.22
3/2			
	7.23	6.90	7.27
5/2			
	7.06	7.16	7.13
7/2			
	6.70	6.80	6.77
9/2			
	6.12	6.19	6.17
11/2			
	5.24	5.29	5.27
13/2			
	3.86		3.87
15/2			

mixes levels of the same spin belonging to rotational bands differing by unit K value, and, in the simplest approximation,

$$H_{\rm cor}(J) = A[(J \mp K)(J \pm K + 1)]^{1/2}\langle j_+ \rangle, \qquad (23)$$

where $\langle j_+ \rangle$ acts between states K and $K + 1$, and $A = (\hbar^2/2\mathcal{J})$ is the rotational constant. We can define a reduced (i.e., spin-independent) interaction energy, h_0, in analogy with the reduced mixing amplitude, ϵ_0, with

$$H_{\rm cor}(J) = [(J \mp K)(J \pm K + 1)]^{1/2}h_0, \qquad (24)$$

whence $h_0 = A\langle j_+ \rangle$. In lowest order, the reduced mixing parameters are related by

$$\epsilon_0 = h_0/(E_{K2} - E_{K1}), \qquad (25)$$

where $(E_{K2} - E_{K1})$ is the (unperturbed) energy separation of the mixed bands at some common representative spin.

The term $\langle j_+ \rangle$ can be calculated in models of the intrinsic wave functions, and we show the results of three different calculations in Table VII. The values from Stephens *et al.* [1] are for a simple Nilsson model. Values from Chasman *et al.* [12] are for a Woods-Saxon calculation. The present particle-rotor values are from the code GAMPN and included higher moments in the shape of the nuclear potential. The

TABLE VIII. Bandhead positions (keV), for the $j_{15/2}$ multiplet in ^{235}U. The present particle-rotor calculation sets $\epsilon = 0.21$, $\epsilon_4 = -0.35$, and the pairing gap = 1.04 MeV. The energy of the core 2^+ state was 38.0 keV.

K	Stephens *et al.* (keV)	Particle-rotor (keV)	Experiment (keV)
1/2	1810	2099	–
3/2	1370	1495	–
5/2	630	633	633
7/2	0	0	0
9/2	820	824	822
11/2	2220	1889	–
13/2	3770	2853	–
15/2	5510	3619	–
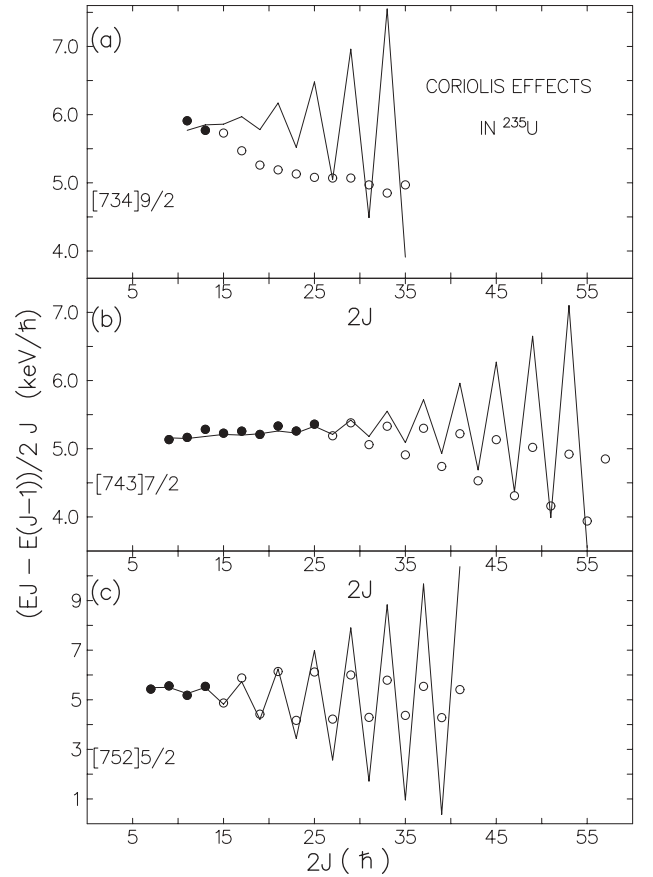
FIG. 15. The rotational constant calculated for members of the $j_{15/2}$ multiplet with the parameters of Ref. [1]. The filled points were known and fitted in Ref. [1]; open points are from the present data. Note that the [734]9/2 Nilsson band is crossed by the $K = 11/2$ γ-vibrational band at spin 17/2.

consistency of these approaches is a good indicator of the robust nature of the properties of high-j intruder orbitals. In fact all these models give results close to the values calculated for the pure-j shell, namely,

$$\langle j_+ \rangle = [(j \mp K)(j \pm K + 1)]^{1/2}, \qquad (26)$$

with $j = 15/2$ in our case.

For each specified value of spin, J, the calculation proceeds with exact diagonalization of a matrix of which the diagonal elements are the unperturbed energies of the (up to eight) rotational levels of spin J in the $j_{15/2}$ multiplet, and of which

TABLE IX. Results for the attenuation of the Coriolis matrix elements derived from a fit to the energies of the $j_{15/2}$ multiplet and from the measured $B(E2)$ values to the ground state.

Spins	$\langle K \pm 1 \mid j_\pm \mid K \rangle$ predicted	Attenuation factor from energies	Attenuation factor from $B(E2)$
1/2–3/2	7.25	(1)	–
3/2–5/2	7.23	0.78	–
5/2–7/2	7.06	0.52	0.40
7/2–9/2	6.70	0.43	0.37
9/2–11/2	6.12	(1)	–

TABLE X. Analysis of Coulomb excitation yields for negative-parity bands in ^{235}U with a ^{40}Ca beam in the CHICO experiment. All the $E2$ matrix elements connecting the ground state to the excited bands may be obtained by substituting the extracted Q_t in Eq. (21), or in the cases of $K = 2$ mixing, in Eq. (22). Mixing parameters and energy denominators refer to the ground-state band [743]7/2. The z parameter is defined in Eq. (35).

Band	Transition moment (e b)	z parameter	ϵ_0	h_0 (keV)	Energy denominator at spin 11/2 (keV)
$K = 3/2$ vib	0.78	-0.055	0.00088	0.62	703
[752]5/2	0.65		0.027	18	674
[734]9/2	0.49		0.020	16	783
$K = 11/2$ vib	0.71	-0.060	0.00087	0.71	818

the off-diagonal elements are the Coriolis interaction energies, H_{cor}. Values for the unperturbed bandhead energies were taken either from our particle-rotor code or from those of Stephens *et al.* [1] shown in Table VIII. The main differences in the two calculations arise from the effects of the hexadecupole deformation, and from effects of the so-called recoil term, which are included in our particle-rotor calculation but not in Ref. [1]. Each rotational band is specified by an unperturbed rotational constant, $A = (\hbar^2/2\mathcal{J})$ [cf. Eq. (11)]: these were chosen in Ref. [1] to be 6.4 keV in common to all bands. Finally, a value for the energy-decoupling factor, a, in the unobserved $K = 1/2$ band must be chosen [cf. Eq. (11)].[5] The authors of Ref. [1] took $a = -7.2$, and this seems to be a reasonable choice: we find $a = -7.16$ in our particle-rotor code, and $a = -7.32$ is used in Chasman *et al.* [12]. In the case of a pure $j_{15/2}$ shell [cf. Eq. (26)] we have $a = -8$, which again illustrates that properties of high-j intruder orbitals are insensitive to the model parameters.

With the parameter set derived in Ref. [1], we find that an exact diagonalization of the Coriolis interactions within the $j_{15/2}$ multiplet reproduces the earlier results (as indeed it should!), as shown in Fig. 15 as the filled points. It may be noted that both the magnitude of the oscillation in the parameter A and the change in its overall magnitude from unperturbed to the observed value are measures of the strength of the Coriolis interactions. This fit involves attenuation of the $(3/2,5/2)$, $(5/2,7/2)$, and $(7/2,9/2)$ Coriolis matrix elements, H_{cor}, shown in Table IX (a result extensively discussed by Stephens *et al.* [1] and by Bohr and Mottelson [11], page 275 ff.).

If we take our present values for the unperturbed bandhead energies, a comparable fit to the oscillations of the [752]5/2 band requires that the attenuation of $H(3/2, 5/2)$ be 0.90 (rather than 0.78 as shown in Table IX). At the same time, the rotor constant for the bands becomes $A = 6.8$, rather than $A = 6.4$ in the older fit. However, having reproduced the [752]5/2 band, these changes do not affect the fit to the strengths $H(5/2, 7/2)$ or $H(7/2, 9/2)$ and these values remain as shown in Table IX and are strongly attenuated.

In view of the assumptions going into the calculation, we feel that the fit at low spins has defined a fundamental problem with the expected Coriolis matrix elements and fine-tuning the parameters to further improve the fit at low spin is not

productive. The case could be reopened if the $K = 1/2$, and $K = 3/2$ bands could be found experimentally.

The new data are shown as open points in Fig. 15, and we see that, with increasing spin, there is a general departure from the predictions of the earlier and of the present best parameters.

The present measurement of $Q_t(\lambda = 2)$ from the ground band [743]7/2 to the [752]5/2 and [734]9/2 bands shown in Table IX imply less mixing than the amplitudes derived from the energies alone. If we assume that the intrinsic $Q_t(\lambda = 2)$ values are zero, so that only admixed amplitudes contribute to the $E2$ transition strength, then for bands which have $\Delta K = 1$ we find[6] in lowest order

$$Q_t(\lambda = 2) = 6^{1/2}\epsilon_0 Q_0, \qquad (27)$$

where ϵ_0 is a reduced mixing amplitude related to the admixed amplitudes by

$$\epsilon(J) = [(J \mp K)(J \pm K + 1)]^{1/2}\epsilon_0. \qquad (28)$$

In Table X we summarize the mixing parameters derived from the Coulomb excitation analysis to fit the [752]5/2 and [734]9/2 bands. Applying Eq. (27) allows us to estimate the values for h_0 and hence $A\langle j_+ \rangle = h_0$. The $B(E2)$ values are virtually a direct measure of the admixed wave functions with the ground-state band [743]7/2. Stephens *et al.* [1] also noted that their experimental $B(E2)$ values imply smaller mixing amplitudes than those derived from the energies alone. They attributed this to a nonzero value of the intrinsic $E2$ transition between the pure Nilsson states, which although small could interfere destructively with the collective transitions between the small admixed components. However, if we turn off the Coriolis matrix elements in our particle-rotor code, we calculate that from the $K = 7/2$, $J = 7/2$ ground state, $B(E2; 7/2 \rightarrow 5/2, 5/2) \ll 0.0001$ and $B(E2; 7/2 \rightarrow 9/2, 9/2) \ll 0.0001$ in units of $(e\,b)^2$. These values are too small to have any measurable effect on the observed $B(E2)$ values.

---

[5]Note that $a = -\langle 1/2|j_+|1/2\rangle$.

[6]This result follows by writing expressions for the $E2$ matrix elements and expanding the Clebsch-Gordan coefficients in their explicit algebraic form. Note that the form of Eq. (27) ensures that the $B(E2)$ values satisfy the Alaga rules, despite the K mixing.

B. Unperturbed rotational energies

In lowest order, the $\Delta K = \pm 1$ Coriolis mixing renormalizes the rotational constant $A = (\hbar^2/2\mathcal{J})$, as well as introduces an oscillating term in the energy spacings. The ground-state band is pushed down to lower energies together with more compressed energy spacings by the interactions with the other bands of the $j_{15/2}$ multiplet, all of which lie above it. The rotational constant for the ground band is therefore decreased by the Coriolis effects. Indeed, the fact that we can fit the initial value of the rotor constant, A, from an unperturbed value $A = 6.4$, to its observed value, $A = 5.2$, at low spin, albeit with some attenuated matrix elements, is good evidence that Coriolis interactions within the $j_{15/2}$ multilplet is at low spins the dominant effect.

The description of the ground band for spins above $\sim 35/2$ can be dramatically improved by predicting the unperturbed energies with inclusion of the next order term in the rotor formula, Eq. (11):

$$E(J) = AJ(J+1) + BJ^2(J+1)^2. \tag{29}$$

This prescription with a negative B coefficient causes the energy denominators between the ground band and the other $j_{15/2}$ bands to increase with spin, and the effect of the Coriolis interactions is damped. One can perhaps justify the introduction of this parameter since effects not described by $\Delta K = \pm 1$ Coriolis mixing could be absorbed into the "unperturbed" energies; such effects might include Coriolis antipairing and $\Delta K = \pm 2$ Coriolis mixing with the γ-vibrational bands. However, since the introduction of a B term into the ground band has little effect on the behavior of the $K = 5/2$ and $K = 9/2$ bands, it it does not appear the primary reason for the damping of the $\Delta K = \pm 1$ mixing at higher spin.

VI. MIXING WITH THE γ-VIBRATIONAL BANDS

A. Formalism for $\Delta K = 2$ mixing

Mixing of vibrational bands with the ground band in deformed nuclei has been known for many years [11] (pages 158–166). Its indicators are (1) deviations of the γ-ray branching ratios from the Alaga rules and (2) the existence of a B term in the ground band energies. Because Coriolis interactions between the ground band and the γ-vibrational bands are $\Delta K = \pm 2$, the spin dependence of the interaction is different from the $\Delta K = \pm 1$ Coriolis mixing we have been considering; neither $Q_t(E2; \text{ground} \to \text{vibrational})$ nor the rotational constant can be just renormalized as was the case for $\Delta K = \pm 1$ interactions.

In the formalism of Mikhailov [11] (pages 149–151) $B(E2)$ between states of the ground and γ bands is given by the parameters M_1 and M_2 [cf. Eqs. (21) and (22)] by

$$B(E2; J_i K_i \to J_f K_f)$$
$$= M_1^2 \langle J_i K_i 22 | J_f K_f \rangle^2 \{1 + a_2 [J_f(J_f+1) - J_i(J_i+1)]\}^2, \tag{30}$$

where $K_f = K_i + 2$ and $K_i \neq 0$.

The parameter a_2 is

$$a_2 = M_2/M_1. \tag{31}$$

Note that the role of J_f and J_i is defined by the restriction that, in applying the Mikhailov equation, a transition must always increase K.

To relate the $B(E2)$ values to admixed wave functions, $\epsilon(J)$, and to the interaction energies, $H_{\text{cor}}(J)$, we note that the spin dependence of $\Delta K = 2$ Coriolis mixing may be written as

$$f(J, K) = [(J - K_L - 1)(J - K_L)(J + K_L + 1)$$
$$\times (J + K_L + 2)]^{1/2}, \tag{32}$$

where K_L refers to the smaller of the K values characterizing the two bands that differ by $\Delta K = 2$.

The spin-independent parameters, ϵ_0 and h_0, are then defined (apart from a sign) by

$$\epsilon(J) = f(J, K_L)\epsilon_0, \tag{33}$$
$$H_{\text{cor}}(J) = f(J, K_L)h_0. \tag{34}$$

In the case of two-band mixing, the admixed amplitudes at a given spin, $\epsilon(J)$, will be equal but will have opposite signs in any pair of admixed levels.

We have found it convenient to apply the formalism of Mottelson as quoted by Hansen [26] in which corrections to the Alaga rules are expressed in terms of a parameter z. Each of the five possible $E2$ transitions between bands must be treated separately, as shown in Table XI. These lowest-order corrections can be derived from the amplitudes in the mixed wave functions by expressing the spin dependence $\epsilon(J)$ as in Eq. (32) and writing the Clebsch-Gordan coefficients in their explicit algebraic form. The parameter z is given by

$$z = 24^{1/2}\epsilon_0 Q_0/Q_t. \tag{35}$$

In Table XI we quote the correction factors for the case $K = 2 \to K = 0$. The general case for $K + 2 \to K$ is shown in Table XII. It will be noted that substituting $K_L = 0$ in Table XII yields the results shown in Table XI.

The lowest-order $B(E2)$ values are given by

$$B(E2; K + 2, J_i \to K, J_f)$$
$$= (5/16\pi)e^2 Q_t^2 \langle J_i K_i 2 - 2 | J_f K_f \rangle^2 F(z, K, J_i, J_f)^2, \tag{36}$$

where $F(z, K, J_i, J_f)$ are the values in Table XII.

Results for the experimental γ-ray branching ratio between the $K = 3/2$ γ-vibrational band and the ground-state band

TABLE XI. Correction factor $F(z, J_i, J_f)$ for the reduced matrix element $M(E2; K = 2, J_i \to K = 0, J_f)$.

Initial $K = 2; J_i$	Final $K = 0; J_f$	$F(z, J_i, J_f)$
$J - 2$	J	$1 + (2J+1)z$
$J - 1$	J	$1 + (J+2)z$
J	J	$1 + 2z$
$J + 1$	J	$1 - (J-1)z$
$J + 2$	J	$1 - (2J+1)z$

TABLE XII. Correction factor $F(z, K, J_i, J_f)$ for the reduced matrix element $M(E2; K + 2, J_i \rightarrow K, J_f)$.

Initial $K + 2; J_i$	Final $K; J_f$	$F(z, K, J_i, J_f)$
$J - 2$	J	$1 + [2(K + J) + 1]z$
$J - 1$	J	$1 + (2K + J + 2)z$
J	J	$1 + 2(K + 1)z$
$J + 1$	J	$1 - (2K - J + 1)z$
$J + 2$	J	$1 - [2(J - K) + 1]z$

and between the $K = 11/2$ γ-vibrational band and the ground-state band interpreted in this way are shown in Tables XIII and XIV, respectively.

To relate this expression to the Mikhailov formalism of Eq. (30), we note that for $J_i = J_f$ the correction factor in Eq. (30) vanishes; therefore, for the case $K_L = 0$, then it follows from Table XI that

$$M_1 = (5/16\pi)^{1/2} eQ_t(1 + 2z). \qquad (37)$$

For $K = 0$, the "renormalizing" factor $(1 + 2z)$ is then generally small. However, in the case of ^{235}U for the $K = 11/2$ γ-vibrational band it is $K_L = 7/2$, and one obtains a factor of $(1 + 9z)$ from Table XII; the data give $z = 0.06$; thus the correction amounts to a factor 2.4 when we square it to consider $B(E2)$ values.

The ratio of Mikhailov parameters M_2/M_1 is very roughly equal to $-z/2$, but this approximation is so poor as to be useless when K is appreciable as in the present case.

B. Crossing of the Nilsson [734]9/2 band with the $K = 11/2$ γ-vibrational band

The spin 11/2 member of the $K = 11/2$ band lies 35.2 keV higher than the corresponding 11/2 member of the $K = 9/2$ band, but since the moment of inertia of the $K = 11/2$ band is larger then the bands will cross at some higher spin. It is clear in the data that the crossing occurs at spin 17/2, as shown in Fig. 16. In this figure, it looks plausible that the unperturbed 17/2 levels are essentially degenerate, i.e., $\Delta E^0 = 0$, and if so, the observed separation energy, ΔE, defines the strength of the mixing interaction, H, since for two-level mixing

FIG. 16. The crossing of the Nilsson [734]9/2 band with the $K = 11/2$ γ-vibrational band at spin 17/2. The reference energy $E = 5.5J(J + 1)$ keV has been subtracted from the experimental values in order to make the crossing easier to visualize. We assume that the unperturbed 17/2 levels are essentially degenerate, in which case the interaction energy at spin 17/2 is one half of the observed separation energy. The dashed lines sketch a plausible locus for the unperturbed bands in the region of the crossing.

we have

$$\Delta E = \Delta E^0(1 + 4R^2)^{1/2}, \qquad (38)$$

where

$$R = H/\Delta E^0. \qquad (39)$$

In this case at spin 17/2, $\Delta E = 15.2$ keV, whence $H = 7.6$ keV. We have sketched a plausible locus for the unperturbed levels in the vicinity of the crossing, as shown in Fig. 16. Comparing the perturbed and unperturbed bands we find that the interaction is within 10% of 7.6 keV over the spin range 13/2–19/2 inclusive. This is not a certain result since we simply made a plausible guess as to where the unperturbed

TABLE XIII. Gamma-ray branching ratios from the $K = 11/2$ γ-vibrational band to the [743]7/2 ground-state band analyzed with two-level mixing in terms of the z parameter. It is seen that a mixing described by $z = -0.06$ gives a much better description of the data than the unmixed ($z = 0$) results.

Transition	E_γ (keV)	I_γ (cf. Table LIII)	$B(E2)$ Experiment	$B(E2)$ $z = 0$	$B(E2)$ $z = -0.06$
11/2–7/2	921	22	1.00	1.00	1.00
11/2–9/2	875	11	0.65	0.39	0.64
11/2–11/2	818	3	0.25	0.1	0.27
13/2–9/2	941	5.0	1.00	1.00	1.00
13/2–11/2	885	6.0	1.63	0.71	1.40
13/2–13/2	818	2.2	0.9	0.26	0.9
15/2–11/2	962	1.4	1.00	1.00	1.00
15/2–13/2	895	3.6	3.69	1.0	2.4
15/2–15/2	817	2.2	3.6	0.45	2.0

TABLE XIV. Gamma-ray branching ratios from the $K = 3/2$ γ-vibrational band to the [743]7/2 ground-state band analyzed with two-level mixing in terms of the z parameter. It is seen that a mixing described by $z = -0.054$ gives a much better description of the data than the unmixed ($z = 0$) results.

Transition	E_γ (keV)	I_γ (cf. Table XLIII)	$B(E2)$ Experiment	$B(E2)$ $z = 0$	$B(E2)$ $z = -0.054$
13/2–15/2	630	0.5	1.00	1.00	1.00
13/2–13/2	708	0.21	0.23	0.68	0.28
15/2–17/2	614	0.5	1.00	1.00	1.00
15/2–15/2	703	0.12	0.24	0.76	0.29
17/2–19/2	615	0.85	1.00	1.00	1.00
17/2–17/2	715	0.35	0.19	0.82	0.28
19/2–21/2	592	0.30	1.00	1.00	1.00
19/2–19/2	703	0.31	0.44	0.87	0.28
21/2–23/2	603	0.60	1.00	1.00	1.00
21/2–21/2	724	0.53	0.35	0.92	0.27
23/2–25/2	569	0.70	1.00	1.00	1.00
23/2–23/2	703	0.60	0.30	0.96	0.26
25/2–27/2	597	0.35	1.00	1.00	1.00
25/2–25/2	737	0.35	0.35	1.00	0.25
27/2–29/2	546	0.31	1.00	1.00	1.00
27/2–27/2	702	0.15	0.14	1.03	0.24
29/2–31/2	594	0.29	1.00	1.00	1.00
29/2–29/2	751	0.26	0.28	1.03	0.22

states might lie. As an orientation, we note that the Coriolis interaction at spin 17/2 between the [734]9/2 and [725]11/2 Nilsson bands, using the values in Table IX with Eq. (24), would be 290 keV (if unattenuated). Furthermore, it would increase by nearly a factor of 2 over the spin range 13/2–19/2. Also, with Eq. (34) and $h_0 = 0.7$ keV from Table X, the strength of the ground-band–γ-band interaction at spin 17/2 measured from the branching ratios is $\sim$35 keV.

A small interaction energy between the $K = 11/2$ γ-vibrational band and the [734]9/2 Nilsson band, although not seen so clearly before, is not unexpected. These bands differ structurally by a phonon plus an orbital.

C. The nature of the $K = 3/2$ γ vibrational band

We have referred to the $K = 3/2$ band beginning at 638 keV as a γ-vibrational band as assigned by Stephens *et al.* [1]. Their reasons for this assignment were originally given as follows: (1) Two γ-vibrational bands are expected, with $K = 3/2$ and $K = 11/2$. (2) Bandheads would be expected to lie at approximately 600–800 keV in the range of the $K = 2$ band in neighboring even nuclei. (3) Stephens *et al.* measured $B(E2; 7/2 \to 3/2)$ as 0.5 W.u., which, although not very collective, is nevertheless large compared with typical values between Nilsson states. (4) There is calculated to be no $K = 3/2$ (negative-parity) Nilsson state in the vicinity.

In the light of the present work it is worth re-examining this assignment, in particular, we raise the following question: Can the $K = 3/2$ band be considered to have large components of the missing [761]3/2 Nilsson state of the $j_{15/2}$ multiplet?

The primary evidence against this is that the bandhead energy ($E_x = 638$ keV) is too low. In our particle-rotor code,

cf. Table VIII, we find $E_x(3/2)$ to be at 1495 keV, whereas Stephens *et al.* [1] gave an estimated 1370 keV, and Bohr and Mottelson ([11], page 280) gave 1050 keV. We will show later (Sec. IX) that $E3$ correlations will depress the bandhead excitation energy, and in our QRPA calculations this amounts to 140 keV for the [761]3/2 level.

The observed $K = 3/2$ level spacings are a near-perfect example of a $K = 3/2$ band strongly perturbed by Coriolis interaction with a $K = 1/2$ band. This is natural if the $K = 3/2$ band is in fact [761]3/2 perturbed by [770]1/2. Specifically, for a $K = 3/2$ band perturbed by a $K = 1/2$ band we have (Ref. [11], page 33)

$$E(J) = AJ(J + 1) + (-1)^{J+3/2} A_3 (J - 1/2)(J + 1/2)$$
$$\times (J + 3/2) - BJ^2(J + 1)^2 + \cdots . \quad (40)$$

The coefficient A_3 gives the strength of the Coriolis interaction:

$$A_3 = A^3 \langle 1/2|j_+|1/2 \rangle \langle 1/2|j_+|3/2 \rangle^2 / (E_{3/2} - E_{1/2})^2, \quad (41)$$

where A is the rotor constant, and $E_{3/2}$ and $E_{1/2}$ are the bandhead energies. From Eq. (40), it follows that the level spacings in the $K = 3/2$ band will be

$$\frac{E(J) - E(J - 1)}{2J} = A + J^2(2B \pm A_3), \quad (42)$$

where the plus sign is taken for states J with positive signature.

Figure 17 shows the level spacings (over $2J$) for the $K = 3/2$ band plotted against J^2. The two signatures of the band give nearly straight lines with a common intercept $A = 5.3$ and slope $+0.01$ for the positive signature and slope -0.008 for the negative signature. This is in good accord with Eq. (42) and implies $B = +0.0005$ and $A_3 = +0.009$. A small positive B value would be expected from mixing with the ground-state band. From Eq. (41) we can estimate a theoretical value for A_3
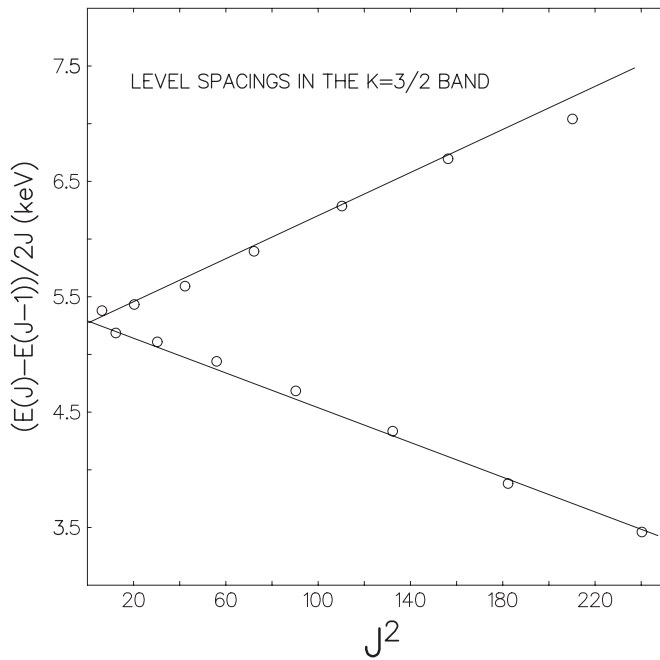
FIG. 17. The rotational constant, A, vs J^2 for the $K = 3/2$ γ-vibrational band at 638 keV. The linear relationship, with nearly equal slopes and a common intercept, is typical of a $K = 3/2$ band perturbed by a $K = 1/2$ band through a Coriolis interaction.

from the Coriolis interaction between [770]1/2 and [761]3/2. Values for j_+ are given in Table IX, we assume $A = 6.4$ keV, and we take the energy denominator $E_{3/2} - E_{1/2} = 1200$ keV. This latter value is extremely uncertain since, in this scenario, the $K = 3/2$ bandhead is much lower than expected in any calculation. Notwithstanding, with these values we predict $A_3 = +0.07$, which is an order of magnitude greater than the observed value.

We conclude that the $K = 3/2$ band does not have the characteristics of the Nilsson [761]3/2 band because its Coriolis interaction with the [770]1/2, and [752]5/2 bands (see below) are much too weak. Nevertheless, the $K = 3/2$ band does have a large Coriolis perturbation from some $K = 1/2$ band lying above it. If it were the [770]1/2 perturbing the $K = 3/2$ band (considered as a γ-vibrational band) then the interaction energy over the spin range shown in Fig. 18 is approximately 13 times weaker than predicted for the interaction between [770]1/2 and [761]3/2. This is comparable to the interaction between the [734]9/2 and the $K = 11/2$ γ-vibrational band, which we showed in Sec. VI B is approximately 16 times weaker than the corresponding [734]9/2-[725]11/2 interaction at spin 17/2.

D. Interaction of the Nilsson [752]5/2 band with the $K = 3/2$ γ-vibrational band

Although there are no crossings between these bands, we can get some idea of their interaction by examining deviations from systematic energy spacings. In Fig. 18 we note that corresponding signatures of the bands are separated by about 30 keV; therefore any interactions between them should be less than 15 keV. We expect an interaction might show up as
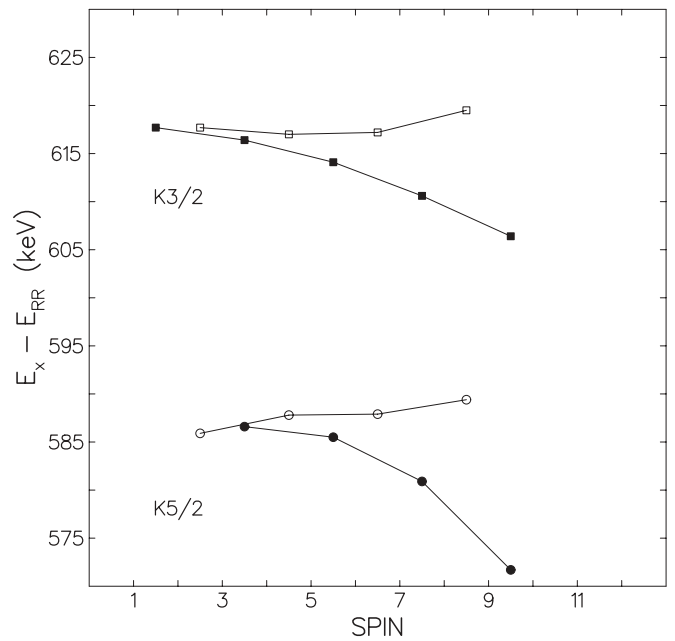
FIG. 18. The energies of low-spin states in the $K = 3/2$ γ-vibrational band and the Nilsson [752]5/2 band after subtraction of a rigid-rotor reference energy of 5.37 $J(J + 1)$ keV. In the text we discuss the possible deviations from systematic behavior that might give some clues to the interactions between the bands. We also note the remarkable isospectral character between corresponding signatures, which is at the level of about 1 to 2 keV over this low-spin range.

a downward shift in the energy of the spin 3/2 member of the $K = 3/2$ band because there is no state of corresponding spin in the $K = 5/2$ band to interact with it. No such trend is observed in Fig. 18 and we estimate that the spin 3/2 member is within 3 keV of its systematically expected position, whence the interaction at low-spin is less than 7 keV. However, caution must be exercised here because, although the admixtures are small at these low spin values, there are multiband interactions that might modify these conclusions.

In a similar vein, we note that the Coriolis interaction between the [743]7/2 and [752]5/2 bands was determined experimentally to be 33 keV at spin 7/2 using the data from Table X and Eq. (24); this implies an upward energy shift of 3 keV on the 7/2 member of the $K = 5/2$ band. This Coriolis shift will be missing for the 5/2 member since there is no corresponding state of spin 5/2 in the $K = 7/2$ ground-state band. Such behavior looks plausible in Fig. 18, where we could argue that the trend of the positive-signature energies implies a downward shift of about 3 keV in the 5/2 level.

Because we do not observe in-band cascade transitions in either the $K = 3/2$ γ-vibrational band or the [752]5/2 bands at low spins, it is easy to overlook the fact that these bands are isospectral at the level of 1–2 keV over the spin range 5/2 to 17/2 inclusive. This is evident from the excitation energies given in Tables XXIX and XXX and from the presentation in Fig. 18. It is all the more remarkable since the bands show a signature splitting of 22 keV by spin 17/2.

TABLE XV. Typical occupation numbers for the $j_{15/2}$ multiplet in ^{235}U in a simple BCS calculation. Single-particle matrix elements such as $\langle j_+ \rangle$ and the $M1$ matrix element G_{M1} will be reduced by the factor $UU + VV$ shown in the last column.

K	U_K	V_K	$U_K U_{K+1} + V_K V_{K+1}$
1/2	0.10	0.99	
			1.00
3/2	0.165	0.986	
			1.00
5/2	0.235	0.972	
			0.81
7/2	0.766	0.643	
			0.87
9/2	0.981	0.192	
			1.00
11/2	0.994	0.105	

VII. EFFECTS OF PAIRING

A. Attenuation of the Coriolis interaction

As discussed in Ref. [1], pairing will reduce the Coriolis matrix elements from the ideal value for states on opposite sides of the Fermi surface and, as shown below, could explain about 10%–15% of the effect in ^{235}U at low spin. The matrix element $\langle j_+ \rangle$ between Nilsson states K to $K + 1$ (within the same multiplet) should be reduced by the factor $P_{K+1,K}$, where

$$P_{K+1,K} = (U_K U_{K+1} + V_K V_{K+1}), \qquad (43)$$

where V and U are the usual occupation numbers in BCS theory. Values typical for the $j_{15/2}$ multiplet for the present case are given in Table XV, where the pairing is treated in the simplest BCS approximation (without blocking each quasiparticle level separately). For the $K = 5/2$ and $K = 7/2$ orbitals discussed above, our calculations give the factor $P_{K+1,K} = 0.81$. Similar occupation numbers are given by the parameters used to set up the QRPA described below. We have also estimated the effect of including blocking from the tables given by Chasman *et al.* [12], specifically for the $K = 5/2$ and $K = 7/2$ orbitals in ^{235}U, but the effect only reduces the factor $P_{K+1,K}$ from 0.81 to 0.72. Since we measure the attenuation of $\langle j_+ \rangle$ between the $K = 5/2$ and $K = 7/2$ orbitals to be 0.40 and between the $K = 7/2$ and $K = 9/2$ states to be 0.37 (cf. Table IX) it seems to us that pairing is unlikely to be the central cause of the discrepancy.

B. Attenuation of $B(M1)$ values between Nilsson states of the same multiplet

Magnetic transitions between bands built on Nilsson states in the same multiplet are also subject to some attenuation if the orbitals lie on opposite sides of the Fermi surface. For example, according to Hjorth *et al.* [27], calculated matrix elements $G_{M1}(K_i \rightarrow K_f)$ should be reduced by the $UU + VV$ factor discussed above. However, the calculated effect in a simple pairing model is far too small to explain the attenuations observed in the $B(M1)$ values described above.

We note that the $M1$ matrix element is closely related to the magnitude of $\langle j_+ \rangle$ via Eqs. (17) and (19), whence any

mechanism which can explain the attenuation of $\langle j_+ \rangle$ will go some way to explaining the anomalously retarded $B(M1)$ values.

VIII. RECOIL EFFECTS

The recoil effect can be viewed in both particle-rotor and cranked shell-model perspectives. In modern particle-rotor codes (such as GAMPN used here) the recoil term is treated explicitly and is not folded into the Nilsson calculation, so that the parameters of the Nilsson model do not take on spurious dependencies (e.g., [28]). The recoil term causes an upward shift in the calculated energies of the Nilsson orbitals; hence its effect on a Coriolis calculation is by changing the input energy denominators for any unseen bands. In particular, the shift is considerable for the low-K relative to the high-K components of a high-j multiplet, such as considered here. According to Osnes *et al.* [28], for the $K = 1/2$ component of a j multiplet,

$$E_{\text{recoil}} \approx Aj(j + 1), \qquad (44)$$

where A is the rotor constant, whereas for the $K = j$ component,

$$E_{\text{recoil}} \approx Aj. \qquad (45)$$

For the $j = 15/2$ multiplet in ^{235}U these estimates give shifts of 380 keV for the $K = 1/2$ Nilsson orbital versus 45 keV for the $K = 15/2$ orbital. Shifts in the quasiparticle bandhead energies will depend on specific cases as to the location of the Fermi level. In the ^{235}U case, inclusion of the recoil term in the particle-rotor model actually decreases the key [770]1/2-[761]3/2 energy denominator and therefore for this pair of orbitals leads to an increased Coriolis effect for a given interaction strength.

In a cranked-shell model approach, the Coriolis effect is known to be weaker than in the particle-rotor model, and this has been interpreted as an effect of the recoil term. In the particle-rotor model, this effect can be regarded as a modified Coriolis term, which is $-(\mathbf{I} - \mathbf{j}) \cdot \mathbf{j}_\perp / \mathcal{J}$ instead of $-\mathbf{I} \cdot \mathbf{j}_\perp / \mathcal{J}$ [29]. If we take the high-spin limit and the particle has alignment i, a reduction factor is approximately given by $(1 - i/I)$. This attenuation becomes weaker at high spin. For instance, by assuming the maximum alignment $i = j = 15/2$ and $I \approx 20$, the simple estimation gives an attenuation factor of $\sim$0.6–0.7.

In our view, the recoil effect is determined explicitly in a particle-rotor calculation and, if the results are incorporated as the unperturbed energies for a Coriolis calculation, then the recoil effect will have been properly taken into account.

IX. EFFECTS OF OCTUPOLE CORRELATIONS

A plausible explanation for the attenuation of Coriolis matrix elements at low spin is that the $j_{15/2}$ multiplet has mixed with other Nilsson states and consequently has a smaller j value than that calculated in a simple model. Since the $j_{15/2}$ system intrudes into a shell of positive-parity levels this mixing can only be through octupole correlations, and indeed we have evidence that there are collective $E3$ excitations in ^{235}U, and there are orbitals nearby, particularly the $g_{9/2}$ multiplet that

TABLE XVI. Analysis of Coulomb excitation yields in ^{235}U with a ^{40}Ca beam in the CHICO experiment for positive-parity bands. As examples, the $M(E3)$ and $B(E3)$ values from the ground state to the lowest state of the excited bands are given. All the $E3$ matrix elements connecting the ground state to the excited bands may be obtained by substituting the extracted Q_t in Eq. (21).

Band (positive parity)	Transition moment $Q_t(\lambda = 3)$ (e 10^{-36} cm^3)	$M(E3; 7/2^- \rightarrow J)$ (e 10^{-36} cm^3)	$B(E3; 7/2^- \rightarrow J)$ (e^2 10^{-72} cm^6)
[631]1/2	2.3	1.21	0.18
		$J = 1/2$	$J = 1/2$
[631]3/2	1.03	0.45	0.025
		$J = 3/2$	$J = 3/2$
[622]5/2	1.38	0.59	0.045
		$J = 5/2$	$J = 5/2$
[633]5/2	1.05	0.45	0.025
		$J = 5/2$	$J = 5/2$
[624]7/2	1.35	0.67	0.055
		$J = 7/2$	$J = 7/2$
[613]7/2	0.80	0.45	0.019
		$J = 7/2$	$J = 7/2$
[615]9/2	0.92	0.55	0.038
		$J = 9/2$	$J = 9/2$
Unassigned (7/2)	0.76	0.37	0.017
		$(J = 7/2)$	$(J = 7/2)$

gives rise to such octupole correlations. A summary of the experimental results is shown in Table XVI. It is of interest to test whether the observed level of octupole collectivity is consistent with a significant drop in the strength of Coriolis matrix elements within the $j_{15/2}$ system. We have calculated octupole mixing in the QRPA, as discussed in the next section. Gareev *et al.* reported generally similar results [10]. Some findings are that the [624]7/2 state contains an admixture of the [743]7/2 state coupled to the $K = 0$ octupole phonon with an amplitude in the range 0.36–0.53, which accounts for the strong $E3$ excitation of the [624]7/2 band. The [622]5/2 state is mixed into the [734]9/2 state via the $K = 2$ phonon with an amplitude in the range 0.4–0.53. This could account for the strong attenuation of the Coriolis matrix element $\epsilon(7/2, 9/2)$. The results are generally in line with the experiments; however, the calculations say that the [631]1/2 is almost a pure Nilsson state, whereas we find that band to be the most strongly populated of the $E3$ excitations. We discuss in Sec. IX D that this may be because the [631]1/2 is yrast for positive parity and picks up unobserved feeding from higher-lying positive-parity bands.

A. Parameters of the model

Details of the formalism are given in Appendix A.

We adopt the Nilsson parameters from Ref. [11]. The quadrupole deformation, $\epsilon = 0.23$, and pairing gaps, $\Delta_n = 657$ keV and $\Delta_p = 905$ keV, were derived from experimental data for ^{234}U. The isoscalar (IS) octupole-octupole residual interactions are in a doubly-stretched form whose coupling strengths are $1.04\chi_{3K}^{HO}$, where χ_{3K}^{HO} are the self-consistent values for the deformed harmonic oscillator potential [30]. The strength of the isovector (IV) dipole interactions were taken from Eqs. (6)–(127) of Ref. [11] with $V_1 = 130$ MeV.

For a model space of the quasiparticle vibration-coupling (QPVC) Hamiltonian, Eq. (A3), we adopt 24 quasiparticle

states and 10 phonon states from those lowest in energy (quasiparticle energy and RPA eigenenergy). The Hamiltonian is diagonalized within the space of $\{a_\mu^\dagger |0\rangle, a_\mu^\dagger X_n^\dagger |0\rangle\}$ with $\mu = 0$–23 and $n = 1$–10.

B. Octupole phonons and dressed quasiparticles

The QRPA calculation predicts octupole phonons with $K = 0$, 1, and 2 that are nearly degenerate in energy ($E_x \sim 700$ keV). The $K = 3$ phonon is calculated somewhat higher in energy ($E_x \sim 1$ MeV). In neighboring even-even nuclei, observed bandhead energies are 786 keV (^{234}U) and 688 keV (^{236}U) for $K^\pi = 0^-$ states, 967 keV (^{236}U) for $K^\pi = 1^-$, and 990 keV (^{234}U) for $K^\pi = 2^-$ [31].

After the calculation of the QRPA + QPVC, we use Eq. (A11) to obtain energies of dressed-quasiparticle bands and Eq. (A10) to obtain $E3$ transition moments. The moment of inertia, $\mathcal{J} = 97\hbar^2/\text{MeV}$, is estimated from the experimental energy spacing between $I = 7/2$ and 11/2 of the ground band ($K = 7/2$). In Table XVII, calculated properties of dressed-quasiparticle states are shown. The excitation energy of the bandhead state relative to the ground state ($I^\pi = K^\pi = 7/2^-$) is defined by

$$E_x(\mu, I) = E^{(\text{lab})}(\mu, I) - E^{(\text{lab})}(0, 7/2)$$
$$= \tilde{E}_\mu - \tilde{E}_0 + \frac{I(I+1) - K_\mu^2 - 7/2}{2\mathcal{J}}, \quad (46)$$

where μ is an index for the (dressed) quasiparticles (cf. Appendix A).

Here we assume the same moment of inertia for all the bands. The quantities $E_x^{(1)}$ in Table XVII are calculated excitation energies of bandhead states $I = K_\mu$. The quantities $E_x^{(0)}$ are quasiparticle energies without coupling to the octupole phonons, calculated with E_μ instead of $\tilde{E}_\mu$ in Eq. (46). Calculated excitation energies are lower than the experimental

TABLE XVII. Calculated low-lying quasiparticle properties for ^{235}U. The Nilsson asymptotic quantum numbers in the first column indicate the main component in each dressed-quasiparticle state. $E_x^{(1)}$ ($E_x^{(0)}$) are excitation energies of one-quasiparticle states with (without) octupole phonon coupling. The corresponding experimental data are shown in the fourth column ($E_x^{\exp}$). P_0 is the probability for zero-phonon states (see text for explanation). Q_t is the calculated $E3$ transition moment to the ground band ([743]7/2) compared with the experimental value, $Q_t^{\exp}$. The experimental value for the [631]1/2 band is probably too large because of feeding, as discussed in Sec. IX D.

$[Nn_3\Lambda]\omega$	$E_x^{(0)}$ (keV)	$E_x^{(1)}$ (keV)	$E_x^{\exp}$ (keV)	P_0	Q_t ($10^3 e$ fm^3)	$Q_t^{\exp}$ ($10^3 e$ fm^3)
[743]7/2	0	0	0	0.95		
[752]5/2	250	170	633	0.86		
[761]3/2	780	640	806	0.58		
[734]9/2	790	440	822	0.59		
[501]1/2	160	210		0.99		
[503]5/2	390	430		0.99		
[631]1/2	60	110	0.08	>0.99	0.10	2.30
[622]5/2	140	120	129	0.91	1.02	1.38
[633]5/2	190	100	333	0.89	0.64	1.05
[631]3/2	280	270	393	0.90	0.66	1.03
[624]7/2	570	420	446	0.75	1.14	1.35
[606]13/2	310	360		>0.99	0.04	

values except for the [631]1/2 band. In particular, the [752]5/2 and [734]9/2 bands of the $j_{15/2}$ multiplet are calculated to be lower than the experimental values by about 400 keV. These may be improved by increasing either the neutron pairing gap or the deformation parameter. The calculations are not very sensitive to getting these energies closely correct. The vibrational states are made up of a superposition of many two-quasiparticle states with energies of approximately 2 MeV, and the 400-keV difference translates to a 20% error in the two-quasiparticle energies. Also, each two-quasiparticle state contributes only about 10% or less to the collective states, reducing any dependence on energy of a particular Nilsson state still further.

In order to see the magnitude of the octupole mixing, we show zero-phonon probabilities

$$P_0(\mu) \equiv \sum_\nu |c_\mu^\nu|^2 = 1 - \sum_{n,\nu} |b_\mu^{n\nu}|^2, \qquad (47)$$

from Eq. (A4). If the state is a pure one-quasiparticle state, we have $P_0 = 1$. The octupole mixing in the ground state ([743]7/2) is relatively weak, but the other members of the $j_{15/2}$ multiplet have strong mixing. In particular, $K = 3/2$ and 9/2 quasiparticles carry about 40% of octupole-phonon components. This mixing will contribute to attenuation of the Coriolis coupling, as discussed below.

C. Coriolis attenuation in the $j_{15/2}$ multiplet

The Coriolis matrix elements are related to those of the operator $j_+ = \sum_{\nu\nu'} j_+(\nu\nu') a_\nu^\dagger a_{\nu'} + (aa, a^\dagger a^\dagger$ terms), among

the dressed quasiparticles,

$$\langle\mu|j_+|\mu'\rangle \equiv \langle 0|\beta_\mu j_+ \beta_{\mu'}^\dagger|0\rangle$$
$$= \sum_{\nu\nu'} \{c_\mu^\nu c_{\mu'}^{\nu'} j_+(\nu\nu') + b_\mu^{n\nu} b_{\mu'}^{n\nu'} j_+(\nu\nu')\} \qquad (48)$$
$$\approx c_\mu^\mu c_{\mu'}^{\mu'} j_+(\mu\mu'), \qquad (49)$$

where all the coefficients are assumed to be real and where we use, in the second line of Eq. (48), the fact that the octupole phonons $X_n^\dagger$ and the angular momentum operator j_+ have different parities. When μ and μ' belong to the $j_{15/2}$ multiplet, the numerical calculation verifies the last equation (49). Thus, the Coriolis matrix elements are attenuated by a factor of $c_\mu^\mu c_{\mu'}^{\mu'}$. Calculated dressed-quasiparticle wave functions are

$$|K = 3/2\rangle = 0.759\ |[761]3/2\rangle + 0.601\ |[633]5/2\rangle$$
$$\otimes \omega_{K=1} + \cdots, \qquad (50)$$
$$|K = 5/2\rangle = 0.918\ |[752]5/2\rangle + 0.323\ |[633]5/2\rangle$$
$$\otimes \omega_{K=0} + \cdots, \qquad (51)$$
$$|K = 7/2\rangle = 0.975\ |[743]7/2\rangle + 0.125\ |[613]7/2\rangle$$
$$\otimes \omega_{K=0} + \cdots, \qquad (52)$$
$$|K = 9/2\rangle = 0.770\ |[734]9/2\rangle + 0.513\ |[622]5/2\rangle$$
$$\otimes \omega_{K=2} + \cdots. \qquad (53)$$

Here we give only the main quasiparticle component and the most-dominant octupole-phonon mode in each dressed state.

The $K = 1/2$, 11/2, 13/2, and 15/2 members of the multiplet are too high in excitation to be accurately treated in QRPA + QPVC theory. This is because at and above 1.5 MeV excitation, there are many collective one-phonon octupole states which can give rise to spurious mixing with the one-quasiparticle states because of accidental degeneracies. These attenuation factors are summarized in Table XVIII. The calculated attenuation factor is approximately 0.7.

D. $E3$ transition amplitude

The $E3$ transition moments are given by Eq. (A10). The collective phonon amplitudes, $t_n[\mathcal{M}_3] \equiv \langle 0|X_n \mathcal{M}_3|0\rangle$, are significantly larger than the quasiparticle amplitude, $\langle 0|a_\mu \mathcal{M}_3 a_{\mu'}^\dagger|0\rangle$. Thus, we can obtain an approximate expression

$$Q_t(\mathcal{M}_3)_{\mu\mu'} \approx \sqrt{(16\pi)/(2\lambda+1)}$$
$$\times \sum_{n\nu} \{c_\mu^\nu b_{\mu'}^{n\nu} t_n[\mathcal{M}_3] + b_\mu^{n\nu} c_{\mu'}^\nu t_n[\mathcal{M}_3]\}. \qquad (54)$$

TABLE XVIII. Calculated attenuation factor for $\langle K+1|j_+|K\rangle$ matrix elements for the $j_{15/2}$ multiplet. $uu' + vv'$ indicates a factor resulting from the pair correlation, and cc' from the octupole-phonon coupling.

	$uu' + vv'$	cc'	Total
$\langle K = 9/2|j_+|K = 7/2\rangle$	0.989	0.696	0.688
$\langle K = 7/2|j_+|K = 5/2\rangle$	0.848	0.895	0.759
$\langle K = 5/2|j_+|K = 3/2\rangle$	0.922	0.751	0.692

Again, all the quantities are assumed to be real. The $E3$ transition moments from positive-parity excited bands to the ground-state $K^\pi = 7/2^-$ band, Q_t, are calculated and shown in Table XVII. Comparing these with the experimental values, we see a reasonable agreement except for the [631]1/2 state. Octupole phonon mixing is essential for reproducing these large Q_t values.

For the [631]1/2 state, the calculation produces a pure quasiparticle state without phonon mixing. Thus, the large Q_t value in the experiment is unexpected. Coriolis mixing within the $j_{15/2}$ multiplet will increase the octupole collectivity of transitions between the ground-state [743]7/2 band and the [631]1/2 band. As can be seen in Table XVII, within the $j_{15/2}$ multiplet the [743]7/2 orbital has the smallest calculated phonon admixture. Taking, for example, values for the admixed K components of the ground-state band at spin 25/2 from Table 12 of Ref. [1], which are also the values we obtain in the present analysis, we estimate that the effect is to increase the Q_t value to the [631]1/2 band by a factor of 2–3 at $I = 25/2$, at most. It is difficult to explain the enhancement by a factor of about 20 in the present theory.

One possible explanation we have considered is that some bands decant a fraction of their population into the [631]1/2 band, thus increasing its apparent cross section in Coulomb excitation. At low spins we have direct evidence for this; for example, the [624]7/2 band has strong branches to the [631]1/2 band at spins below ∼15/2 (cf. Table LIX). But our cross-section measurement is based on yields averaged over spins 21/2 through 27/2 (cf. Fig. 5). At these higher spins, and higher γ-ray energies, we have a good sensitivity for detecting feeding transitions in γ-ray coincidences, and there are none. This does not rule out a scenario where many bands feed into the [631]1/2 band via a myriad of weak, undetectable γ branches.

The [631]1/2 band is special in that it is yrast for positive parities. Since interband $E1$ transitions tend to be inhibited, it is likely that the [631]1/2 band will be fed to some extent from all the higher-lying positive-parity bands. Bearing in mind that the direct population of the band by Coulomb excitation is weak, this feeding might account for a considerable fraction of its yield. We have performed a detailed calculation to test this effect with the GOSIA 2008 Coulomb excitation code [32]. Unfortunately, many of the needed $E2$ and $M1$ matrix elements governing the γ-ray branching ratios are unknown, and average experimental values or plausible guesses have to be made. From this calculation, it is tenable that most, if not all, of the [631]1/2 yield could be due to unobserved feeding from higher-lying states. It is interesting to realize that in the limiting situation where all decays from positive-parity bands fed into the yrast positive-parity band, this latter would have an apparent $B(E3)$ for excitation equal to the sum of all $B(E3)$'s to the excited bands!

X. SUMMARY AND CONCLUDING DISCUSSION

We have populated rotational bands in ^{235}U in sub-barrier Coulomb excitation with ^{136}Xe and ^{40}Ca beams. Experiments performed at various times detected γ rays with the 8pi Spectrometer and with Gammasphere, the latter both in stand-alone mode and in coincidence with scattered ^{40}Ca particles. Many new levels have been observed and organized into rotational bands.

Our principle motivation was to reexamine the strength of the Coriolis interaction between members of the $j_{15/2}$ Nilsson multiplet. Indicators of that strength are (a) the magnitude of the oscillation in the energy spacings for each rotational band of the multiplet, (b) the observed moment of inertia compared to the even neighboring nuclei, and (c) the $E2$ transition moments between the ground-state band based on the $K = 7/2$ member of the multiplet and the $K = 5/2$ and $K = 9/2$ bands which are determined from the Coulomb excitation cross section.

Clearly, it would be advantageous to identify all members of the multiplet, but this key objective was not met: we did not find evidence for any new members of the $j_{15/2}$ multiplet. We have demonstrated that due to the high γ-ray transition density there is no information content in γ-ray energy sums in the singles (γ) spectrum recorded with Gammasphere in coincidence with backscattered ions. This is described in Sec. II C. All new levels were based on γ-γ coincidence results. This criterion made it impossible to assign the low-spin levels near the bandhead of any previously unseen bands unless they had decay branches to the low-spin levels of known excited bands. In the few cases where this happened, we have made use of it (e.g., Sec. III).

At spins below ∼23/2, the oscillation in the energy spacings of the [752]5/2 band is consistent with the parameter set derived by Stephens *et al.* [1] in their analysis of Coriolis effects, and which implies a damping of the Coriolis interaction energy by factors $\alpha \approx 0.7$, $\alpha \approx 0.5$, and $\alpha \approx 0.5$, respectively, for $H(3/2, 5/2)$, $H(5/2, 7/2)$, and $H(7/2, 9/2)$. If we use a more realistic model to predict the excitation energies of the (unseen) $K = 1/2$ and $K = 3/2$ bandheads, which increases the energy denominators, our analysis indicates that $H(3/2, 5/2)$ should only be attenuated by $\alpha = \sim0.9$, but the other attenuation factors were unchanged. In both the present and earlier experiments, it was found that the wave function admixtures in the 5/2, 7/2, and 9/2 bands derived from Coulomb-excitation cross sections indicate more attenuation than derived from the energy spacings. This discrepancy is approximately 20% (cf. Table IX).

We now find that above spin 23/2 in the [752]5/2 and [743]7/2 bands, even these attenuated parameters produce too much Coriolis interaction. With the parameters of Stephens *et al.* [1] the [734]9/2 band is predicted to show large oscillations above spin 17/2; however, this is just the spin where the band is crossed by the $K = 11/2$ γ-vibrational band, and we lose sight of it. In the [752]5/2 band, the oscillations in the energy spacings actually begin to damp out above spin 25/2.

We think it makes sense to consider two separate regions defined roughly by a boundary at spin ∼25/2. This boundary corresponds to ∼1500 keV in the $K = 5/2$ and 9/2 bands and to ∼800 keV in the ground-state $K = 7/2$ band. In the low-spin region, Coriolis damping factors are typically in the range 0.4–0.5. Explanations for this have been given in terms of (i) pairing and (ii) the recoil effect. We have shown that at least in a simple BCS calculation the effect of pairing on the interaction most affected [i.e., $H(5/2, 7/2)$] is ∼0.8. The effect of the recoil term is mainly to change the calculated bandhead energies.

The γ-vibrational bands based on the ground state do not seem to play an active role in the experimental determination of the Coriolis mixing. Despite their proximity to the Nilsson bands of interest, they appear to have very little interaction with them. We have presented evidence for a very weak interaction between the γ-vibrational bands built on the ground-state $K = 3/2$ and $K = 11/2$ bands and other bands of the $j = 15/2$ multiplet, specifically the [752]5/2 and the [734]9/2 bands. These vibrational bands are mixed with the ground-state band: the admixed amplitudes are small but produce large effects on the $B(E2)$ values (cf. Tables XIII and XIV). These $B(E2)$ values are well represented either in a Mikhailov formalism or in a z-parameter formulation, which we have extended to general K values in this paper (cf. Table XII).

A new factor considered here is the effect of octupole correlations. We have treated these in a QRPA calculation and the resulting $E3$ collectivity from the ground-state band to several positive-parity Nilsson bands agrees well with experiment, except in the one case of the [631]1/2 band as discussed above in Sec. IX. This band is yrast for positive parity and we have argued that most of its yield originates in unobserved feeding from higher-lying positive-parity states. These same calculations show that the Coriolis matrix elements within the $j_{15/2}$ multiplet will be attenuated by factors in the range $\sim$0.7–0.9. Combining all these calculated effects in the low-spin regime produces attenuation factors $\sim$0.7, which are still too small compared with experiment in the low-spin region.

The $M1$ transition amplitude between $K^\pi = 7/2^-$ and $K^\pi = 5/2^-$ and between $K^\pi = 7/2^-$ and $K^\pi = 9/2^-$ are drastically weakened according to these experiments. The reduction factors are much more severe than those of the Coriolis attenuation. A survey of all odd-Z and odd-N nuclei above mass $A = 140$ searching for cases where decays between high-j intruders have been observed shows that this is a universal problem, although there are no cases so clear as the present ^{235}U case.

Taken together, the strong attenuation of the Coriolis interaction and of the magnetic transitions between high-j intruder states indicate that we need deeper study of why the single-particle degrees of freedom are so suppressed in heavy nuclei.

ACKNOWLEDGMENTS

APPENDIX A: QUASIPARTICLE RANDOM PHASE APPROXIMATION CALCULATIONS

We briefly recapitulate a method for the QRPA-plus-quasiparticle-vibration coupling (QRPA + QPVC). See Refs. [33,34] for details.

1. The quasiparticle random phase approximation and quasiparticle-vibration coupling for octupole phonons

The model Hamiltonian has been assumed to be of the form

$$H = h_{\text{s.p.}} + H_{\text{int}}, \quad (A1)$$

where $h_{\text{s.p.}}$ is a single-particle Nilsson-BCS Hamiltonian

$$h_{\text{s.p.}} = h_{\text{Nilsson}} - \sum_{\tau=n,p} \Delta_\tau (P_\tau^\dagger + P_\tau) - \sum_{\tau=n,p} \lambda_\tau N_\tau. \quad (A2)$$

The residual interaction, H_{int}, is a separable multipole interaction. The isoscalar octupole and the isovector dipole interactions are used in the calculation. We assume axial symmetry and R symmetry of the Nilsson potential.

First, the octupole phonon energy $\hbar\omega_n$ and its creation operator $X_n^\dagger$ are constructed by solving the RPA equation of motion [33]. The Hamiltonian for an odd-A nucleus (^{235}U) is

$$H = \text{const.} + \sum_\mu E_\mu a_\mu^\dagger a_\mu + \sum_n \hbar\omega_n X_n^\dagger X_n$$
$$\times \sum_{\mu\nu} \sum_n f_n(\mu\nu) a_\mu^\dagger a_\nu X_n^\dagger + \text{H.c.}, \quad (A3)$$

where a_μ (E_μ) is a quasiparticle operator (energy) and the coupling coefficient $f_n(\mu\nu)$ is determined by the standard procedure using the RPA solutions [34]. Then, we achieve dressed-quasiparticle states by diagonalizing the Hamiltonian, Eq. (A3), within the space of one-quasiparticle states and one-phonon-plus-one-quasiparticle states, $\{a_\mu^\dagger|0\rangle, a_\mu^\dagger X_n^\dagger|0\rangle\}$. Dressed-quasiparticle operators can be written as

$$\beta_\mu^\dagger = \sum_\nu c_\mu^\nu a_\nu^\dagger + \sum_{n,\nu} b_\mu^{n\nu} a_\nu^\dagger X_n^\dagger \quad (A4)$$

as shown schematically in Fig. 19.

The corresponding dressed-quasiparticle energy is denoted by $\tilde{E}_\mu$ in this paper. Note that each quasiparticle state has a definite K quantum number, $I_z \beta_\mu^\dagger|0\rangle = K_\mu \beta_\mu^\dagger|0\rangle$.

2. Transformation from the intrinsic to the laboratory frame

Calculations of the QRPA and quasiparticle-vibration-coupling (QRPA + QPVC) are carried out in the intrinsic (body-fixed) frame. We construct wave functions in the laboratory frame by assuming the strong coupling scheme:

$$|IKM;\mu\rangle = \left(\frac{2I+1}{16\pi^2}\right)^{1/2} \left(D_{MK}^I|\mu\rangle + R\text{-conj.}\right)$$
$$(K = K_\mu \neq 0), \quad (A5)$$
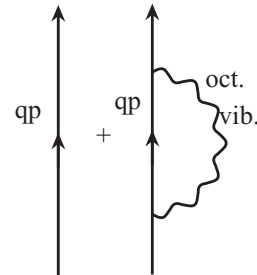
FIG. 19. The lowest-order diagrams for the quasiparticle-vibration coupling for octupole phonons. The quasiparticle energy is modified by the phonon coupling.

where $|\mu\rangle = \beta_\mu^\dagger|0\rangle$ and R-conj. indicates $R_i^{-1} R_e D_{MK}^I |\mu\rangle$ [11]. The Coriolis coupling couples states with different K, and the wave function becomes

$$|IM;\mu\rangle = \sum_\nu C_\mu^\nu(I)|IK_\nu M;\nu\rangle$$

$$= \sum_\nu \left(\frac{2I+1}{16\pi^2}\right)^{1/2} C_\mu^\nu(I)\left(D_{MK_\nu}^I \beta_\nu^\dagger|0\rangle + R\text{-conj.}\right).$$

(A6)

Of course, the Coriolis coupling does not couple states with different parity, and thus $C_\mu^\nu = 0$ if $|\mu\rangle$ and $|\nu\rangle$ have different parities. The coupling is especially strong when $|\mu\rangle$ and $|\nu\rangle$ belong to the same multiplet of high-j orbitals.

The multipole operators are also transformed as

$$\mathcal{M}^{(\text{laboratory})}(\lambda\mu) = \sum_{K=-\lambda}^{\lambda} D_{\mu K}^\lambda \mathcal{M}_{\lambda K},$$

(A7)

where $\mathcal{M}_{\lambda K}$ is the intrinsic moment operator whose matrix elements can be calculated in the QRPA + QPVC scheme. Then, by using the expression (A6), the reduced transition amplitude for a multipole operator can be written as

$$\frac{\langle I_f;\mu||\mathcal{M}(\lambda)||I_i;\mu'\rangle}{\sqrt{2I_i+1}} = \sum_{\nu,\nu'} \sum_{\Delta K} C_\mu^{\nu*}(I_f) C_{\mu'}^{\nu'}(I_i)$$

$$\times \langle I_i K_{\nu'} \lambda \Delta K | I_f K_\nu \rangle \langle \nu|\mathcal{M}_{\lambda \Delta K}|\nu'\rangle.$$

(A8)

Here, contributions from the decoupling terms are omitted. If we neglect the Coriolis effect ($C_\mu^\nu = \delta_\mu^\nu$, $C_{\mu'}^{\nu'} = \delta_{\mu'}^{\nu'}$), this leads

to the usual leading-order intensity relation [11]

$$\frac{\langle I_f;\mu||\mathcal{M}(\lambda)||I_i;\mu'\rangle}{\sqrt{2I_i+1}} = \langle I_i K_{\mu'} \lambda \Delta K | I_f K_\mu \rangle \langle \mu|\mathcal{M}_{\lambda \Delta K}|\mu'\rangle.$$

(A9)

Without the Coriolis coupling, the transition moment, Q_t, is also given by a simple expression,

$$Q_t(\mathcal{M}_\lambda)_{\mu\mu'} = \sqrt{(16\pi)/(2\lambda+1)}\langle\mu|\mathcal{M}_{\lambda\Delta K}|\mu'\rangle.$$

(A10)

The energy is also transformed by assuming the strong-coupling scheme. By using a calculated dressed-quasiparticle energy $\tilde{E}_\mu$ and a moment of inertia $\mathcal{J}$, the energy in the laboratory frame is given by

$$E^{(\text{lab})}(\mu, I) = \tilde{E}_\mu + \frac{I(I+1) - K_\mu^2}{2\mathcal{J}}.$$

(A11)

When we consider the Coriolis coupling, we should diagonalize the Coriolis term,

$$H_{\text{Cor}} = -\frac{\mathbf{I} \cdot \mathbf{j}_\perp}{\mathcal{J}} = -\frac{I_+ j_- + I_- j_+}{2\mathcal{J}}.$$

(A12)

APPENDIX B: DETAILED LEVEL SCHEMES

The detailed level schemes are shown in Figs. 20–27.
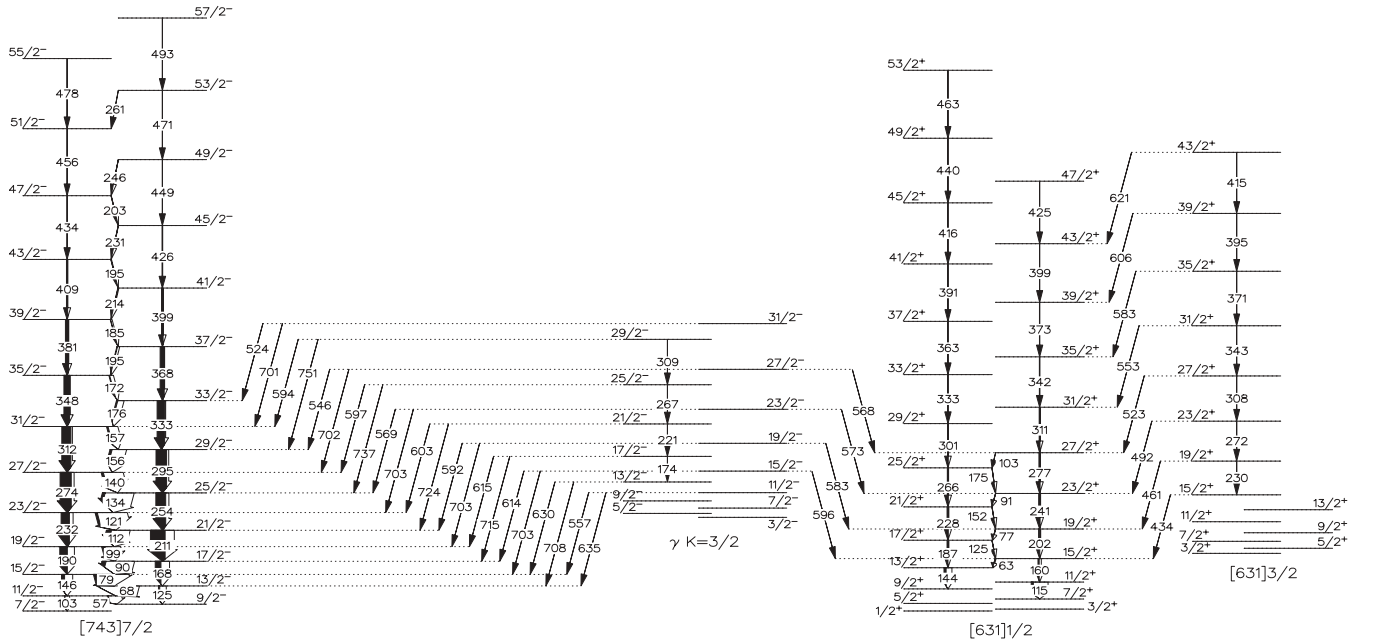
FIG. 20. Partial level scheme based on γ-γ coincidences from the 8Pi and Gammasphere stand-alone experiments showing transitions within the [743]7/2 ground-state band (Tables XXXVII and XXXVIII), within the [631]1/2 band (Table XXXIX), within the [631]3/2 band and its decay to the [631]1/2 band (Table XLII), and within the $K = 3/2$ γ-vibrational band and its decay to both the [631]1/2 band and to the ground-state band (Table XLIII). The width of the arrows is proportional to the observed intensity of the transitions and was normalized to the $21/2^- \rightarrow 17/2^-$ transition of the ground-state band.
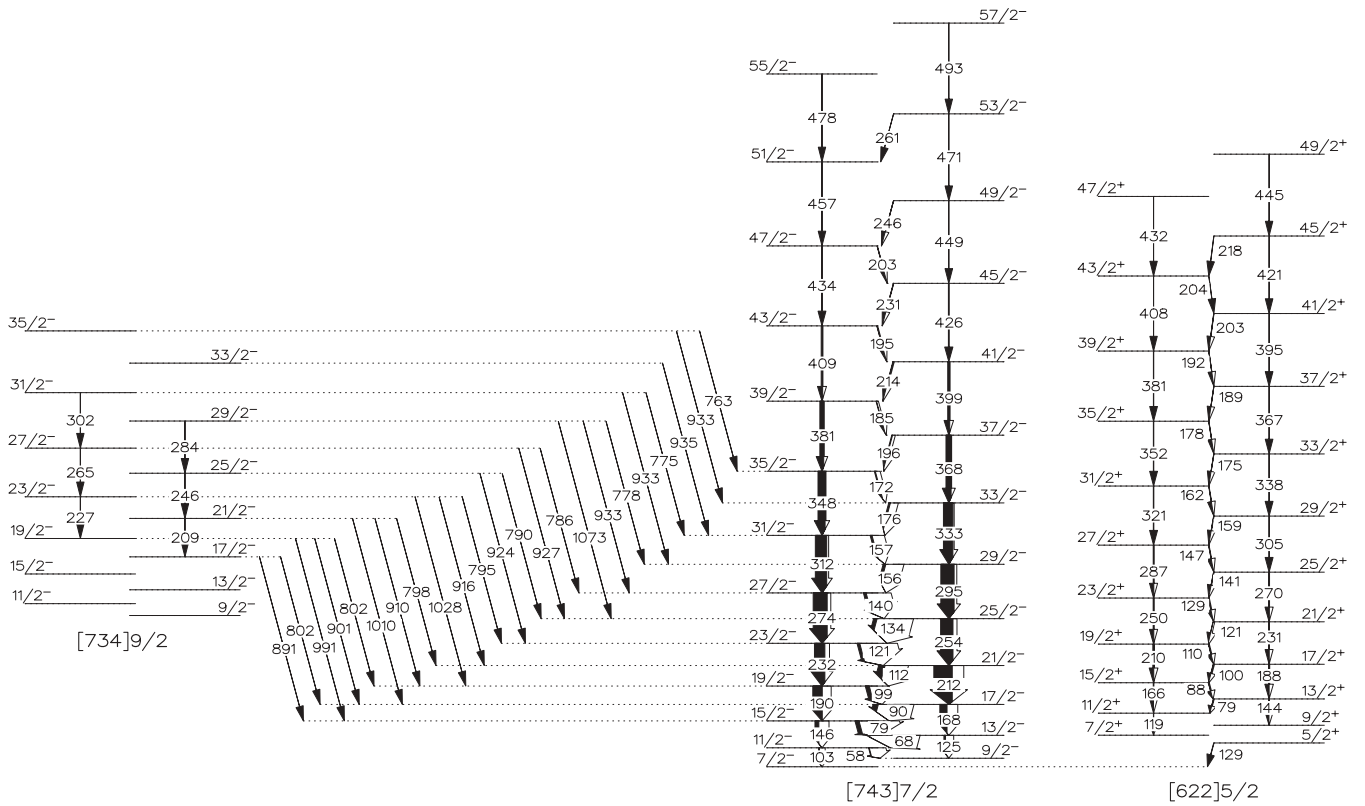
FIG. 21. Partial level scheme based on γ-γ coincidences from the 8Pi and Gammasphere stand-alone experiments showing transitions within the [743]7/2 ground-state band (Tables XXXVII and XXXVIII), within the [622]5/2 band and its decay to the ground-state band (Tables XL and XLI), and within the [734]9/2 band and its decay to the ground-state band (Table XLVI). The width of the arrows is proportional to the observed intensity of the transitions and was normalized to the $21/2^- \rightarrow 17/2^-$ transition of the ground-state band.
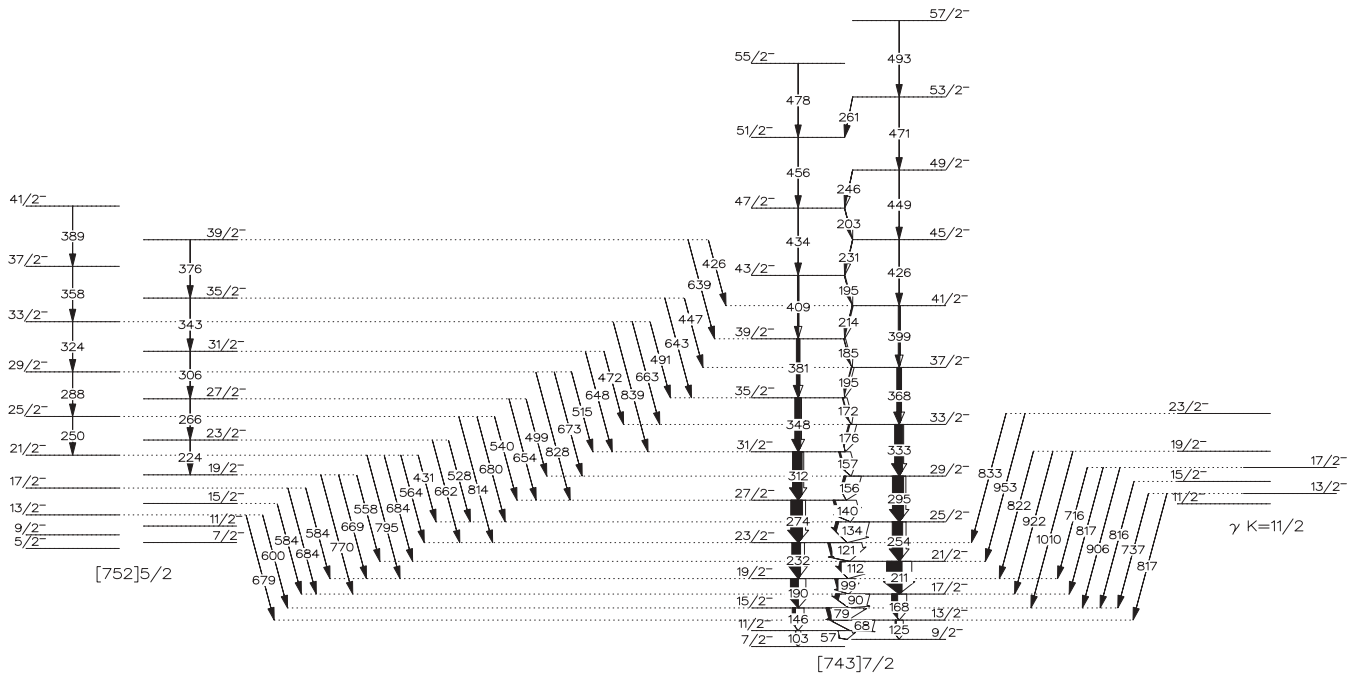
FIG. 22. Partial level scheme based on γ-γ coincidences from the 8Pi and Gammasphere stand-alone experiments showing transitions within the [743]7/2 ground-state band (Tables XXXVII and XXXVIII), within the [752]5/2 band and its decay to the ground-state band (Tables XLIV and XLV), and the decay from the $K = 11/2$ γ-vibrational band to the ground-state band (Tables XLVII and XLVIII). The width of the arrows is proportional to the observed intensity of the transitions and was normalized to the $21/2^- \rightarrow 17/2^-$ transition of the ground-state band.
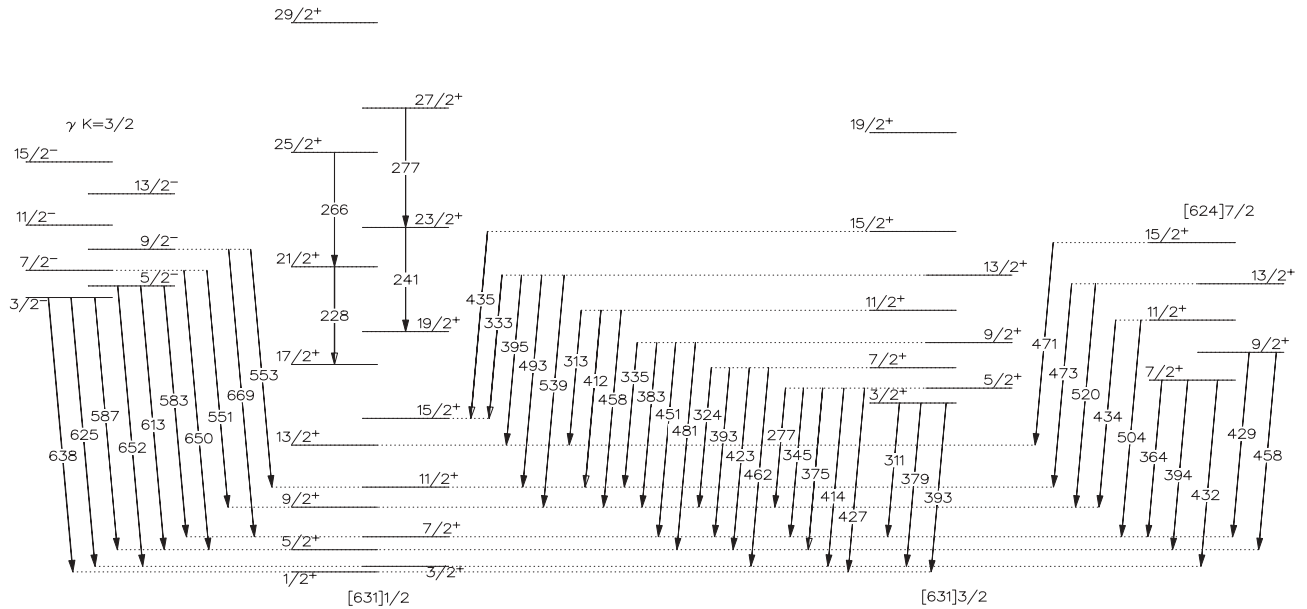
FIG. 23. Partial level scheme based on the Gammasphere and CHICO data showing transitions within the [631]1/2 band (Table XXXV), the decay from the $K = 3/2$ γ-vibrational band to the [631]1/2 band (Table L), the decay from the [631]3/2 to the [631]1/2 band (Table LIV), and the decay from the [624]7/2 to the [631]1/2 band (Table LIX). The width of the arrows is proportional to the observed intensity of the transitions and was normalized to the $19/2^- \rightarrow 15/2^-$ transition of the ground-state band.
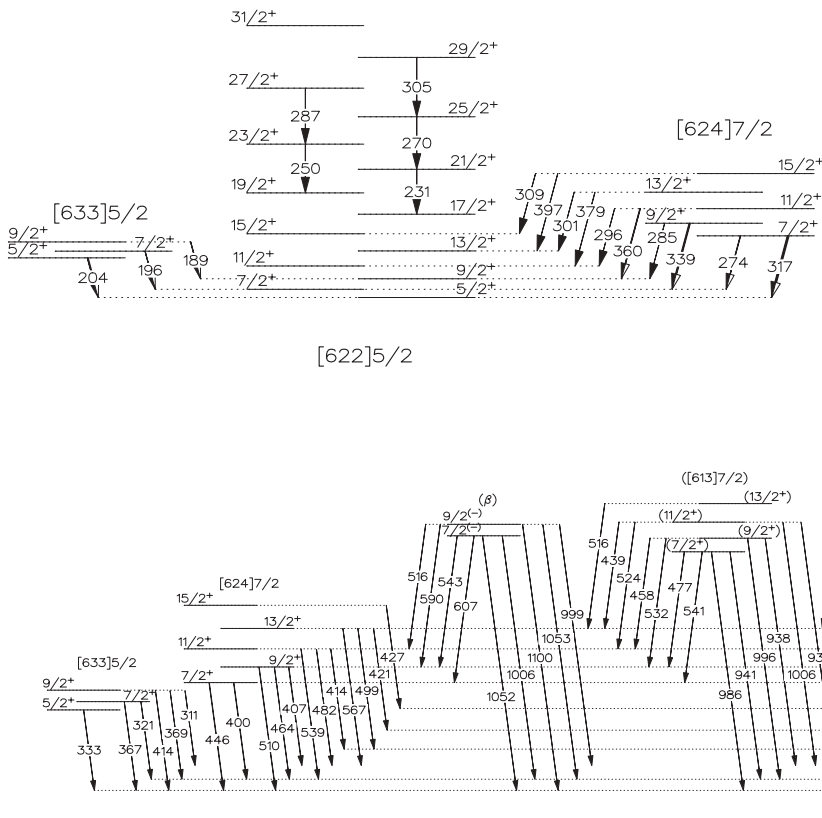
FIG. 24. Partial level scheme based on the Gammasphere and CHICO data showing transitions within the [622]5/2 band (Table XXXIV), the decay from the [633]5/2 band to the [622]5/2 band (Table LV), and the decay from the [624]7/2 band to the [622]5/2 band (Table LVIII). The width of the arrows is proportional to the observed intensity of the transitions and was normalized to the $19/2^- \rightarrow 15/2^-$ transition of the ground-state band.
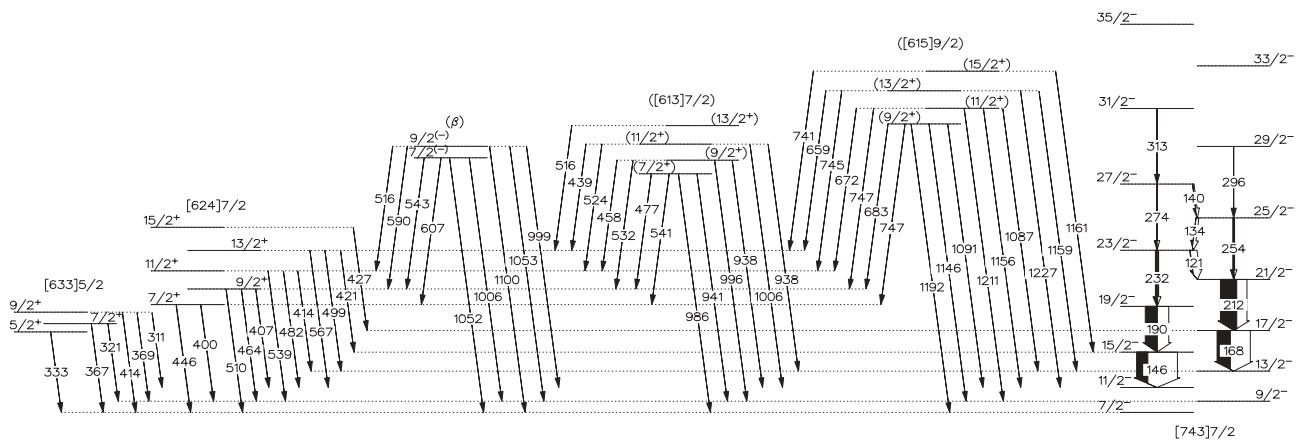
FIG. 25. Partial level scheme based on the Gammasphere and CHICO data showing transitions within the [743]7/2 ground-state band (Table XXXIII), the decay from the [633]5/2 band to the ground-state band (Table LV), the decay from the [624]7/2 band to the ground-state band (Table LVIII), the decay from the [615]9/2 band to both the [624]7/2 band and the ground-state band (Table LVII), the decay from the [613]7/2 band to both the [624]7/2 band and the ground-state band (Table LVI), and the decay from the presumed β-vibrational band to both the [624]7/2 band and the ground-state band (Table LX). The width of the arrows is proportional to the observed intensity of the transitions and was normalized to the $19/2^- \rightarrow 15/2^-$ transition of the ground-state band.
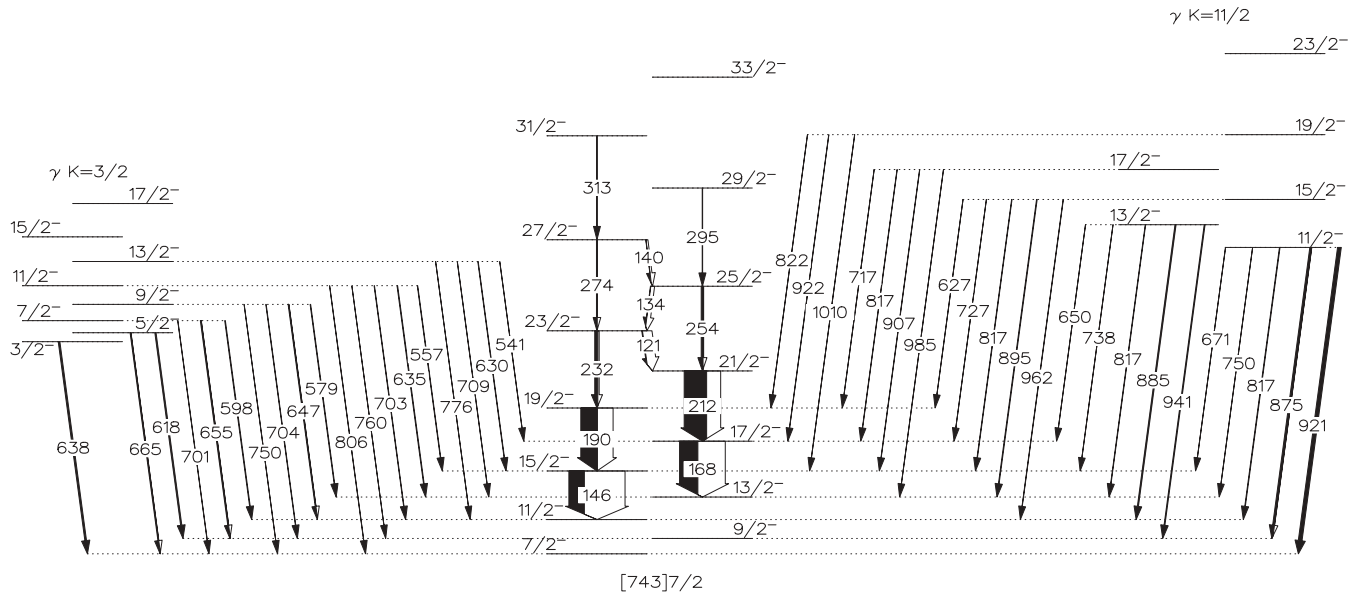
FIG. 26. Partial level scheme based on the Gammasphere and CHICO data showing transitions within the [743]7/2 ground-state band (Table XXXIII), the decay from the $K = 3/2$ γ-vibrational band to the ground-state band (Table XLIX), and the decay from the $K = 11/2$ γ-vibrational band to the ground-state band (Table LIII). The width of the arrows is proportional to the observed intensity of the transitions and was normalized to the $19/2^- \rightarrow 15/2^-$ transition of the ground-state band.
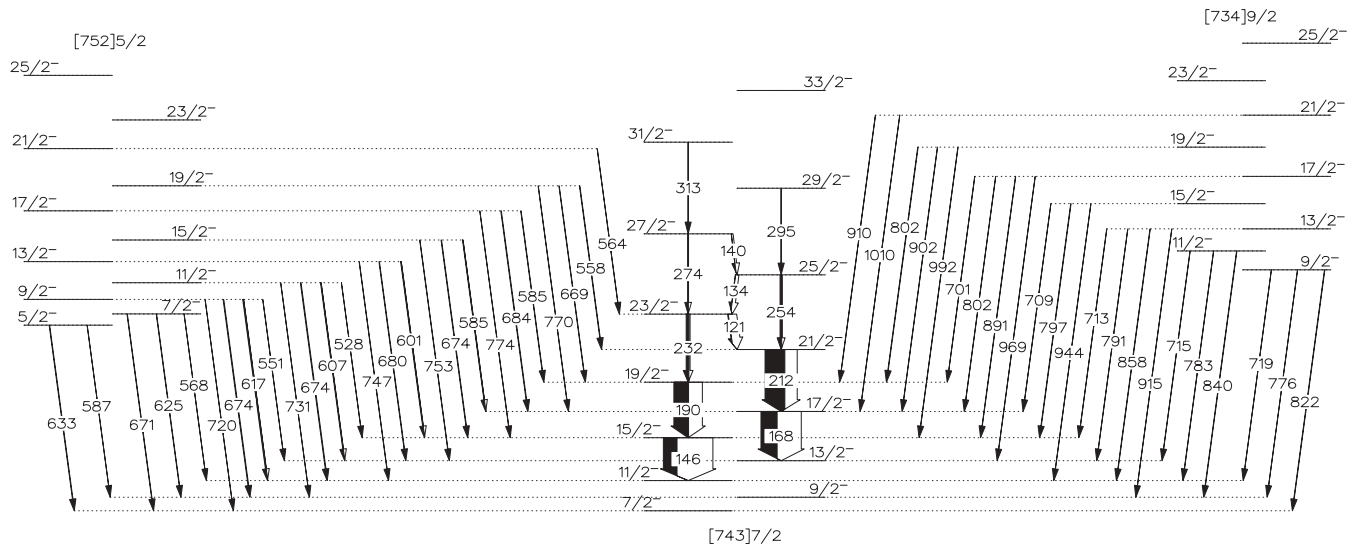
FIG. 27. Partial level scheme based on the Gammasphere and CHICO data showing transitions within the [743]7/2 ground-state band (Table XXXIII), the decay from the [752]5/2 to the ground-state band (Table LI), and the decay from the [734]9/2 to the ground-state band (Table LII). The width of the arrows is proportional to the observed intensity of the transitions and was normalized to the $19/2^- \rightarrow 15/2^-$ transition of the ground-state band.

APPENDIX C: DATA TABLES

1. Comments to the tables

The results in the tables are coded as follows: Letters before the comma indicate the source of the γ-ray energy or

TABLE XIX. Rotational bands observed in these experiments. Comments: (a) tentative assignment; (b) bands that cross at spin 17/2.

Spherical shell	Nilsson orbital	K^π	Max. spin observed
$i_{11/2}$	[631]	$3/2^+$	$43/2^+$
	[622]	$5/2^+$	$49/2^+$
	[613](a)	$7/2^+$	$13/2^+$
$g_{9/2}$	[633]	$5/2^+$	$9/2^+$
	[624]	$7/2^+$	$15/2^+$
	[615](a)	$9/2^+$	$15/2^+$
$d_{5/2}$	[631]	$1/2^+$	$53/2^+$
$j_{15/2}$	[752]	$5/2^-$	$41/2^-$
	[743]	$7/2^-$	$57/2^-$
	[734](b)	$9/2^-$	$35/2^-$
(γ vibration)		$3/2^-$	$31/2^-$
	(b)	$11/2^-$	$23/2^-$

level energy quoted in the table. Letters following the comma indicate that the γ ray, or level, was also confirmed in these experiments as coded.

For Tables XX–XLVIII: (a) 8pi Spectrometer with the Xe beam in γ-γ coincidence. (b) Gammasphere (stand-alone) with the Xe beam in γ-γ coincidence. (c) Gammasphere (singles) with the Ca beam and with CHICO coincidence. (d) Gammasphere (γ-γ) with the Ca beam and with CHICO coincidence. (e) Not seen in these experiments, or there are more accurate values in the Data Sheets of Ref. [4].

For Tables XLIX–LX: These data are entirely Gammasphere (singles γ rays) with CHICO and the ^{40}Ca beam. The letter (f) denotes γ rays with multiple assignments in these tables.

TABLE XX. Excitation energies of the ground-state band.

Level energy (keV)	J^π	Comments
Ground-state band [743]7/2	(odd signature)	
0.0	$7/2^-$	
103.0	$11/2^-$	e,abc
249.1	$15/2^-$	e,abc
438.4(5)	$19/2^-$	a,bc
670.5(6)	$23/2^-$	a,bc
944.2(6)	$27/2^-$	a,bc
1256.7(7)	$31/2^-$	a,bc
1605.0(7)	$35/2^-$	a,b
1985.6(8)	$39/2^-$	a,b
2394.6(9)	$43/2^-$	a,b
2828.8(13)	$47/2^-$	a,b
3285.1(20)	$51/2^-$	ab
3762.7(20)	$55/2^-$	b
Ground-state band [743]7/2	(even signature)	
46.2	$9/2^-$	e
170.7	$13/2^-$	e,abc
338.6(5)	$17/2^-$	a,bc
549.8(6)	$21/2^-$	a,bc
804.4(6)	$25/2^-$	a,bc
1099.7(7)	$29/2^-$	a,bc
1433.0(7)	$33/2^-$	a,b
1800.9(7)	$37/2^-$	a,b
2199.7(8)	$41/2^-$	a,b
2625.5(10)	$45/2^-$	a,b
3074.5(19)	$49/2^-$	a,b
3546.1(17)	$53/2^-$	b
4039(3)	$57/2^-$	b

TABLE XXI. Excitation energies of the [631]1/2 Nilsson band.

Level energy (keV)	J^π	Comments
[631]1/2	(even signature)	
0.1	$1/2^+$	e
51.7	$5/2^+$	e
150.5	$9/2^+$	e,ab
294.7	$13/2^+$	e,ab
482.1(4)	$17/2^+$	a,b
709.2(4)	$21/2^+$	a,bc
975.1(5)	$25/2^+$	a,bc
1276.5(7)	$29/2^+$	a,bc
1610.1(1.0)	$33/2^+$	ab
1972.8(1.0)	$37/2^+$	ab
2364.(1.5)	$41/2^+$	ab
2780.(1.5)	$45/2^+$	ab
3220.(1.5)	$49/2^+$	b
3683.(1.5)	$53/2^+$	b
[631]1/2	(odd signature)	
13.0	$3/2^+$	e
81.7	$7/2^+$	e
197.1	$11/2^+$	e
356.9(4)	$15/2^+$	a,b
558.6(4)	$19/2^+$	a,b
800.6(4)	$23/2^+$	a,bc
1078.1(7)	$27/2^+$	a,bc
1388.0(8)	$31/2^+$	a,bc
1731.2(1.0)	$35/2^+$	a,b
2102.5(1.0)	$39/2^+$	a,b
2501.8(1.5)	$43/2^+$	a,b
2927.5(1.5)	$47/2^+$	b

TABLE XXII. Excitation energies of the [622]5/2 Nilsson band.

Level energy (keV)	J^π	Comments
[622]5/2	(odd signature)	
171.4	$7/2^+d$	e
291.1	$11/2^+$	e
456.4(5)	$15/2^+$	a,b
666.2(5)	$19/2^+$	a,bc
916.4(7)	$23/2^+$	a,bc
1203.7(1.0)	$27/2^+$	a,bc
1524.7(1.0)	$31/2^+$	a,b
1876.7(1.0)	$35/2^+$	ab
2257.8(1.0)	$39/2^+$	ab
2665.4(1.5)	$43/2^+$	ab
3097.5(1.5)	$47/2^+$	b
[622]5/2	(even signature)	
129.3	$5/2^+$	e
225.4	$9/2^+$	e
368.4(5)	$13/2^+$	a,b
556.7(5)	$17/2^+$	a,b
787.3(5)	$21/2^+$	a,bc
1056.9(7)	$25/2^+$	a,bc
1361.5(7)	$29/2^+$	ab,c
1699.(1.0)	$33/2^+$	ab
2066.(1.0)	$37/2^+$	ab
2461.6(1.0)	$41/2^+$	ab
2882.6(1.5)	$45/2^+$	ab
3327.0(2.0)	$49/2^+$	ab

TABLE XXIII. Excitation energies of the [631]3/2 Nilsson band.

Level energy (keV)	J^π	Comments
[631]3/23/2	(odd signature)	
392.6(4)	$3/2^+$	e,c
474.6(4)	$7/2^+$	e,c
608.1(4)	$11/2^+$	c
791.3(5)	$15/2^+$	a,bc
1021.0(5)	$19/2^+$	a,b
1293.0(5)	$23/2^+$	a,b
1601.0(5)	$27/2^+$	a,b
1942.8(8)	$31/2^+$	a,b
2314(1)	$35/2^+$	b
2708(1)	$39/2^+$	b
3124(1)	$43/2^+$	b
[631]3/2	(even signature)	
427.2(4)	$5/2^+$	e,c
533.0(4)	$9/2^+$	e,c
689.8(4)	$13/2^+$	e,c

TABLE XXIV. Excitation energies of the [633]5/2 Nilsson band (both signatures).

Level energy (keV) [633]5/2	J^π (both signatures)	Comments
332.8(3)	$5/2^+$	c,e
367.1(3)	$7/2^+$	c,e
414.5(4)	$9/2^+$	c,e

TABLE XXV. Excitation energies of the tentative [613]7/2 Nilsson band (both signatures).

Level energy (keV) [613]7/2	J^π (both signatures)	Comments
986.7(6)	$7/2^+$	d,c
1042.9(6)	$9/2^+$	d,c
1109.3 (6)	$11/2^+$	d,c
1186(1)	$13/2^+$	d

TABLE XXVI. Excitation energies of the tentative [615]9/2 Nilsson band (both signatures).

Level energy (keV) [615]9/2	J^π (both signatures)	Comments
1192.9(6)	$9/2^+$	d,c
1257.5(6)	$11/2^+$	d,c
1330(1)	$13/2^+$	d,s
1411(1)	$15/2^+$	d

TABLE XXVII. Excitation energies of the [624]7/2 Nilsson band (both signatures).

Level energy (keV) [624]7/2	J^π (both signatures)	Comments
445.8(4)	$7/2^+$	c,e
510.4(4)	$9/2^+$	c,e
585.3(5)	$11/2^+$	c,e
669.7(6)	$13/2^+$	c,d
765.4(10)	$15/2^+$	c,d

TABLE XXVIII. Excitation energies of an unassigned rotational band ($K = 7/2$) (both signatures). This band is probably the one identified as a β-vibrational band in Ref. [1].

Level energy (keV) ($K = 7/2$) unassigned	J (both signatures)	Comments
1052.9(1)	7/2	c
1100.3(1)	9/2	c

TABLE XXIX. Excitation energies of the $K = 3/2$ γ-vibrational band.

Level energy (keV)	J^π	Comments
$K = 3/2$ γ band	(odd signature)	
637.8(4)	$3/2^-$	c
701.0(4)	$7/2^-$	c
806.1(5)	$11/2^-$	c,b
952.9(12)	$15/2^-$	b
1142.1(4)	$19/2^-$	b
1373.8(4)	$23/2^-$	b
1646.0(4)	$27/2^-$	b
1957.5(4)	$31/2^-$	b
$K = 3/2$ γ band	(even signature)	
664.7(4)	$5/2^-$	c
749.9(4)	$9/2^-$	c
878.8(5)	$13/2^-$	c,b
1053.1(5)	$17/2^-$	b
1274.1(5)	$21/2^-$	b
1541.2(5)	$25/2^-$	b
1850.2(5)	$29/2^-$	b

TABLE XXX. Excitation energies of the [752]5/2 Nilsson band.

Level energy (keV)	J^π	Comments
[752]5/2	(even signature)	
632.9(3)	$5/2^-$	c
720.7(4)	$9/2^-$	c
849.5(5)	$13/2^-$	b,c
1022.7(5)	$17/2^-$	b
1234.7(8)	$21/2^-$	b
1484.5(8)	$25/2^-$	b
1772.2(8)	$29/2^-$	b
2096.0(1.0)	$33/2^-$	b
2453(1)	$37/2^-$	b
2842(1)	$41/2^-$	b
[752]5/2	(odd signature)	
671.2(3)	$7/2^-$	c
777.5(4)	$11/2^-$	c
923.2(5)	$15/2^-$	c
1108.0(8)	$19/2^-$	b
1332.5(1.0)	$23/2^-$	b
1598.5(1.0)	$27/2^-$	b
1904.9(1.0)	$31/2^-$	b
2248.3(1.0)	$35/2^-$	b
2624.9(1.2)	$39/2^-$	b

TABLE XXXI. Excitation energies of the [734]9/2 Nilsson band (crossed by the $K = 11/2$ γ-vibrational band at spin 17/2).

Level energy (keV)	J^π	Comments
[734]9/2	(odd signature)	
885.9(4)	$11/2^-$	c
1047.1(4)	$15/2^-$	c
1239.8(8)	$19/2^-$	c,b
1466.3(1.1)	$23/2^-$	b
1730.5(1.3)	$27/2^-$	b
2031.9(1.3)	$31/2^-$	b
2367.3(1.4)	$35/2^-$	b
[734]9/2	(even signature)	
821.5(4)	$9/2^-$	c
961.2(4)	$13/2^-$	c
1140.1(8)	$17/2^-$	c,b
1348.8(1.1)	$21/2^-$	b,c
1594.2(1.2)	$25/2^-$	b
1877.8(1.2)	$29/2^-$	b
2192.2(1.6)	$33/2^-$	b

TABLE XXXII. Excitation energies of the $K = 11/2$ γ-vibrational band (crossed by the [734]9/2 band at spin 17/2).

Level energy (keV)	J^π	Comments
$K = 11/2$ γ band	(even signature)	
987.4(5)	$13/2^-$	c
1155.3(5)	$17/2^-$	c,b
$K = 11/2$ γ band	(odd signature)	
921.1(4)	$11/2^-$	c
1065.3(8)	$15/2^-$	c,b
1260.1(1.2)	$19/2^-$	c, b
1503.8(1.5)	$23/2^-$	b

TABLE XXXIII. Relative intensities in the ground-state rotational band [743]7/2 in the CHICO experiment used in the Winther–de Boer calculations. Relative intensities are normalized to the $(19/2^- \rightarrow 15/2^-)$ transition, $E_\gamma = 189.6$ keV, with $I_\gamma = 100$. The transition marked † is assigned $\approx 60\%$ to the $(21/2^- \rightarrow 17/2^-)$ in ^{235}U, and the remainder mainly to the $(8^+ \rightarrow 6^+)$ transition in ^{238}U (cf. text).

E_i (keV)	$J_i^\pi \rightarrow J_f^\pi$	E_γ (keV)	I_γ	Comments
249	$15/2^- \rightarrow 11/2^-$	146.2(3)	93(9)	c
438	$19/2^- \rightarrow 15/2^-$	189.6(3)	100	c
671	$23/2^- \rightarrow 21/2^-$	120.9(3)	4.1(8)	c
671	$23/2^- \rightarrow 19/2^-$	232.6(3)	18.4(20)	c
944	$27/2^- \rightarrow 25/2^-$	140.1(4)	1.27(25)	c
944	$27/2^- \rightarrow 23/2^-$	273.9(4)	4.5(7)	c,f
1257	$31/2^- \rightarrow 27/2^-$	312.9(4)	1.00(16)	c,f
339	$17/2^- \rightarrow 13/2^-$	168.2(3)	110(10)	c
550	$21/2^- \rightarrow 17/2^-$	211.5(4)	135(12)†	c
804	$25/2^- \rightarrow 23/2^-$	134.1(4)	2.21(40)	c
804	$25/2^- \rightarrow 21/2^-$	254.6(3)	11(1)	c
1100	$29/2^- \rightarrow 25/2^-$	295.5(3)	2.0(3)	c,f

TABLE XXXIV. Relative intensities in the [622]5/2 Nilsson rotational band (both signatures) in the CHICO experiment used in the Winther–de Boer calculations. Relative intensities are normalized to the $19/2^- \to 15/2^-$ transition, $E_\gamma = 189.6$ keV, with $I_\gamma = 100$.

E_i (keV)	$J_i^\pi \to J_f^\pi$	E_γ (keV)	I_γ	Comments
787	$21/2^+ \to 17/2^+$	230.4(3)	0.75(15)	c
916	$23/2^+ \to 19/2^+$	250.5(3)	1.1(1)	c
1057	$25/2^+ \to 21/2^+$	270.0(4)	0.8(1)	c
1204	$27/2^+ \to 23/2^+$	287.6(3)	0.30(5)	c
1362	$29/2^+ \to 25/2^+$	304.4(4)	0.10(2)	c

TABLE XXXV. Relative intensities in the [631]1/2 Nilsson rotational band (both signatures) in the CHICO experiment used in the Winther–de Boer calculations. Relative intensities are normalized to the $19/2^- \to 15/2^-$ transition, $E_\gamma = 189.6$ keV, with $I_\gamma = 100$.

E_i (keV)	$J_i^\pi \to J_f^\pi$	E_γ (keV)	I_γ	Comments
709	$21/2^+ \to 17/2^+$	228.3(3)	1.8(3)	c
801	$23/2^+ \to 19/2^+$	241.3(3)	1.2(2)	c
975	$25/2^+ \to 21/2^+$	266.3(4)	0.60(10)	c
1078	$27/2^+ \to 23/2^+$	276.9(3)	0.35(10)	c,f

TABLE XXXVI. Relative intensities in the ground-state rotational band and decays from the $K = 0^-$ octupole band in ^{238}U in the CHICO experiment used in the Winther–de Boer calculations. Relative intensities are normalized to the $19/2^- \to 15/2^-$ transition in the ground-state band of ^{235}U, $E_\gamma = 189.6$ keV, with $I_\gamma = 100$. The transition † is approximately 40% the $8^+ \to 6^+$ transition in ^{238}U, the main component ($\approx$60%) being the $21/2^- \to 17/2^-$ transition in ^{235}U.

E_i (keV)	$J_i^\pi \to J_f^\pi$	E_γ (keV)	I_γ	Comments
45	$2^+ \to 0^+$	45	–	c
148	$4^+ \to 2^+$	103.0(3)	50(5)	c
307	$6^+ \to 4^+$	159.3(3)	75(8)	c
518	$8^+ \to 6^+$	211.5(3)	135(10)†	c
776	$10^+ \to 8^+$	257.9(3)	18(2)	c
1077	$12^+ \to 10^+$	300.7(3)	3.3(5)	c,f
1416	$14^+ \to 12^+$	339.2(5)	0.40(8)	d
732	$3^- \to 2^+$	687.1(3)	2.2(3)	c
827	$5^- \to 6^+$	519.5(3)	0.45(5)	cdf
966	$7^- \to 6^+$	659.3(3)	0.5(3)	cdf
966	$7^- \to 8^+$	448.3(3)	0.16(5)	cdf
1151	$9^- \to 8^+$	633.0(5)	0.7(3)	cdf
1151	$9^- \to 10^+$	374.9(3)	0.2(1)	cdf

TABLE XXXVII. Gamma-ray assignments, transition energies, and relative intensities in the [743]7/2 ground-state rotational band (even signature) in the ^{136}Xe experiment. Relative intensities are normalized to the $21/2^- \to 17/2^-$ transition, $E_\gamma = 211.67$ keV, with $I_\gamma = 100$.

E_i (keV)	$J_i^\pi \to J_f^\pi$	E_γ (keV)	I_γ	Comments
171	$13/2^- \to 11/2^-$	68.30(3)	17(5)	a
171	$13/2^- \to 9/2^-$	124.79(4)	8.6(22)	a,bc
339	$17/2^- \to 15/2^-$	90.17(3)	27.5(20)	a,bc
339	$17/2^- \to 13/2^-$	168.13(3)	39(3)	a,bc
550	$21/2^- \to 19/2^-$	111.67(3)	34(5)	a,bc
550	$21/2^- \to 17/2^-$	211.67(4)	100(3)	a,bc
804	$25/2^- \to 23/2^-$	134.16(4)	18.6(8)	a,bc
804	$25/2^- \to 21/2^-$	254.42(3)	67(3)	a,bc
1100	$29/2^- \to 27/2^-$	155.74(4)	14.2(7)	a,bc
1100	$29/2^- \to 25/2^-$	295.21(3)	72(3)	a,bc
1433	$33/2^- \to 31/2^-$	176.45(4)	8.9(5)	a,b
1433	$33/2^- \to 29/2^-$	333.26(3)	51.1(20)	a,b
1801	$37/2^- \to 35/2^-$	196.18(6)	4.2(4)	a,b
1801	$37/2^- \to 33/2^-$	367.89(3)	27.7(12)	a,b
2200	$41/2^- \to 39/2^-$	214.10(3)	2.0(3)	a,b
2200	$41/2^- \to 37/2^-$	398.76(4)	10.7(6)	a,b
2626	$45/2^- \to 43/2^-$	231.04(18)	0.63(24)	a,b
2626	$45/2^- \to 41/2^-$	425.77(6)	4.1(3)	a,b
3075	$49/2^- \to 47/2^-$	245.6(5)	0.29(11)	a,b
3075	$49/2^- \to 45/2^-$	449.20(15)	1.00(12)	a,b
3546	$53/2^- \to 51/2^-$	261.0(10)	0.1(6)	b
3546	$53/2^- \to 49/2^-$	471.4(10)	0.6(6)	b
4039	$57/2^- \to 53/2^-$	493.1(10)	0.1(6)	b

TABLE XXXVIII. Gamma-ray assignments, transition energies, and relative intensities in the [743]7/2 ground-state rotational band (odd signature) in the ^{136}Xe experiment. Relative intensities are normalized to the $21/2^- \to 17/2^-$ transition, $E_\gamma = 211.67$ keV, with $I_\gamma = 100$.

E_i (keV)	$J_i^\pi \to J_f^\pi$	E_γ (keV)	I_γ	Comments
103	$11/2^- \to 9/2^-$	57.50(4)	3.4(17)	a
103	$11/2^- \to 7/2^-$	103.(4)	2.7(3)	a,bc
249	$15/2^- \to 13/2^-$	78.78(3)	21.2(25)	a,bc
249	$15/2^- \to 11/2^-$	146.25(3)	21(4)	a,bc
438	$19/2^- \to 17/2^-$	98.92(3)	21(4)	a,bc
438	$19/2^- \to 15/2^-$	189.56(3)	51.4(21)	a,bc
671	$23/2^- \to 21/2^-$	120.93(3)	14.3(10)	a,bc
671	$23/2^- \to 19/2^-$	232.40(3)	56.4(25)	a,bc
944	$27/2^- \to 25/2^-$	140.13(4)	14.4(7)	a,bc
944	$27/2^- \to 23/2^-$	273.63(3)	76(3)	a,bc
1257	$31/2^- \to 29/2^-$	157.31(4)	9.9(6)	a,bc
1257	$31/2^- \to 27/2^-$	312.43(3)	61.7(23)	a,bc
1605	$35/2^- \to 33/2^-$	172.28(5)	5.0(4)	a,b
1605	$35/2^- \to 31/2^-$	348.18(3)	38.4(15)	a,b
1986	$39/2^- \to 37/2^-$	184.81(5)	2.4(3)	a,b
1986	$39/2^- \to 35/2^-$	380.55(3)	20.7(10)	a,b
2395	$43/2^- \to 41/2^-$	195.21(20)	1.02(24)	a,b
2395	$43/2^- \to 39/2^-$	409.00(5)	7.9(5)	a,b
2829	$47/2^- \to 45/2^-$	202.90(18)	0.43(13)	a,b
2829	$47/2^- \to 43/2^-$	434.14(10)	2.57(25)	a,b
3285	$51/2^- \to 47/2^-$	456.80(13)	0.71(14)	a,b
3763	$55/2^- \to 51/2^-$	477.5(5)	0.12(1)	b

TABLE XXXIX. Gamma-ray assignments, transition energies, and relative intensities in the [631]1/2 rotational band in the ^{136}Xe experiment. Relative intensities are normalized to the $21/2^- \rightarrow 17/2^-$ transition of the [743]7/2 ground-state band, $E_\gamma = 211.67$ keV, with $I_\gamma = 100$.

E_i (keV)	$J_i^\pi \rightarrow J_f^\pi$	E_γ (keV)	I_γ	Comments
295	$13/2^+ \rightarrow 9/2^+$	144.39(4)	14.3(14)	a,b
482	$17/2^+ \rightarrow 15/2^+$	125.2(10)	0.11(4)	a,b
482	$17/2^+ \rightarrow 13/2^+$	187.48(4)	6.3(8)	a,b
709	$21/2^+ \rightarrow 19/2^+$	152.0(10)	0.10(4)	a,bc
709	$21/2^+ \rightarrow 17/2^+$	228.06(4)	8.2(6)	a,bc
975	$25/2^+ \rightarrow 23/2^+$	174.6(10)	0.11(5)	a,bc
975	$25/2^+ \rightarrow 21/2^+$	265.93(4)	6.7(4)	a,bc
1277	$29/2^+ \rightarrow 25/2^+$	300.90(4)	4.7(3)	a,b
1610	$33/2^+ \rightarrow 29/2^+$	333.20(6)	2.57(24)	a,b
1973	$37/2^+ \rightarrow 33/2^+$	363.05(7)	1.52(16)	a,b
2364	$41/2^+ \rightarrow 37/2^+$	390.71(13)	0.63(11)	a,b
2780	$45/2^+ \rightarrow 41/2^+$	416.37(20)	0.30(7)	a,b
3220	$49/2^+ \rightarrow 45/2^+$	440.44(8)	0.055(4)	b
3683	$53/2^+ \rightarrow 49/2^+$	462.91(10)	0.0242(20)	b
197	$11/2^+ \rightarrow 7/2^+$	115.31(14)	14.3(14)	a
357	$15/2^+ \rightarrow 13/2^+$	62.6(10)	0.31(8)	a,bc
357	$15/2^+ \rightarrow 11/2^+$	160.08(4)	8.0(16)	a,bc
559	$19/2^+ \rightarrow 17/2^+$	76.6(10)	0.22(4)	a,bc
559	$19/2^+ \rightarrow 15/2^+$	202.08(4)	8.1(8)	a,bc
801	$23/2^+ \rightarrow 21/2^+$	90.65(6)	0.17(5)	a,bc
801	$23/2^+ \rightarrow 19/2^+$	241.19(4)	9.4(6)	a,bc
1078	$27/2^+ \rightarrow 25/2^+$	102.9(10)	0.04(5)	a,bc
1078	$27/2^+ \rightarrow 23/2^+$	277.44(4)	7.7(4)	a,bc
1388	$31/2^+ \rightarrow 27/2^+$	311.20(5)	5.3(3)	a,b
1731	$35/2^+ \rightarrow 31/2^+$	342.42(5)	3.41(23)	a,b
2103	$39/2^+ \rightarrow 35/2^+$	371.71(8)	2.18(20)	a,b
2502	$43/2^+ \rightarrow 39/2^+$	398.9(10)	0.71(13)	a,b
2928	$47/2^+ \rightarrow 43/2^+$	425.40(5)	0.163(7)	b

TABLE XL. Gamma-ray assignments, transition energies, and relative intensities in the [622]5/2 rotational band (odd signature) in the ^{136}Xe experiment. Relative intensities are normalized to the $21/2^- \rightarrow 17/2^-$ transition of the [743]7/2 ground-state band, $E_\gamma = 211.67$ keV, with $I_\gamma = 100$.

E_i (keV)	$J_i^\pi \rightarrow J_f^\pi$	E_γ (keV)	I_γ	Comments
291	$11/2^+ \rightarrow 7/2^+$	119.0(10)	0.21(24)	a,b
456	$15/2^+ \rightarrow 13/2^+$	88.0(10)	0.64(20)	a,b
456	$15/2^+ \rightarrow 11/2^+$	165.70(6)	1.3(3)	a,b
666	$19/2^+ \rightarrow 17/2^+$	110.0(10)	1.12(16)	a,b
666	$19/2^+ \rightarrow 15/2^+$	209.84(8)	4.8(6)	a,b
916	$23/2^+ \rightarrow 21/2^+$	129.0(10)	0.43(8)	a,b
916	$23/2^+ \rightarrow 19/2^+$	250.17(8)	3.3(3)	a,b
1204	$27/2^+ \rightarrow 25/2^+$	146.5(10)	0.29(8)	a,b
1204	$27/2^+ \rightarrow 23/2^+$	287.28(8)	3.1(3)	a,b
1525	$31/2^+ \rightarrow 29/2^+$	162.0(10)	0.29(6)	a,b
1525	$31/2^+ \rightarrow 27/2^+$	320.97(8)	2.29(23)	a,b
1877	$35/2^+ \rightarrow 33/2^+$	178.0(10)	0.21(6)	a,b
1877	$35/2^+ \rightarrow 31/2^+$	352.37(11)	1.93(18)	a,b
2258	$39/2^+ \rightarrow 37/2^+$	192.0(10)	0.14(7)	a,b
2258	$39/2^+ \rightarrow 35/2^+$	381.10(15)	1.64(20)	a,b
2666	$43/2^+ \rightarrow 41/2^+$	203.6(10)	0.13(8)	a,b
2666	$43/2^+ \rightarrow 39/2^+$	407.6(10)	0.43(12)	a,b
3098	$47/2^+ \rightarrow 43/2^+$	432.1(1)	0.19(4)	b

TABLE XLI. Gamma-ray assignments, transition energies, and relative intensities in the [622]5/2 rotational band (even signature) in the ^{136}Xe experiment. Relative intensities are normalized to the $21/2^- \rightarrow 17/2^-$ transition of the [743]7/2 ground-state band, $E_\gamma = 211.67$ keV, with $I_\gamma = 100$.

E_i (keV)	$J_i^\pi \rightarrow J_f^\pi$	E_γ (keV)	I_γ	Comments
129	$5/2^+ \rightarrow 7/2^-$	129.3(10)	1.4(14)	a,bc
368	$13/2^+ \rightarrow 11/2^+$	78.7(10)	0.36(14)	a,b
368	$13/2^+ \rightarrow 9/2^+$	143.7(10)	0.9(4)	a,b
557	$17/2^+ \rightarrow 15/2^+$	100.0(10)	1.15(24)	a,b
557	$17/2^+ \rightarrow 13/2^+$	188.30(13)	3.3(6)	a,b
787	$21/2^+ \rightarrow 19/2^+$	121.4(10)	0.64(11)	a,b
787	$21/2^+ \rightarrow 17/2^+$	230.64(10)	2.4(4)	a,bc
1057	$25/2^+ \rightarrow 23/2^+$	141.0(10)	0.31(8)	a,b
1057	$25/2^+ \rightarrow 21/2^+$	269.60(9)	3.7(3)	a,bc
1362	$29/2^+ \rightarrow 27/2^+$	159.0(10)	0.30(9)	a,b
1362	$29/2^+ \rightarrow 25/2^+$	305.08(9)	2.50(24)	a,bc
1699	$33/2^+ \rightarrow 31/2^+$	175.0(10)	0.15(7)	a,b
1699	$33/2^+ \rightarrow 29/2^+$	337.66(9)	2.4(3)	a,b
2066	$37/2^+ \rightarrow 35/2^+$	189.0(10)	0.13(6)	a,b
2066	$37/2^+ \rightarrow 33/2^+$	367.37(15)	1.38(23)	a,b
2462	$41/2^+ \rightarrow 39/2^+$	203.0(10)	0.36(9)	a,b
2462	$41/2^+ \rightarrow 37/2^+$	395.27(7)	1.43(13)	a,b
2883	$45/2^+ \rightarrow 43/2^+$	217.8(10)	0.15(8)	a,b
2883	$45/2^+ \rightarrow 41/2^+$	420.96(7)	0.71(8)	a,b
3327	$49/2^+ \rightarrow 45/2^+$	444.96(10)	0.22(8)	a,b

TABLE XLII. Gamma-ray assignments, transition energies, and relative intensities in the [631]3/2 rotational band (odd signature) in the ^{136}Xe experiment. Relative intensities are normalized to the $21/2^- \rightarrow 17/2^-$ transition of the [743]7/2 ground-state band, $E_\gamma = 211.67$ keV, with $I_\gamma = 100$.

E_i (keV)	$J_i^\pi \rightarrow J_f^\pi$	E_γ (keV)	I_γ	Comments
791	$15/2^+ \rightarrow 15/2^+$	434.1(10)	0.4(4)	a,bc
1021	$19/2^+ \rightarrow 15/2^+$	230.0(10)	0.12(12)	a,b
1021	$19/2^+ \rightarrow 19/2^+$	461.2(10)	0.41(20)	a,b
1293	$23/2^+ \rightarrow 19/2^+$	272.0(10)	0.08(10)	a,b
1293	$23/2^+ \rightarrow 23/2^+$	491.6(3)	0.50(12)	a,b
1601	$27/2^+ \rightarrow 23/2^+$	308.0(10)	0.17(9)	a,b
1601	$27/2^+ \rightarrow 27/2^+$	522.9(10)	0.33(10)	a,b
1943	$31/2^+ \rightarrow 27/2^+$	342.6(10)	0.137(7)	b
1943	$31/2^+ \rightarrow 31/2^+$	554.21(5)	0.174(6)	b
2314	$35/2^+ \rightarrow 31/2^+$	371.1(10)	0.124(6)	b
2314	$35/2^+ \rightarrow 35/2^+$	583.3(10)	0.156(4)	b
2708	$39/2^+ \rightarrow 35/2^+$	395.5(10)	0.062(3)	b
2708	$39/2^+ \rightarrow 39/2^+$	605.7(10)	0.0311(22)	b
3124	$43/2^+ \rightarrow 39/2^+$	415.0(10)	0.0035(25)	b
3124	$43/2^+ \rightarrow 43/2^+$	621.3(10)	0.0111(22)	b

TABLE XLIII. Gamma-ray assignments, transition energies, and relative intensities within the $K = 3/2$ γ vibrational band, and across to the [743]7/2 ground-state band, in the ^{136}Xe experiment. Relative intensities are normalized to the $21/2^- \to 17/2^-$ transition of the [743]7/2 ground-state band, $E_\gamma = 211.67$ keV, with $I_\gamma = 100$. Decays across to the [631]1/2 Nilsson rotational band were not detected from the even signature states. Decays within the odd signature of the γ vibrational band are nearly degenerate with cascades in the ground-state band and were impossible to characterize.

E_i (keV)	$J_i^\pi \to J_f^\pi$	E_γ (keV)	I_γ	Comments
806	$11/2^- \to 15/2^-$	557.0(5)	0.62(15)	b,ac
806	$11/2^- \to 13/2^-$	635.3(5)	0.6(6)	b,ac
953	$15/2^- \to 15/2^+$	595.8(5)	0.19(2)	b,a
953	$15/2^- \to 17/2^-$	614.2(5)	0.50(5)	b,a
953	$15/2^- \to 15/2^-$	702.9(5)	0.12(1)	b,a
1142	$19/2^- \to 19/2^+$	583.1(5)	0.26(3)	b,a
1142	$19/2^- \to 21/2^-$	592.0(5)	0.30(6)	b,a
1142	$19/2^- \to 19/2^-$	702.9(5)	0.31(6)	b,a
1374	$23/2^- \to 25/2^-$	568.7(5)	0.7(2)	b,a
1374	$23/2^- \to 23/2^+$	573.4(5)	0.19(2)	b,a
1374	$23/2^- \to 23/2^-$	703.1(5)	0.6(1)	b,a
1646	$27/2^- \to 29/2^-$	545.8(5)	0.31(3)	b,a
1646	$27/2^- \to 27/2^+$	568.2(5)	0.19(3)	b
1646	$27/2^- \to 27/2^-$	701.8(5)	0.15(2)	b
1957	$31/2^- \to 33/2^-$	524.5(5)	0.19(3)	b
1957	$31/2^- \to 31/2^-$	701.0(5)	0.17(3)	b
879	$13/2^- \to 15/2^-$	629.7(5)	0.50(6)	b,ac
879	$13/2^- \to 13/2^-$	708.4(5)	0.21(6)	b,ac
1053	$17/2^- \to 13/2^-$	174.3(5)	0.20(8)	b,a
1053	$17/2^- \to 19/2^-$	614.6(5)	0.85(30)	b,a
1053	$17/2^- \to 17/2^-$	714.6(8)	0.35(7)	b,a
1274	$21/2^- \to 17/2^-$	221.0(6)	0.10(5)	b,a
1274	$21/2^- \to 23/2^-$	603.3(5)	0.60(10)	b,a
1274	$21/2^- \to 21/2^-$	724.1(4)	0.53(20)	b,a
1541	$25/2^- \to 21/2^-$	267.1(7)	0.28(10)	b,a
1541	$25/2^- \to 27/2^-$	596.9(5)	0.35(10)	b,a
1541	$25/2^- \to 25/2^-$	736.7(6)	0.35(12)	b,a
1850	$29/2^- \to 25/2^-$	309.1(10)	0.17(6)	b
1850	$29/2^- \to 31/2^-$	593.5(6)	0.29(9)	b
1850	$29/2^- \to 29/2^-$	750.7(10)	0.26(9)	b

TABLE XLIV. Gamma-ray assignments, transition energies, and relative intensities in the [752]5/2 rotational band (even signature) in the ^{136}Xe experiment. Relative intensities are normalized to the $21/2^- \to 17/2^-$ transition of the [743]7/2 ground-state band, $E_\gamma = 211.67$ keV, with $I_\gamma = 100$.

E_i (keV)	$J_i^\pi \to J_f^\pi$	E_γ (keV)	I_γ	Comments
850	$13/2^- \to 15/2^-$	600.47(6)	0.53(8)	b,ac
850	$13/2^- \to 13/2^-$	679.22(3)	0.40(9)	b,ac
1023	$17/2^- \to 19/2^-$	583.90(12)	0.87(4)	b,ac
1023	$17/2^- \to 17/2^-$	683.99(7)	0.76(5)	b,ac
1235	$21/2^- \to 25/2^-$	431.4(10)	0.31(3)	b,ac
1235	$21/2^- \to 23/2^-$	563.5(10)	0.31(5)	b,ac
1235	$21/2^- \to 21/2^-$	684.1(10)	0.31(5)	b,a
1235	$21/2^- \to 19/2^-$	795.2(10)	0.12(4)	b,a
1484	$25/2^- \to 21/2^-$	250.4(10)	0.3(1)	b,a
1484	$25/2^- \to 27/2^-$	539.80(10)	0.47(12)	b,a
1484	$25/2^- \to 25/2^-$	680.10(9)	0.44(17)	b,a
1484	$25/2^- \to 23/2^-$	813.6(10)	0.2(1)	b,a
1772	$29/2^- \to 25/2^-$	287.7(10)	0.4(1)	b,a
1772	$29/2^- \to 31/2^-$	515.40(8)	0.31(10)	b
1772	$29/2^- \to 29/2^-$	672.7(3)	0.5(2)	b
1772	$29/2^- \to 27/2^-$	827.8(10)	0.3(1)	b
2096	$33/2^- \to 29/2^-$	323.8(10)	0.3(1)	b
2096	$33/2^- \to 35/2^-$	490.6(10)	0.19(6)	b
2096	$33/2^- \to 33/2^-$	663.2(10)	0.25(9)	b
2096	$33/2^- \to 31/2^-$	839.1(10)	0.19(9)	b
2453	$37/2^- \to 33/2^-$	357.5(10)	0.2(1)	b
2842	$41/2^- \to 37/2^-$	388.7(10)	0.10(5)	b

TABLE XLV. Gamma-ray assignments, transition energies, and relative intensities in the [752]5/2 rotational band (odd signature) in the ^{136}Xe experiment. Relative intensities are normalized to the $21/2^- \to 17/2^-$ transition of the [743]7/2 ground-state band, $E_\gamma = 211.67$ keV, with $I_\gamma = 100$.

E_i (keV)	$J_i^\pi \to J_f^\pi$	E_γ (keV)	I_γ	Comments
923	$15/2^- \to 17/2^-$	584.5(5)	0.24(6)	b,ac
1108	$19/2^- \to 21/2^-$	557.6(5)	0.4(6)	b,ac
1108	$19/2^- \to 19/2^-$	669.3(5)	0.6(6)	b,ac
1108	$19/2^- \to 17/2^-$	769.6(5)	0.5(6)	b,ac
1333	$23/2^- \to 19/2^-$	224.5(5)	0.1(6)	b,a
1333	$23/2^- \to 25/2^-$	527.8(5)	0.3(13)	b,a
1333	$23/2^- \to 23/2^-$	661.8(5)	0.47(22)	b,a
1599	$27/2^- \to 23/2^-$	266.1(5)	0.3(6)	b,a
1599	$27/2^- \to 29/2^-$	498.5(5)	0.3(6)	b,a
1599	$27/2^- \to 27/2^-$	654.2(5)	0.3(6)	b,a
1905	$31/2^- \to 27/2^-$	306.4(5)	0.4(6)	b
1905	$31/2^- \to 33/2^-$	472.0(5)	0.1(6)	b
1905	$31/2^- \to 31/2^-$	647.8(5)	0.2(6)	b
2248	$35/2^- \to 31/2^-$	343.4(5)	0.5(6)	b
2248	$35/2^- \to 37/2^-$	447.3(5)	0.1(6)	b
2248	$35/2^- \to 35/2^-$	643.0(5)	0.2(6)	b
2625	$39/2^- \to 35/2^-$	376.2(5)	0.1(6)	b
2625	$39/2^- \to 41/2^-$	425.6(5)	0.1(6)	b
2625	$39/2^- \to 39/2^-$	639.4(5)	0.1(6)	b

TABLE XLVI. Gamma-ray assignments, transition energies, and relative intensities in the [734]9/2 rotational band in the ^{136}Xe experiment. Relative intensities are normalized to the $21/2^- \rightarrow 17/2^-$ transition of the [743]7/2 ground-state band, $E_\gamma = 211.67$ keV, with $I_\gamma = 100$. Note that the Nilsson [734]9/2 band is crossed by the $K = 11/2$ γ-vibrational band at spin 17/2.

E_i (keV)	$J_i^\pi \rightarrow J_f^\pi$	E_γ (keV)	I_γ	Comments
1140	$17/2^- \rightarrow 17/2^-$	802.0(5)	0.30(4)	b,a
1140	$17/2^- \rightarrow 15/2^-$	890.9(5)	0.30(6)	b,ac
1349	$21/2^- \rightarrow 17/2^-$	209.0(5)	0.05(3)	b,a
1349	$21/2^- \rightarrow 21/2^-$	798.3(5)	0.30(4)	b,a
1349	$21/2^- \rightarrow 19/2^-$	910.1(5)	0.50(3)	b,ac
1349	$21/2^- \rightarrow 17/2^-$	1010.5(5)	0.30(3)	b,a
1594	$25/2^- \rightarrow 21/2^-$	245.5(5)	0.10(6)	b,a
1594	$25/2^- \rightarrow 25/2^-$	789.7(5)	0.4(1)	b,a
1594	$25/2^- \rightarrow 23/2^-$	923.9(5)	0.6(2)	b,a
1878	$29/2^- \rightarrow 25/2^-$	284.0(5)	0.15(6)	b,a
1878	$29/2^- \rightarrow 29/2^-$	778.2(5)	0.20(6)	b
1878	$29/2^- \rightarrow 27/2^-$	933.53(7)	0.4(1)	b
1878	$29/2^- \rightarrow 25/2^-$	1073.3(5)	0.10(6)	b
2192	$33/2^- \rightarrow 31/2^-$	934.9(5)	0.20(6)	b
1240	$19/2^- \rightarrow 19/2^-$	801.6(5)	0.6(2)	b,ac
1240	$19/2^- \rightarrow 17/2^-$	901.4(5)	0.6(2)	b,ac
1240	$19/2^- \rightarrow 15/2^-$	991.0(5)	0.6(2)	b,ac
1466	$23/2^- \rightarrow 19/2^-$	227.0(5)	0.10(5)	b,a
1466	$23/2^- \rightarrow 23/2^-$	795.3(5)	0.3(1)	b,a
1466	$23/2^- \rightarrow 21/2^-$	916.2(5)	0.3(1)	b,a
1466	$23/2^- \rightarrow 19/2^-$	1027.8(5)	0.3(1)	b,a
1731	$27/2^- \rightarrow 23/2^-$	264.6(5)	0.2(1)	b,a
1731	$27/2^- \rightarrow 27/2^-$	785.9(5)	0.3(1)	b
1731	$27/2^- \rightarrow 25/2^-$	926.5(5)	0.3(1)	b
2032	$31/2^- \rightarrow 27/2^-$	301.7(5)	0.10(5)	b
2032	$31/2^- \rightarrow 31/2^-$	774.8(5)	0.10(5)	b
2032	$31/2^- \rightarrow 29/2^-$	932.8(5)	0.2(1)	b
2367	$35/2^- \rightarrow 35/2^-$	762.6(5)	0.10(5)	b
2367	$35/2^- \rightarrow 33/2^-$	934.0(5)	0.10(5)	b

TABLE XLVII. Gamma-ray assignments, transition energies, and relative intensities for decays from the $K = 11/2$ γ-vibrational band (odd signature) to the [743]7/2 ground-state band in the ^{136}Xe experiment. Relative intensities are normalized to the $21/2^- \rightarrow 17/2^-$ transition of the [743]7/2 ground-state band, $E_\gamma = 211.67$ keV, with $I_\gamma = 100$. Note that the $K = 11/2$ γ-vibrational band crosses the Nilsson [734]9/2 band at spin 17/2.

E_i (keV)	$J_i^\pi \rightarrow J_f^\pi$	E_γ (keV)	I_γ	Comments
1065	$15/2^- \rightarrow 15/2^-$	816.5(5)	0.6(2)	b,ac
1260	$19/2^- \rightarrow 19/2^-$	822.0(5)	0.6(2)	b,ac
1260	$19/2^- \rightarrow 17/2^-$	921.8(5)	0.6(2)	b,ac
1260	$19/2^- \rightarrow 15/2^-$	1010.4(5)	0.6(2)	b,ac
1504	$23/2^- \rightarrow 23/2^-$	833.3(5)	0.3(1)	b,a
1504	$23/2^- \rightarrow 21/2^-$	953.2(5)	0.2(1)	b

TABLE XLVIII. Gamma-ray assignments, transition energies, and relative intensities for decays from the $K = 11/2$ γ-vibrational band (even signature) to the [743]7/2 ground-state band in the ^{136}Xe experiment. Relative intensities are normalized to the $21/2^- \rightarrow 17/2^-$ transition of the [743]7/2 ground-state band, $E_\gamma = 211.67$ keV, with $I_\gamma = 100$. Note that the $K = 11/2$ γ-vibrational band crosses the Nilsson [734]9/2 band at spin 17/2.

E_i (keV)	$J_i^\pi \rightarrow J_f^\pi$	E_γ (keV)	I_γ	Comments
987	$13/2^- \rightarrow 15/2^-$	737.2(5)	0.3(1)	b,ac
987	$13/2^- \rightarrow 13/2^-$	816.7(5)	0.2(1)	b,ac
1155	$17/2^- \rightarrow 19/2^-$	716.1(5)	0.3(1)	b,ac
1155	$17/2^- \rightarrow 17/2^-$	816.7(5)	0.3(1)	b,ac
1155	$17/2^- \rightarrow 15/2^-$	906.3(5)	0.6(2)	b,ac

TABLE XLIX. Transition energies and relative intensities for decays from the $K = 3/2$ γ-vibrational band to the [743]7/2 ground-state band in the CHICO experiment. Relative intensities are normalized to the $19/2^- \to 15/2^-$ transition in the ground-state band, $E_\gamma = 189.6$ keV, with $I_\gamma = 100$.

J_i	$J \to J+2$		$J \to J+1$		$J \to J$		$J \to J-1$		$J \to J-2$	
	E_γ (keV)	I_γ	E_γ (keV)	I_γ	E_γ (keV)	I_γ	E_γ (keV)	I_γ	E_γ (keV)	I_γ
3/2	637.8	9.6(24)f	–	–	–	–	–	–	–	–
5/2	618.2	6.9(20)	664.6	4.8(8)	–	–	–	–	–	–
7/2	598.1	3.6(10)	654.8	5.0(10)	701.2	1.0(5)f	–	–	–	–
9/2	579.5	3.1(6)	647.1	4.2(10)	703.7	≈2 f	750.0	0.5(3)f	–	–
11/2	557.4	2.4(6)	635.4	3.2(4)	(703.7)	≈2 f	760.3	0.2(2)	806.3	1.0(5)
13/2	541.2	0.5(3)f	630.3	2.1(4)	708.6	0.69(5)f	775.9	0.2(2)f	–	–

TABLE L. Transition energies and relative intensities for decays from the $K = 3/2$ γ-vibrational band to the [631]1/2 Nilsson band in the CHICO experiment. Relative intensities are normalized to the $19/2^- \to 15/2^-$ transition in the ground-state band, $E_\gamma = 189.6$ keV, with $I_\gamma = 100$. Because there is a parity change, the transitions $E_\gamma(J \to J \pm 2)$ need not be considered.

J_i	$J \to J+1$		$J \to J$		$J \to J-1$	
	E_γ (keV)	I_γ	E_γ (keV)	I_γ	E_γ (keV)	I_γ
3/2	586.8	0.5(2)f	624.9	3.8(20)f	637.8	3.0(1.0)f
5/2	583.0	2.5(10)	613.0	2.1(5)	651.6	2.0(4)
7/2	550.7	0.55(20)f	–	–	649.5	0.9(2)f
9/2	553.2	0.8(2)	–	–	668.8	0.8(4)f

TABLE LI. Transition energies and relative intensities for decays from the [752]5/2 Nilsson band to the [743]7/2 ground-state band in the CHICO experiment. Relative intensities are normalized to the $19/2^- \to 15/2^-$ transition in the ground-state band, $E_\gamma = 189.6$ keV, with $I_\gamma = 100$.

J_i	$J \to J+2$		$J \to J+1$		$J \to J$		$J \to J-1$		$J \to J-2$	
	E_γ (keV)	I_γ	E_γ (keV)	I_γ	E_γ (keV)	I_γ	E_γ (keV)	I_γ	E_γ (keV)	I_γ
5/2	586.8	0.5(3)f	633.1	3.0(10)f	–	–	–	–	–	–
7/2	568.2	0.2(1)	624.9	2.0(10)f	671.1	2.1(8)f	–	–	–	–
9/2	550.7	0.55(20)f	617.4	5.7(10)	674.5	4(1)	719.9	0.6(3)	–	–
11/2	528.5	0.25(10)	607.2	3.8(10)f	674.5	4(1)	731.4	0.7(3)	–	–
13/2	–	–	601.0	4.1(10)	679.6	2.7(10)f	746.9	1.3(10)f	–	–
15/2	–	–	584.6	3.1(10)f	674.5	3(1)	752.8	1.5(5)	–	–
17/2	–	–	584.6	2.1(10)f	684.2	3.3(10)	774.5	0.8(3)	–	–
19/2	–	–	557.4	2.4(10)	668.9	1.9(7)f	769.9	1.1(4)	–	–
21/2	–	–	563.9	0.6(2)	–	–	–	–	–	–

TABLE LII. Transition energies and relative intensities for decays from the [734]9/2 Nilsson band to the [743]7/2 ground-state band in the CHICO experiment. Relative intensities are normalized to the $19/2^- \to 15/2^-$ transition in the ground-state band, $E_\gamma = 189.6$ keV, with $I_\gamma = 100$. Note that the $K = 11/2$ γ-vibrational band crosses the Nilsson [734]9/2 band at spin 17/2.

J_i	$J \to J+2$		$J \to J+1$		$J \to J$		$J \to J-1$		$J \to J-2$	
	E_γ (keV)	I_γ	E_γ (keV)	I_γ	E_γ (keV)	I_γ	E_γ (keV)	I_γ	E_γ (keV)	I_γ
9/2	–	–	719.4	0.2(1)f	775.9	0.2(1)f	821.6	2.4(5)f	–	–
11/2	–	–	715.2	0.8(2)	783.4	1.0(3)	839.7	2.1(5)	–	–
13/2	–	–	712.7	0.5(1)	791.1	0.6(2)	857.8	1.9(5)	915.1	0.5(2)
15/2	–	–	708.6	0.30(20)f	797.3	2.2(5)f	–	–	943.7	0.6(2)
17/2	–	–	701.2	0.2(2)f	801.5	0.9(3)f	891.0	1.5(3)	969.4	0.8(2)
19/2	–	–	–	–	802.1	(2.5)	902.1	1.0(3)	992.1	1.2(3)
21/2	–	–	–	–	–	–	910.6	0.7(3)	1010.2	0.25(20)f

TABLE LIII. Transition energies and relative intensities for decays from $K = 11/2$ γ-vibrational band to the [743]7/2 ground-state band in the CHICO experiment. Relative intensities are normalized to the $19/2^- \to 15/2^-$ transition in the ground-state band, $E_\gamma = 189.6$ keV, with $I_\gamma = 100$. Note that the $K = 11/2$ γ-vibrational band crosses the Nilsson [734]9/2 band at spin 17/2.

J_i	$J \to J+2$		$J \to J+1$		$J \to J$		$J \to J-1$		$J \to J-2$	
	E_γ (keV)	I_γ	E_γ (keV)	I_γ	E_γ (keV)	I_γ	E_γ (keV)	I_γ	E_γ (keV)	I_γ
11/2	671.1	0.35(15)f	750.0	0.4(3)f	≈817	(3.1)f	875.0	11(2)	920.7	22(3)
13/2	649.5	0.25(15)f	737.9	0.25(10)	≈817	(2.2)f	884.6	6(2)	941.2	5.0(10)f
15/2	627.3	–	727.1	0.2(1)	≈817	(2.2)f	894.5	3.6(10)	961.8	1.4(2)
17/2	–	–	717.4	0.2(2)f	≈817	(1.3)f	906.6	1.3(3)	≈985	0.1(1)
19/2	–	–	–	–	821.6	0.2(1)f	921.5	0.9(4)	1010.1	0.25(20)f

TABLE LIV. Transition energies and relative intensities for decays from the [631]3/2 Nilsson band to the [631]1/2 Nilsson band in the CHICO experiment. Relative intensities are normalized to the $19/2^- \to 15/2^-$ transition in the ground-state band, $E_\gamma = 189.6$ keV, with $I_\gamma = 100$.

J_i	$J \to J+2$		$J \to J+1$		$J \to J$		$J \to J-1$		$J \to J-2$	
	E_γ (keV)	I_γ	E_γ (keV)	I_γ	E_γ (keV)	I_γ	E_γ (keV)	I_γ	E_γ (keV)	I_γ
3/2	311.0	0.30(10)f	–	–	379.4	0.7(3)f	392.9	0.6(2)	–	–
5/2	276.9	0.05(5)f	345.3	0.15(5)	375.3	1.0(3)f	414.2	0.6(3)f	427.4	0.3(2)f
7/2	–	–	324.2	0.1(1)	392.9	0.55(20)	422.7	0.5(2)	462.1	0.3(1)
9/2	–	–	335.2	0.4(2)	382.9	0.6(2)	451.4	0.5(2)	481.4	0.2(2)f
11/2	–	–	312.9	0.36(30)f	411.5	1.6(3)	457.7	0.17(7)f	–	–
13/2	–	–	333.0	1.3(3)	395.3	0.7(2)	492.9	0.9(3)	539.0	1.0(3)
15/2	–	–	–	–	435.0	1.5(4)	–	–	–	–

TABLE LV. Transition energies and relative intensities for decays from the [633]5/2 Nilsson band to the [743]7/2 ground-state band and across to the [622]5/2 band in the CHICO experiment. Relative intensities are normalized to the $19/2^- \to 15/2^-$ transition in the ground-state band, $E_\gamma = 189.6$ keV, with $I_\gamma = 100$.

J_i	$J \to J+1$ gsb		$J \to J$ gsb		$J \to J$ [622]5/2	
	E_γ (keV)	I_γ	E_γ (keV)	I_γ	E_γ (keV)	I_γ
5/2	333.1	1.3(3)	–	–	203.0	1.4(3)
7/2	321.3	0.26(5)	367.3	0.6(1)	196.0	0.25(5)
9/2	311.0	0.47(9)f	368.8	0.45(9)	189f	–

TABLE LVI. Transition energies and relative intensities for decays from the band tentatively assigned [613]7/2 to the [743]7/2 ground-state band and across to the [624]7/2 Nilsson band in the CHICO experiment. Relative intensities are normalized to the $19/2^- \to 15/2^-$ transition in the ground-state band, $E_\gamma = 189.6$ keV, with $I_\gamma = 100$. Note that the γ rays in the first two columns were not confirmed by coincidence measurements (see text).

J_i	$J \to J+1$ gsb		$J \to J$ gsb		$J \to J$ [624]		$J \to J+1$ [624]	
	E_γ (keV)	I_γ	E_γ (keV)	I_γ	E_γ (keV)	I_γ	E_γ (keV)	I_γ
7/2	941.2	0.6(2)f	986.4	0.53(10)	541.2	1.0(5)f	476.6	0.16(5)
9/2	938.3	0.19(10)f	996.3	0.56(10)	532.3	0.7(3)	457.7	0.2(1)f
11/2	938.3	0.19(10)f	1006.5	0.13(5)f	524.4	0.2(1)	439.3	0.16(6)
13/2	–	–	–	–	516.4	0.11(6)	–	–

TABLE LVII. Transition energies and relative intensities for decays from the band tentatively assigned [615]9/2 to the [743]7/2 ground-state band and across to the [624]7/2 Nilsson band in the CHICO experiment. Relative intensities are normalized to the $19/2^- \rightarrow 15/2^-$ transition in the ground-state band, $E_\gamma = 189.6$ keV, with $I_\gamma = 100$. Note that the γ rays in the first three columns were not confirmed by coincidence measurements (see text).

J_i	$J \rightarrow J+1$		$J \rightarrow J$		$J \rightarrow J-1$		$J \rightarrow J-1$ [624]		$J \rightarrow J$ [624]	
	E_γ (keV)	I_γ	E_γ (keV)	I_γ	E_γ (keV)	I_γ	E_γ (keV)	I_γ	E_γ (keV)	I_γ
9/2	1090.6	0.17(4)	1145.8	0.30(6)	1192.3	0.30(6)	747.1	1.0(4)f	682.6	0.3(2)f
11/2	1086.8	0.4(8)	1155.9	0.36(20)	≈ 1211	0.1(1)	746.9	0.4(3)f	672.0	0.3(2)f
13/2	–	–	1159.0	0.2(1)	1226.7	0.05(3)	745.1	0.19(6)	659.3	≈0.5f
15/2	–	–	1161.4	0.2(1)	–	–	740.8	0.06(3)	–	–

TABLE LVIII. Transition energies and relative intensities for decays from the [624]7/2 Nilsson band to the [743]7/2 ground-state band (first three sets of columns) and across to the [622]5/2 Nilsson band (last two sets of columns). Relative intensities are normalized to the $19/2^- \rightarrow 15/2^-$ transition in the ground-state band, $E_\gamma = 189.6$ keV, with $I_\gamma = 100$.

J_i	$J \rightarrow J+1$		$J \rightarrow J$		$J \rightarrow J-1$		$J \rightarrow J$ [622]		$J \rightarrow J-1$ [622]	
	E_γ (keV)	I_γ	E_γ (keV)	I_γ	E_γ (keV)	I_γ	E_γ (keV)	I_γ	E_γ (keV)	I_γ
7/2	399.6	2.8(5)	445.8	3.0(8)	–	–	273.9	1.0(10)f	316.5	5.0(10)
9/2	407.3	2.5(5)	463.9	1.3(3)	510.4	2.4(4)	285.1	0.2(1)	338.7	3.9(8)
11/2	414.3	1.0(5)f	481.5	0.4(2)f	539.4	1.0(2)	295.5	0.2(1)f	359.7	2.1(4)
13/2	421.1	0.8(2)	499.0	0.1(1)	566.8	0.4(1)	300.7	0.2(2)f	379.4	0.7(3)f
15/2	427.2	0.6(3)	–	–	–	–	308.7	0.24(5)	397.0	0.6(2)

TABLE LIX. Transition energies and relative intensities for decays from the [624]7/2 Nilsson band to the [631]1/2 Nilsson band in the CHICO experiment. Relative intensities are normalized to the $19/2^- \rightarrow 15/2^-$ transition in the ground-state band, $E_\gamma = 189.6$ keV, with $I_\gamma = 100$.

J_i	$J \rightarrow J$		$J \rightarrow J-1$		$J \rightarrow J-2$	
	E_γ (keV)	I_γ	E_γ (keV)	I_γ	E_γ (keV)	I_γ
7/2	363.7	0.07 to 0.14	394.0	0.2(1)	432.1	0.6(2)
9/2	–	–	429.1	0.9(3)	457.7	0.3(1)f
11/2	–	–	≈434.1	0.7(3)	503.8	0.3(1)f
13/2	–	–	472.7	0.5(2)	519.7	≈0.1 f
15/2	–	–	470.8	0.5(2)	–	–

TABLE LX. Transition energies and relative intensities for decays from an unassigned ($K = 7/2$) band to the [743]7/2 ground-state band (first three sets of columns) and across to the [624]7/2 Nilsson band (last two sets of columns). Relative intensities are normalized to the $19/2^- \rightarrow 15/2^-$ transition in the ground-state band, $E_\gamma = 189.6$ keV, with $I_\gamma = 100$. Note that the γ rays in the first three columns were not confirmed by coincidence measurements (see text).

J_i	$J \rightarrow J+1$		$J \rightarrow J$		$J \rightarrow J-1$		$J \rightarrow J$ [624]		$J \rightarrow J+1$[624]	
	E_γ (keV)	I_γ	E_γ (keV)	I_γ	E_γ (keV)	I_γ	E_γ (keV)	I_γ	E_γ (keV)	I_γ
7/2	1006.5	0.13(5)f	1052.0	0.5(1)	–	–	606.9	0.5(5)f	542.9	0.6(3)f
9/2	998.6	0.2(1)	1053.3	0.4(1)	1099.5	0.5(1)	589.5	0.1(1)f	515.5	0.8(2)

[1] F. S. Stephens *et al.*, Nucl. Phys. A **115**, 129 (1968).

[2] A. Winther and J. de Boer, *Coulomb Excitation* (Academic, New York, 1966).

[3] M. W. Simon *et al.*, Nucl. Instrum. Methods Phys. Res. A **452**, 205 (2000).

[4] E. Browne, Nucl. Data Sheets **98**, 665 (2003).

[5] R. S. Simon *et al.*, Z. Phys. A **298**, 121 (1980).

[6] J. de Bettencourt *et al.*, Phys. Rev. C **34**, 1706 (1986).

[7] R. C. Thompson, J. R. Huizenga, and Th. W. Elze, Phys. Rev. C **13**, 638 (1976).

[8] T. H. Braid, R. R. Chasman, J. R. Erskine, and A. M. Friedman, Phys. Rev. C **1**, 275 (1970).

[9] F. A. Rickey, E. T. Jurney, and H. C. Britt, Phys. Rev. C **5**, 2072 (1972).

[10] F. A. Gareev, S. P. Ivanova, A. Malov, and V. G. Soloviev, Nucl. Phys. A **171**, 134 (1971).

[11] A. Bohr and B. R. Mottelson, *Nuclear Structure*, Vol. 2 (Benjamin, New York, 1975).

[12] R. R. Chasman, I. Ahmed, A. M. Friedman, and J. R. Erskine, Rev. Mod. Phys. **49**, 833 (1977).

[13] E. Browne and F. R. Femenia, At. Data Nucl. Data Tables **10**, 81 (1971).

[14] A. E. Stuchbery, ANU Internal Report 1998 ANU-P/1388. Australian National University, Canberra, Australia, 2005.

[15] B. E. Chi, Nucl. Phys. **83**, 97 (1966); Erratum, Nucl. Phys. **89**, 706 (1966).

[16] Code GAMPN by I. Ragnarsson and P. B. Semmes (unpublished). Based on work described in S. E. Larsson, G. Leander, and I. Ragnarsson, Nucl. Phys. A **307**, 189 (1978).

[17] S. G. Nilsson *et al.*, Nucl. Phys. A **131**, 1 (1969).

[18] I. Ragnarsson *et al.*, Nucl. Phys. A **307**, 189 (1978).

[19] R. Bengtsson *et al.*, Phys. Scr. **39**, 196 (1989).

[20] P. Rozmej *et al.*, in *Proceedings of the XXIV International Winter Meeting on Nuclear Physics, Bormio, Italy*, edited by I. Iori, (Uniersita degli studi Milano, Milano, 1986), p. 567.

[21] C.-D. Herrmann *et al.*, Nucl. Phys. A **493**, 83 (1989).

[22] Z. Bochnacki and S. Ogaza, Nucl. Phys. **83**, 619 (1966).

[23] N. J. Stone, At. Data Nucl. Data Tables **90**, 75 (2005).

[24] F. E. Chukreev, V. E. Makarenko, and M. J. Martin, Nucl. Data Sheets **97**, 129 (2002).

[25] K. E. G. Lobner *et al.*, Nucl. Data Tables A **7**, 495 (1970).

[26] P. G. Hansen, O. B. Nielson, and R. K. Sheline, Nucl. Phys. **12**, 413 (1959).

[27] S. A. Hjorth, A. Johnson, and G. Ehrling, Nucl. Phys. A **184**, 113 (1972).

[28] E. Osnes, J. Rekstad, and O. K. Gjotterud, Nucl. Phys. A **253**, 45 (1975).

[29] A. J. Kreiner, Phys. Rev. Lett. **42**, 829 (1979).

[30] H. Sakamoto and T. Kishimoto, Nucl. Phys. A **501**, 205 (1989).

[31] E. Browne and J. K. Tuli, Nucl. Data Sheets **108**, 681 (2007); **107**, 2649 (2006).

[32] GOSIA website, http://www.pas.rochester.edu/~cline/Gosia.

[33] T. Nakatsukasa, K. Matsuyanagi, S. Mizutori, and Y. R. Shimizu, Phys. Rev. C **53**, 2213 (1996).

[34] T. Nakatsukasa, S. Mizutori, and K. Matsuyanagi, Prog. Theor. Phys. **89**, 847 (1993).